DIGITAL IMAGE ANALYSIS OF VITILIGO FOR MONITORING OF VITILIGO TREATMENT

HERMAWAN NUGROHO

DEPARTMENT OF ELECTRICAL AND ELECTRONICS ENGINEERING
UNIVERSITI TEKNOLOGI PETRONAS
JANUARY 2008

STATUS OF THESIS

Title of thesis | Digital Image Analysis of Vitiligo for Monitoring of Vitiligo Treatment

I, HERMAWAN NUGROHO ,

hereby allow my thesis to be placed at the Information Resource Center (IRC) of Universiti Teknologi PETRONAS (UTP) with the following conditions:

1. The thesis becomes the properties of UTP.
2. The IRC of UTP may make copies of the thesis for academic purposes only.
3. This thesis is classified as

☐ Confidential

☑ Non-confidential

If this thesis is confidential, please state the reason:

\-

The contents of the thesis will remain confidential for - years.

Remarks on disclosure:

\-

Endorsed by

Signature of Author

Jl Merdeka 593,
Pontianak,
Indonesia

Date : 8-1-2008

Signature of Supervisor

Universiti Teknologi PETRONAS

Professor Ir Dr Ahmad Fadzil M Hani
Dept of Electrical & Electronic Engineering
Universiti Teknologi PETRONAS

Date : 8/1/08

UNIVERSITI TEKNOLOGI PETRONAS

Approval by Supervisor (s)

The undersigned certify that they have read, and recommend to The Postgraduate Studies Programme for acceptance, a thesis entitled "Digital Image Analysis of Vitiligo" submitted by (Hermawan Nugroho) for the fulfillment of the requirements for the degree of Master of Science in Electrical and Electronics Engineering.

_____

Date

Signature : _____

Main supervisor : Professor Ir Dr Ahmad Fadzil M Hani
Dept of Electrical & Electronic Engineering
Universiti Teknologi PETRONAS

Date : 9-1-08

Signature : _____

Co-Supervisor : _____

Date : _____

TITLE PAGE

UNIVERSITI TEKNOLOGI PETRONAS

Digital Image Analysis of Vitiligo for Monitoring of Vitiligo Treatment

By

Hermawan Nugroho

A THESIS
SUBMITTED TO THE POSTGRADUATE STUDIES PROGRAMME
AS A REQUIREMENT FOR THE
DEGREE OF MASTER OF SCIENCE
ELECTRICAL AND ELECTRONICS ENGINEERING
BANDAR SERI ISKANDAR,
PERAK

2007

DECLARATION

I hereby declare that the thesis is based on my original work except for quotations and citations which have been duly acknowledged. I also declare that it has not been previously or concurrently submitted for any other degree at UTP or other institutions.

Signature: 

Name : HERMAWAN NUGROHO

Date : 8th January 2008

ACKNOWLEDGEMENT

First and foremost, I would like to give my sincere thanks to ALLAH SWT, the almighty God, the source of my life and hope for giving me the strength and wisdom to complete the research.

I am most grateful to my supervisor Professor Ahmad Fadzil M.H for giving me an opportunity to pursue a master degree. Many times, his patience and constant encouragement has steered me to the right direction.

I would like also express my gratitude to Dr. Norashikin Shamsudin and Puan Sri from Dermatology Department, Hospital Kuala Lumpur, for their effort in helping and providing me with the all data and guidance that I need for this research. Special thanks also to my postgraduate friends for their encouragement and friendship. My sincerity thanks also to postgraduate office staffs, Kak Norma, Pn Kamaliah and Bang Fadhil for their assistance during my study.

At last and most importantly, I would like to thank my family for their open-mindedness and endless support. They are always close to my heart.

ABSTRACT

Vitiligo is an acquired pigmentary skin disorder characterized by depigmented macules that result from damage to and destruction of epidermal melanocytes. Visually, the vitiligous areas are paler in contrast to normal skin or completely white due to the lack of pigment melanin. The course of vitiligo is unpredictable where the vitiligous skin lesions may remain stable for years before worsening.

Vitiligo treatments have two objectives, to arrest disease progression and to re-pigment the vitiligous skin lesions. To monitor the efficacy of the treatment, dermatologists observe the disease directly, or indirectly using digital photos. Currently there is no objective method to determine the efficacy of the vitiligo treatment. Physician's Global Assessment (PGA) scale is the current scoring system used by dermatologists to evaluate the treatment. The scale is based on the degree of repigmentation within lesions over time. This quantitative tool however may not be help to detect slight changes due to treatment as it would still be largely dependent on the human eye and judgment to produce the scorings. In addition, PGA score is also subjective, as it varies with dermatologists.

The progression of vitiligo treatment can be very slow and can take more than 6 months. It is observed that dermatologists find it visually hard to determine the areas of skin repigmentation due to this slow progress and as a result the observations are made after a longer time frame. The objective of this research is to develop a tool that enables dermatologists to determine and quantify areas of repigmentation objectively over a shorter time frame during treatment. The approaches towards achieving this objective are based on digital image processing techniques.

Skin color is due to the combination of skin histological parameters, namely pigment melanin and haemoglobin. However in digital imaging, color is produced by combining

three different spectral bands, namely red, green, and blue (RGB). It is believed that the spatial distribution of melanin and haemoglobin in skin image could be separated.
It is found that skin color distribution lies on a two-dimensional melanin-haemoglobin color subspace. In order to determine repigmentation (due to pigment melanin) it is necessary to perform a conversion from RGB skin image to this two-dimensional color subspace. Using principal component analysis (PCA) as a dimensional reduction tool, the two-dimensional subspace can be represented by its first and second principal components. Independent component analysis is employed to convert the two-dimensional subspace into a skin image that represents skin areas due to melanin and haemoglobin only.

In the skin image that represents skin areas due to melanin, vitiligous skin lesions are identified as skin areas that lack melanin. Segmentation is performed to separate the healthy skin and the vitiligous lesions. The difference in the vitiligous surface areas between skin images before and after treatment will be expressed as a percentage of repigmentation in each vitiligo lesion. This percentage will represent the repigmentation progression of a particular body region.

Results of preliminary and pre-clinical trial study show that our vitiligo monitoring system has been able to determine repigmentation progression objectively and thus treatment efficacy on a shorter time cycle. An intensive clinical trial is currently undertaken in Hospital Kuala Lumpur using our developed system.

ABSTRAK

Vitiligo diperolehi daripada ketidakseimbangan pigmen kulit yang digambarkan oleh macula yang terdepigmentasi kesan daripada kerosakan dan gangguan ke atas epidermis *melanocytes*. Secara visual, kawasan vitiligo adalah pudar berbanding dengan kulit normal, atau boleh dikatakan bewarna putih keseluruhannya kesan daripada kekurangan pigmen Melanin. Faktor terjadinya Vitiligo adalah sukar dikesan kerana penyakit kulit virtiligo ini akan kekal stabil untuk beberapa tahun sebelum menjadi lebih buruk.

Terdapat dua objektif perawatan vitiligo; untuk menahan penyebaran penyakit dan untuk repigmentasi kulit berpenyakit vitiligo. Bagi mengawasi keberkesanan rawatan, pakar kulit memerhati penyakit ini secara langsung atau tidak langsung dengan menggunakan gambar digital. Pada masa ini, tiada kaedah yang matlamatnya untuk menentukan keberkesanan rawatan vitiligo. Skala *Physician's Global Assessment* (PGA), adalah kaedah terkini yang digunakan oleh pakar kulit untuk menguji rawatn. Alat pengukur ini adalah berdasarkan darjah *repigmentation* dalam kulit berpenyakit keatas masa. Walaubagaimanapun, alat pengiraan ini mungkin tidak cukup untuk membantu dalam mengesan perubahan kecil yang terjadi daripada rawatan kerana kebanyakan masih lagi bergantung kepada mata kasar manusia untuk membuat keputusan. Tambahan pula, keputusan PGA juga subjektif kerana ia berbeza mengikut pakar kulit.

Perkembangan rawatan vitiligo adalah sangat perlahan dan memakan masa lebih daripada enam(6) bulan. Ini terjadi kerana para dermatologis sukar untuk menentukan kawasan kulit yg *repigmentation* secara visual kerana perkembangan yang perlahan. Ini menyebabkan pemerhatian hanya dapat dilakukan setelah melalui suatu jangka masa yang sangat lama. Objektif kajian ini adalah untuk menghasilkan alat yang membolehkan para dermatologis menentukan dan mengira kawasan *repigmentation* dalam jangka masa

yang singkat sepanjang tempoh rawatan. Pendekatan yang digunakan untuk mencapai objektif ini adalah berdasarkan kepada teknik pemprosesan imej digital.

Warna kulit terbentuk daripada kombinasi parameter histologi kulit yang dinamai melanin dan hemoglobin. Walaubagaimanapun, dalam imej digital, warna terbentuk dari kombinasi tiga jalur gelombang spectrum yang berbeza iaitu merah, hijau dan biru (RGB).

Dipercayai bahawa, ruang penyebaran melanin dan hemoglobin dalam imej kulit dapat boleh dipisahkan.Penyebaran kulit didapati bergantung kepada dua dimensi melanin-hemoglobin ruang warna. Untuk menentukan repigmentation (kesan daripada pigmen melanin), adalah perlu untuk melaksanakan pertukaran daripada imej RGB kepada dua dimensi ruang warna. Dengan menggunakan *Principle Component Analysis* (PCA) sebagai alat pendarap dimensi, ruang dua dimensi dapat ditunjukkan daripada prinsip pertama dan kedua komponen-komponen berkenaan. Independent Component Analysis (ICA) dijalankan untuk menukar ruang dua dimensi kepada imej kulit yang mengandungi melanin dan hemoglobin sahaja.

Pada imej kulit yg mewakili kawasan melanin, kulit berpenyakit vitiligo dapat ditentukan berdasarkan kawasan kulit yang mengandungi kurang melanin. *Segmentation* dijalankan untuk memisahkan kulit sihat daripada kuit berpenyakit vitiligo. Perbandingan ke atas kawasan kulit vitiligo untuk sebelum dan selepas rawatan diungkapkan sebagai peratusan *repigmentation* di dalam setiap kulit vitiligo. Peratusan ini akan mewakili perkembangan repigmentation keatas kawasan jasad tertentu.

Keputusan menunjukkan bahawa, kaedah ini mampu mencapai matlamat dalam menetukan perkembangan *repigmentation* dan membawa kepada keberkesanan rawatan dalam tempoh masa yang singkat.

TABLE OF CONTENT

LIST OF FIGURES

LIST OF TABLES

Chapter 1

INTRODUCTION

1.1 Background of Study

1.1.1 Background

Medical imaging which leads to computer-aided diagnosis and monitoring is a multidisciplinary research field that brings together clinicians, scientists, engineers and physicians. The clinical applications span from non-invasive methods (image interpretation, monitoring and diagnostics) to a growing number of invasive methods (robotic surgery). Different types of image may require different types of processing, and advances in image acquisition systems, image processing and computer vision techniques continuously open up new possibilities for medical applications. All of these medical applications require the manipulation and integration of medical image information.

In dermatological practice and studies, visual cues play an important role for enabling dermatologists make accurate diagnosis. In this research, medical analysis of vitiligo skin images is studied. Vitiligo is an acquired pigmentary skin disorder characterized by depigmented macules that result from damage to and destruction of epidermal melanocytes. Visually, the vitiligo areas are paler in contrast to normal skin or completely white due to the lack of pigment melanin [Roberts, 2003]. Figure 1.1 shows samples of vitiligo lesions. The prevalence of vitiligo varies from 0.1% to 2% in various global populations without any sex, racial, skin types or socioeconomic predilection [Pajonk, 2001]. Onset may occur at any age but 50% of patients acquire it before the age of 20. The course of vitiligo is unpredictable where the vitiligo skin lesions may remain stable for years before worsening. The disease is most disfiguring in dark-skinned racial or ethnic groups where the contrast between the depigmented and healthy skin is more discernable. It has been reported that patients with vitiligo will have an increased risk of auto-immune diseases such as thyroid disease (Hashimoto's thyroiditis and Grave's disease), and Addison's disease [Kovacs, 1998].

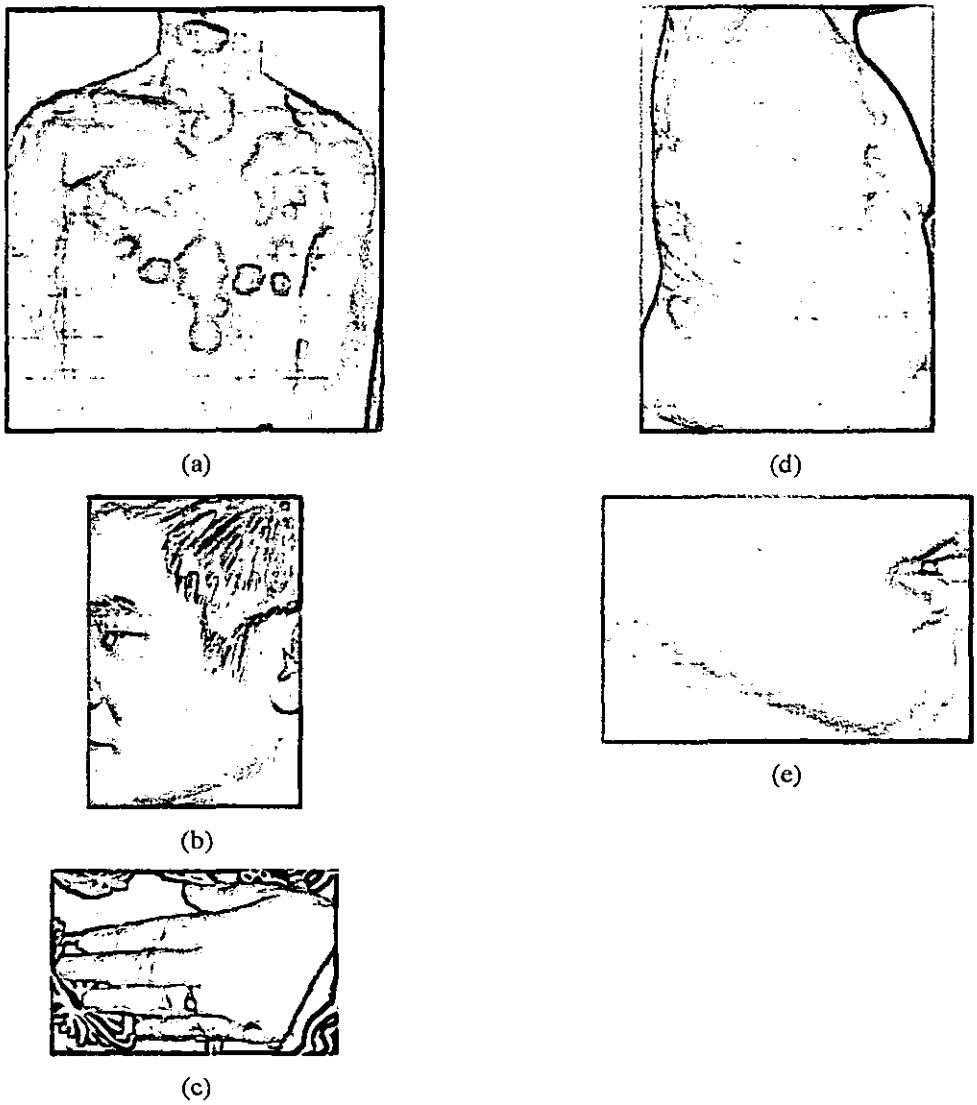

Figure 1.1 Samples of vitiligo lesions; (a) generalized vitiligo, (b) segmental vitiligo, (c) acrofacial vitiligo, (d) universal vitiligo, (e) focal vitiligo

Vitiligo treatments have two objectives, namely to arrest disease progression and to re-pigment the vitiligo skin lesions [Roberts, 2003]. To monitor the efficacy of the treatment, dermatologists observe the disease directly, or indirectly using digital photos. These digital skin images are manually analyzed for purpose of diagnosis by dermatologists. As a result, a large number of skin images are being taken that require manual analysis and diagnosis. At present, dermatologist analyzes the disease by comparing patient's images before and after the treatment. A dermatologist studies the

photographs and assesses the efficacy of the therapeutic response of vitiligo treatment. This requires a high degree of skill and experience as the dermatologist has to be trained to enable an accurate assessment to be made. However the technique is still subjective as it is possible to have different assessments due to the varying degrees of experience of dermatologists.

In addition, the progression of vitiligo treatment is very slow and usually takes more than 6 months. Dermatologists may not be able to detect the delicate changes in treatment effects as it would still largely depends on the human eye and judgments to produce the assessments and diagnosis. As a result, the observations of the disease are made after a longer time frame, typically every 6 months.

In the Dermatology Department of Hospital Kuala Lumpur, dermatologists observe patient's vitiligo skin areas with help of digital images. They compare features of vitiligo lesions before and after treatment. However, since there were no fixed image acquisition procedures, it is found that the vitiligo images sometimes are not well-illuminated and in most cases calibrations of scale in the images are not performed. As a result, it is hard to determine the actual size and subsequent changes in size of the vitiligo lesions and the repigmentation areas due to treatment.

1.1.2 Role of Digital Image Analysis

During treatment for vitiligo, skin images are produced using a digital SLR (Single Lens Reflection) camera. Digital SLR camera provides many advantages compare to digital compact camera. The principal advantage of digital SLR cameras over other digital cameras is the defining characteristic of an SLR: the image in the optical viewfinder is parallax-free because its light is routed directly from the main lens itself, rather than from an off-axis viewfinder [Barnett, 2005].

The skin images produced by the camera are presented as arrays of pixels having discrete intensity values. These intensity values are produced by the camera's CCD (Charge-

coupled device). CCD is an image sensor consisting of integrated circuits containing an array of coupled light sensitive capacitors. It is reported that CCD and photographic film respond to 70% and 40% of the incident light respectively, thus making CCD more efficient than photographic film [Peterson, 2001]. In digital image camera, CCD sensors are equipped with Bayer mask to produce color images. Bayer mask filters all of incoming light before in contact to CCD into three colors light; red, green and blue [Bayer, 1976].

In signal processing, digital skin image can be seen as a two-dimensional signal that contains information of skin. Using computing techniques, skin image can be analyzed and used as a tool for assisting dermatologists. Moreover, with the decrease in cost and increase in computation power of personal computers, it is now reasonable to develop a sophisticated and cost-effective computer-based image analysis system. Computer aided analysis of digital skin image offers quantitative and repeatable measurements, reducing the subjectivity of diagnosis. In addition, it also has the potential to enable dermatologist monitors vitiligo on a shorter time cycle.

Malaysia is now embarking on telemedicine, which is one of the Multimedia Supercoridor (MSC) projects. It is envisioned that the schemes presented in the thesis will form part of the telemedicine initiative in Malaysia. Telemedicine can be defined as the practice of medicine from a distance. It provides health care services through a combination of telecommunications and multimedia technologies with medical expertise. The purpose of telemedicine is to provide equal access to quality healthcare regardless of income, status or geographical location [Multimedia University, 2004]. This work contributes to the computer aided diagnosis, especially for assisting dermatologist to monitor vitiligo disease.

1.2 Problem Statement

Assessment of therapeutic response of vitiligo has always been unsatisfactory as currently there is no objective way to measure and quantify the repigmentation response. The current scoring systems used to evaluate treatment outcome is largely arbitrary and is highly subjective with inter and intra-observer variations [Norashikin, 2007]. There is no validated quantitative scale that allows vitiligo to be characterized parametrically [Hamzavi, 2004]

PGA (Physician's Global Assessment) scale is the current scoring system used by dermatologists. The scale is based on the degree of repigmentation within lesions over time. However, it is found that most of the studies on vitiligo treatments vary in width and number of points of the PGA scale with different authors. The degree of repigmentation that defines success has often been set somewhat arbitrarily at 50-75% repigmentation based largely on the global impression of the overall response [Lepe, 2003]. It is difficult to compare treatment outcomes given differences in the PGA scale used to assess repigmentation. In this research, we use PGA scale that is shown in Table 1.1.

Table 1.1 Physician's Global Assessment Scale

Repigmentation	Scale
0-25%	Mild
26-50%	Moderate
51-75%	Good
76-100%	Excellent to Complete

Furthermore, the evaluation of the treatment would still be largely dependent on the human eye and judgment to produce the scorings. In addition, the judgment is also subjective, as it varies with dermatologists.

The progression of vitiligo treatment can be very slow and can take more than 6 months [Roberts, 2003]. It is observed that dermatologists find it visually hard to determine the

areas of skin repigmentation due to this slow progress and as a result the observations are made after a longer time frame.

It is also known that patients respond differently to the vitiligo treatment. Therapeutic response of a particular treatment could be very different from different patients. It is therefore useful for dermatologists to know the efficacy of a particular treatment earlier, in order that treatment can be adjusted.

The development of a quantitative tool that is highly sensitive to assist dermatologists to evaluate vitiligo treatment outcomes is therefore necessary. Such tools should ideally be able to analyze the overall repigmentation surface area more objectively with repeatable and reliable results.

1.3 Research Objective and Scope of Work

As described in earlier section, the current therapeutic response assessment for vitiligo disease is Physician's Global Assessment (PGA) scale [Middelkamp-Hup, 2007]. However, these are subjective as it is possible to have different judgments due to the varying degrees of experience of dermatologists. To be able to perform PGA scoring accurately, a dermatologist has to be trained extensively. Another problem is that most of the studies on vitiligo treatments have different PGA scale. It is hard to compare treatment outcomes given differences in the scoring systems used to assess repigmentation. In addition, the progression of vitiligo treatment is very slow [Roberts, 2003]. During treatment, areas of repigmentation are found to be small and patchy. Dermatologists found it difficult to visually discern these areas of skin repigmentation during treatment. As a result, the observation and assessment process is made after a longer time cycle.

From all reasons above, it is necessary to develop a qualitative tool that is highly sensitive to assist dermatologists for monitoring vitiligo treatment outcome objectively. The system should be able to analyze, determine and quantify vitiligo skin and repigmentation areas efficiently and reliable. More importantly, it can provide objective

efficacy assessment to assist dermatologist making accurate diagnosis and therapeutic response. The system is expected to provide dermatologist with an objective tool to determine repigmentation areas.

In order to contribute in the development of such tool, the objective of this project is to develop techniques to determine and quantify the repigmentation surface areas objectively over a shorter time frame, based on digital signal and image processing techniques. A combination of signal, image processing and analysis techniques is develop to convert the skin images into images that represents skin areas due to pigment melanin only followed by a segmentation process. Areas of repigmentation are measured by comparing images before and after treatment. The developed algorithm consists of a variety of image processing techniques such as image rotation, geometrical transformation, median cut segmentation, morphological operations and a variety of signal processing techniques such as principal component analysis and independent component analysis. The algorithm is implemented using MATLAB 7.1 software and converted into a stand alone system for use in the field.

1.4 An Overview of Thesis Structure

The thesis is structured according to the respective identification tasks of the digital image analysis of vitiligo monitoring as follows

Chapter 2 introduces the medical background that is anatomy of skin, types of vitiligo diseases and treatments of vitiligo. This chapter also provides a literature review on segmentation of skin diseases systems and algorithms.

Chapter 3 discusses the method and techniques in image processing and signal processing that are used in the thesis. This chapter focuses on the mathematical formulations of the techniques used in the developed system.

Chapter 4 describes the development of the system. The system is presented and devised by a block diagram. This chapter also provides and describes the development of skin models which are used to measure the accuracy of the developed system.

Chapter 5 presents the determination of the developed system algorithm from two data sets, namely historical data and pre-clinical trial data. The performance of the system algorithm is presented in this chapter.

Chapter 6 presents the achievement and contribution of this research work, conclusions and future avenues of investigation.

Chapter 2

VITILIGO AND DIGITAL IMAGING OF SKIN

2.1 Introduction

In this chapter, the basic medical background regarding vitiligo disease is introduced. This will cover the anatomy of human skin, characteristic of vitiligo disease and its histology properties, forms and screening. This chapter wills also presents an overview of previous and related research of digital image analysis systems.

2.2 Anatomy of Skin

Skin is the largest organ of the human body. It is made up of multiple layers of epithelial tissues which protect muscles and organs. Skin functions are insulation and temperature regulation, sensation, vitamin D and B synthesis, and protection against pathogens. Skin has three primary layers, the epidermis, the dermis and the hypodermis (subcutaneous tissue) [Rosebury, 1969; Revis, 2006]. The epidermis provides protection to infection. The dermis serves as location for the appendages of skin. The hypodermis serves as the basement of skin membrane. The epidermis consists of keratinocytes, melanocytes, Langerhans cells and Merkels cells. There are no blood vessels in epidermis and it is nourished by diffusion from the dermis. Epidermis is divided into 5 sub-layers (strata), which are (from superficial to deep) strata corneum, strata lucidum, strata granulosum, strata spinosum and strata basale. Epidermis cells are formed through mitosis at the innermost layers.

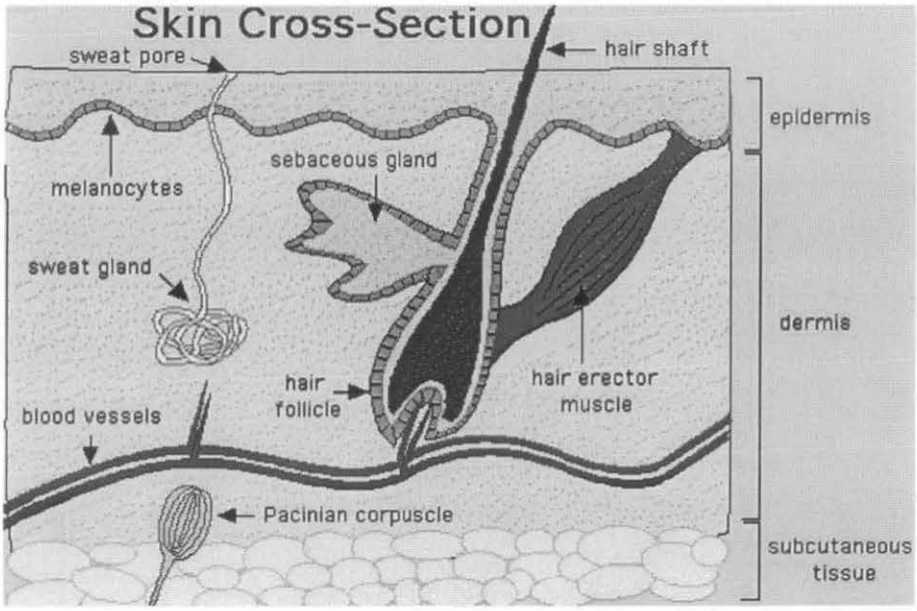

Figure 2.1 Anatomy of Skin (taken from www.enchantedlearning.com)

Skin has pigment melanin which absorbs some of the potentially dangerous ultraviolet radiation in sunlight. Melanin is color pigment found in skin, eyes and hair. It is produced by melanocytes through processes called melanogenesis [Romero-Graillet, 1996; Ito, 2003]. Melanocytes are epidermis cells that are located in the bottom layer of the epidermis as shown in Figure 2.2. The density of melanocytes in skin does not vary among different ethnic origins, however skin pigmentation differs due to variations in the rate of melanin production.

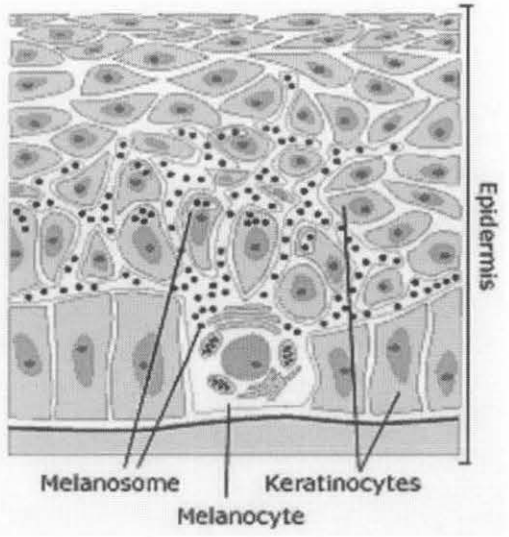

Figure 2.2 Melanocyte (reproduced from Revis [Revis, 2006])

The dermis is the second primary layer of skin and located beneath the epidermis. It is connected to the epidermis by a basement membrane. There are many sensor and glands located in the dermis. The nerves that are related to sense of touch and heat, hair follicles, sweat glands, sebaceous glands, apocrine glands and blood vessels are all located in the dermis. The blood vessels in the dermis provide nourishment and waste removal.

The hypodermis is the last layer of skin and lies below the dermis. It attaches the skin to underlying bone and muscle, and supplies skin with blood vessels and nerves. It consists of loose connective tissue and elastin. The hypodermis contains 50% of body fat where fat serves as padding and insulation for the body.

2.3 Vitiligo

Vitiligo is an acquired, idiopathic pigmentary disorder characterized by depigmented macules that result from damage to and destruction of epidermal melanocytes [Norashikin, 2007]. The loss of melanocytes alters both structure and function of skin, mucous membranes, eyes and hair bulbs and results in the absence of pigment melanin.

Melanin, the pigment that determines color of skin, hair, and eyes is produced in melanocytes. If these cells cannot produce melanin, the skin becomes paler or completely white in contrast to normal skin color [Roberts, 2003].

The causes of vitiligo disease are unknown. Theories concerning the cause of vitiligo have concentrated on four different mechanisms: autoimmune, autocytotoxic, neural and genetic [Tonsi, 2004]. In auto immune theory, the extent of skin depigmentation is correlated with the incidence and the level of anti-bodies against melanocytes. It is found that there is increased occurrence of vitiligo in certain autoimmune diseases such a thyroid disease (Hashimoto's thyroiditis and Grave's disease), Addison's disease, pernicious anemia, insulin-dependent diabetes mellitus, and alopecia areata [Beterle, 1985]. In autocytotoxicity theory, it is reported that an intermediate or metabolic product of melanin synthesis causes melanocytes destruction. A second mechanism by which autocytotoxicity occurs is through the inhibition of thioredoxin reductase enzyme. In neural theory, it is believed that a neurochemical mediator destroys melanocytes or inhibits melanin production. Lerner initiated this theory on the basis of reports of patients afflicted with a nerve injury and vitiligo, with decreased or absent skin finding in denervated areas [Lerner, 1959]. In genetic theory, melanocytes have an inherent abnormality that impedes their growth and differentiation in conditions that support normal melanocytes.

The impact of vitiligo on patient psychology is varying. However, most of them find it irritating. Vitiligo can have a major impact on patients' psychology [Porter, 1979]. The disease is most prominent in dark-skinned patients resulting major impact to their psychological condition. Vitiligo can increase the risk of developing autoimmune disease [Kovacs, 1998], such as thyroid disease, Addison's disease, pernicious anemia and alopecia areata.

2.4 Clinical Features of Vitiligo

Vitiligo is seen as acquired white or hypopigmented maculae or patches as shown in Figures 2.3-2.7. The disease is categorized according to the distribution and the extent of

involvement of depigmentation. Clinical presentations may vary and are categorized as generalized, acral or acrofacial, localized and segmental vitiligo.

2.4.1 Generalized Vitiligo

Figure 2.3 depicts the generalized type which is the most common pattern with bilateral, symmetric depigmentation of the face (typically the periofícial areas), torso, neck, extensor surfaces, or bony prominences of the hands, wrists, legs.

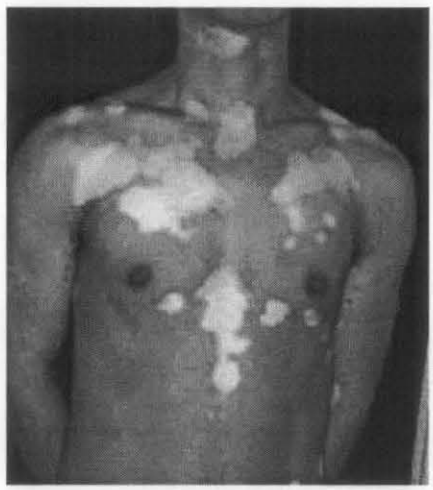

Figure 2.3 Generalized vitiligo (courtesy of Hospital Kuala Lumpur)

2.4.2 Acrofacial Vitiligo

Acrofacial vitiligo is limited to the distal digits and periorificial facial areas, the latter in a circumferential pattern (Figure 2.4).

Figure 2.4 Acrofacial vitiligo (courtesy of Hospital Kuala Lumpur)

2.4.3 Segmental Vitiligo

Segmental vitiligo, as shown in Figure 2.5, is the least common pattern and occurs in a unilateral, dermatomal or quasi-dermatomal distribution, often following the distribution of the trigerminal nerve. It is known for its early onset and rapid initial growth with non-progression within 2 years.

Figure 2.5 Segmental Vitiligo (courtesy of Hospital Kuala Lumpur)

2.4.4 Focal Vitiligo

Focalized vitiligo has a limited and localized distribution, as seen in Figure 2.6. However, it may develop into generalized vitiligo or follow a stable course.

Figure 2.6 Focal Vitiligo (courtesy of Hospital Kuala Lumpur)

2.4.5 Universal Vitiligo

Universal vitiligo implies loss of pigment melanin over the entire body surface area. This can be seen in Figure 2.7.

Figure 2.7 Universal Vitiligo (courtesy of Hospital Kuala Lumpur)

2.5 Vitiligo Treatment

Vitiligo can be treated in many ways, as shown in Table 2.1. Overall, it can be categorized as three types of treatment; medical treatment, surgical and UVB/Laser treatment.

Table 2.1 Vitiligo Treatments

Medical Treatment	Surgical	UVB/ Laser Therapy
1.Topical and systemic corticosteroids	1. Mini grafting	1. Narrow band UVB therapy
2.Psorelen with exposure to ultraviolet A radiation therapy	2.Transplantation of cultured melanocytes	2. 380 nm laser
3. Heliotherapy	3.Transplantation of non-cultured melanocytes	3.Depigmentation with Q-switched ruby laser
4. Depigmentation therapy with monobenzylether of hydroquinone		
5. Tacrolimus Ointment		

2.5.1 Medical Treatment

In topical and systemic corticosteroids therapy, topical corticosteroids are used. Topical corticosteroids are effective repigmenting agents. From experiments, it is reported that optimal success of treatment with topical corticosteroids requires applications for 3 to 4 months or longer [Tonsi, 2004]. Mid or lower potency corticosteroids may be preferable to avoid the toxicity associated with long term applications of corticosteroids. Corticosteroid cream is applied to depigmented skin once daily for 3 to 4 months and the response is monitored with Wood's lamp examination at 6-weeks interval. Therapy is continued if repigmentation occurs, but stopped if there is no evidence of response after 3 months. Photographs may assist in evaluating progress.

Psoralen-ultraviolet A (PUVA) is a repigmentation therapy using medication known as psoralen. This chemical is able to make human skin very sensitive to light. Then the skin is treated with a special type of ultraviolet light. Treatment with PUVA is reported to have a 50 to 70% chance of returning color on the face, trunk, upper arms and upper legs [Kenny, 1971]. There are two types of PUVA therapy; oral psoralen photochemotherapy and topical therapy. Oral psoralen photochemotherapy is used for patients with more

extensive vitiligo or for patients who are unmanageable with topical therapy. It is found that darker pigmented patients respond better to PUVA therapy because of the increased tolerance to greater cumulative UVA dosage. Children also experience repigmentation to a greater extent than adults. Vitiligo on the trunk, proximal extremities, and face respond well to PUVA therapy, although distal extremities and periorificial areas do not. The potential side effects include burn, erythema, pruritus, xerosis, carcinogenicity, pigmented lesions, cataracts and aging. Topical therapy psoralen photochemotherapy is another PUVA therapy used for patients with limited vitiligo lesion areas (less than 20% of the body surface) or for children older than 5 years with localized vitiligo.

Heliotherapy is a repigmentation therapy using a combination of trisoralen and sunlight. Trisoralen is a photosensitizer used to increase skin tolerance to sunlight and enhance pigmentation. It darkens the skin and thickens skin layers.

Depigmentation therapy is a treatment of vitiligo to remove remaining pigment melanin of normal skin and make the whole body an even white color. This therapy is considered for patients with extensive involvement or patients with more than 50% involvement of the skin and has demonstrated therapeutic resistance. This treatment could be done by using 20% monobenzoether or hydroquinone applied to the skin once or twice daily for one to three years. The pigment removal is permanent and irreversible, resulting in permanent photosensitivity.

For some cases, patients have poor clinical response to topical steroid and PUVA therapy due to undesirable side effects. For such cases, dermatologists will consider a treatment with vitamin D analogues (topical taclacitol).

Tacrolimus ointment [Travis, 2003] is an immunosuppressant that is derived from the fungus *Streptomyces tsukubaensis*. Topical tacrolimus offers several advantages in treating vitiligo. It is well tolerated in adults and children and prolonged use does not cause atrophy and adverse potential ocular side effects. There is also no limitation for application to facial and intertriginous areas. The efficacy of tacrolimus for vitiligo was first reported in a case series of 6 patients with generalized vitiligo. Five of the 6 patients

achieved at least a 50% repigmentation of the affected areas [Lepe, 2003]. Tacrolimus ointment has been found to be safe and efficacious in both adult and childhood vitiligo patients in North America, Mexico, Europe and India. Conjunction with this research, a study of efficacy and safety of tacrolimus ointment in Malaysia is conducted in Hospital Kuala Lumpur, Malaysia. The study concentrates on repigmentation evaluation using objective and subjective methods whilst our developed digital image analysis system is used as the objective method.

2.5.2 Surgical

There are two types of surgical (mini grafting); micropigmentation (tattooing) and dermabrasion [van Geel, 2001]. Micropigmentation involves tattooing vitiligo skin, in order to match the normal skin color. However, an exact match of pigment is difficult to obtain. In dermabrasion, vitiligo skin areas are superficially dermabraded. It may result a darker repigmentation.

In transplantation of cultured-melanocytes, initially melanocytes are harvested from a small fragment of pigmented skin from patient. The melanocytes is then isolated and grown in cell culture for 3 weeks. It is found that in vitro transplantation method, the repigmentation areas can be as large as 10 times from the donor areas [Issa, 2003]. A method that resembles in vitro cultured melanocytes is transplantation of non cultured melanocytes.

2.5.3 UVB/Laser Therapy

In narrow band UVB therapy [Menchini, 2003], a new device that produces focused beam of narrow UVB is used. The dose is gradually increased until 50% repigmentation is observed. Photographs of the patients are taken for helping the observation. Another therapy that resembles UVB therapy is the therapy using excimer laser with wavelength of 380 nm [Baltas, 2002]. For depigmentation cases, it is known that bleaching creams may have serious side effects. Q-switched (QS) ruby laser could be used as an alternative for depigmentation [Kim, 2001].

2.6 Efficacy Assessment

The assessment of vitiligo therapeutic response is based on the degree of skin repigmentation within vitiligo areas over time by dermatologists. Currently there is no objective way to measure and quantify the repigmentation response. The evaluation of vitiligo treatment outcome is largely dependent on the human eye and judgment to produce the scorings.

Physician's Global Assessment (PGA) is the current scoring systems used to evaluate treatment outcome. However, there is no standard PGA scales as it vary in width and number of points [Norashikin, 2007]. The degree of repigmentation that defines success however has often been set somewhat arbitrarily at 50-75% repigmentation based largely on the global impression of the overall response. For this project, we use PGA scales as shown in Table 1.1.

2.7 Digital Image Analysis of Vitiligo

Digital image processing is now becoming very useful due to the availability of digital camera and personal computer. A combination of personal computer and digital camera has the potential to become an intelligent analysis system for analyzing digital images.

Digital image analysis of repigmentation of vitiligo areas is a complicated task particularly because of the variability of the images in terms of brightness and angle of observation, and the size of repigmentation areas which is very small to be discerned visually and patchy.

Skin is considered to be a layered construction of epidermis, dermis and hypodermis. All possible colors occurring within normal human skin could be analytically modeled by exploiting the physics related to the optical interface between these layers. In other terms, skin color is due to the combination of skin histological parameters. However in digital imaging, color is created by combining three different spectral bands: red, green

and blue (RGB). Moreover, the image formation process within a digital camera is a process involving the spectrum of the incoming light, the spectral characteristic of camera's CCD and the spectral transmittance of Bayer filter. The incoming light is a result of the light source properties and the properties of reflecting material, in our cases, human skin.

2.7.1 Interaction of Light and Skin

Light is the portion of electromagnetic radiation that can be detected by human eyes. The wavelengths visible to human eyes lies from violet at about 380 nm ($1nm=10^{-9}m$) to deep red at about 770 nm. Light can interfere with each other, become directionally polarized, and bend when passing an edge [Anderson, 1982]. It may be characterized by its spectrum and direction. The spectrum indicates the radiant power at a given wavelength and its composition defines its color.

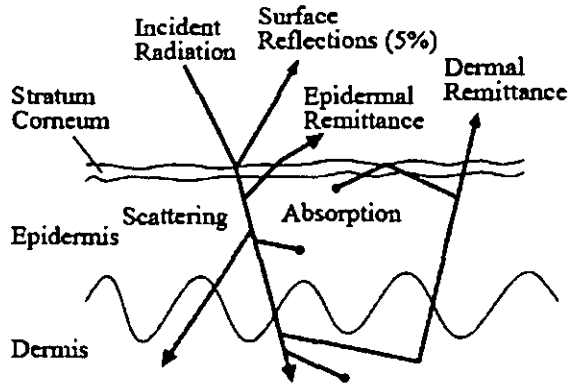

Figure 2.8 Schematic representation of the major optical pathways in human skin, reproduced from Anderson and Parish [Anderson, 1982]

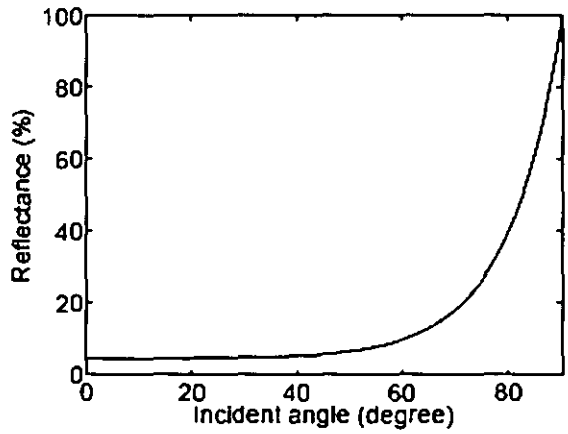

Figure 2.9 Surface reflectance as a function of the incident angle (with respect to the surface normal) at a planar interface of a material with refractive index $n_D = 1.55$, reproduced from Moritz Storring [Storring, 2004]

The light reflections of skin could be defined by several components, as illustrated in Figure 2.8. At incident angles close to normal about 5% of the incident light coming in contact to skin is directly reflected at the surface. This is mainly due to the change in refractive index between air ($n_D = 1.0$) and skin ($n_D = 1.5$). Surface reflections increase for larger incident angles, as described by Fresnel's equation and as shown in Figure 2.9. Fresnel's equations describe the reflection and transmission of light as electromagnetic waves at an interface. When a wave (light in our case) reaches a boundary between two different interfaces (two different dielectric constants), part of the wave is reflected and part is transmitted, with the sum of the energies in these two waves equal to the original wave. Electromagnetic waves are transverse, as a result there are separate coefficients in the directions perpendicular to and parallel to the surface of the dielectric. These are depicted in Figure 2.10. The coefficients for reflection and transmission of the transverse electric are denoted $r_\perp$ and $t_\perp$, respectively, while the coefficients for reflection and transmission of the transverse magnetic field are denoted, $r_{||}$ and $t_{||}$, respectively. Figure 2.11 shows the incident light and their reflectance and transmission coefficients. In addition to the amplitude coefficients, power coefficients are often defined as the square of the corresponding amplitude coefficients. Since we are only interested in the reflectance coefficients, R, the formula can be written as,

$$R_{\perp} = |r_{\perp}|^2 = \left[\frac{\sin(\theta_t - \theta_i)}{\sin(\theta_t + \theta_i)}\right]^2$$

$$R_{||} = |r_{||}|^2 = \left[\frac{\tan(\theta_t - \theta_i)}{\tan(\theta_t + \theta_i)}\right]^2 \qquad (2.1)$$

where $R_{\perp}$ represents power of the reflection coefficient of transverse electric field, $R_{||}$ represents the power of the reflection coefficient of transverse magnetic field, θ_i represents incident angle and θ_t represents reflectance angle. Figure 2.11 shows the graph of reflectance of light versus incident angle.

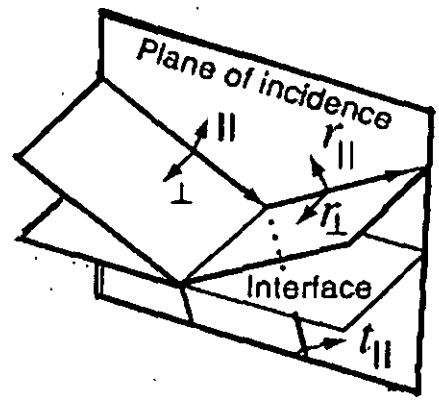

Figure 2.10 Fresnel's equations

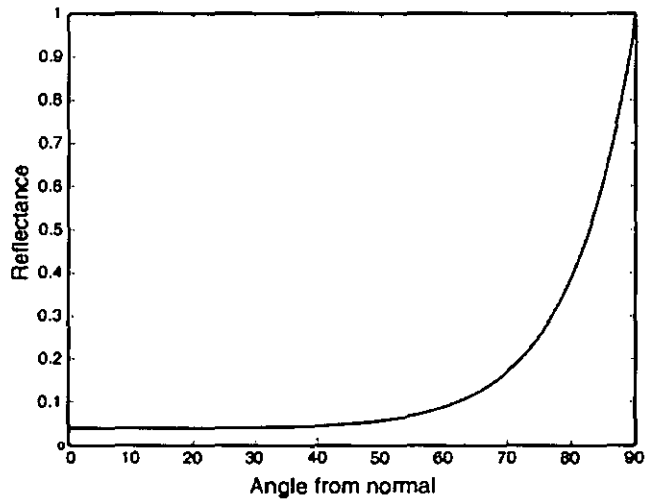

Figure 2.11 Reflectance vs Incident Angle

Most of the incident light (nearly 95%) penetrates into skin and follows a complex path until it exits back out of the skin or gets attenuated by skin choromophores [Preece, 2004]. Figure 2.10 shows the absorption spectra of the visible light and pigments of human skin. It is observed that pigment melanin which is located in the epidermis absorbs light radiation over the entire visible range. As a result, skin tends to be darker. Melanin also absorbs more of the radiation in the shorter than in the longer wavelengths.

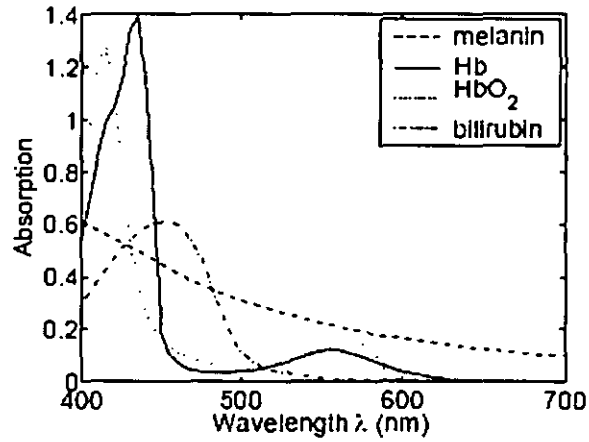

Figure 2.12 Absorption spectra of a major visible-light-absorbing pigments of human skin, melanin, deoxy-hemoglobin (Hb), oxy-hemoglobin (HbO_2), and bilirubin, reproduced from Anderson and Parish [Anderson, 1982]

In the dermis the light is scattered and absorbed. The absorption is mainly due to the properties in the blood such as haemoglobin, bilirubin and beta-carotene. Haemoglobin may be oxygenated (oxy-haemoglobin) giving blood a reddish color or deoxygenated giving blood a bluish color.

2.7.2 Digital Camera

Skin reflectance is considered to be continuous. However, digital camera's CCD uses finite set samples to describe the spectrum. Sample measurements are obtained by filtering the incoming light spectrum and integrating over this filtered spectrum.

CCD (Charge Coupled Device) is an integrated circuit containing an array of coupled, light sensitive capacitors [Peterson, 2001]. It is used primarily as image sensor devices. To generate an image, there are four processes in CCD. Firstly, it generates electric charges due to the photoelectric effect of incoming light coming in contact with CCD. Secondly, it collects the charge in the electrodes (gates). Thirdly, under the control of an external circuit, each electrode transfers its electric charge to one or other of its neighbors. Lastly, the individual charge packets are converted to an output voltage and digitally encoded.

Digital color camera usually uses a Bayer mask over the CCD to generate a digital color image. Bayer mask is a color filter array used for arranging red, green and blue (RGG) color filters on a square grid of CCD sensor [Bayer, 1976]. The mask pattern is 50% green, 25% red and 25% blue as depicted in Figure 2.13. There are twice as many green elements as red or blue in order to mimic the human eyes which are more sensitive with green color than red and blue.

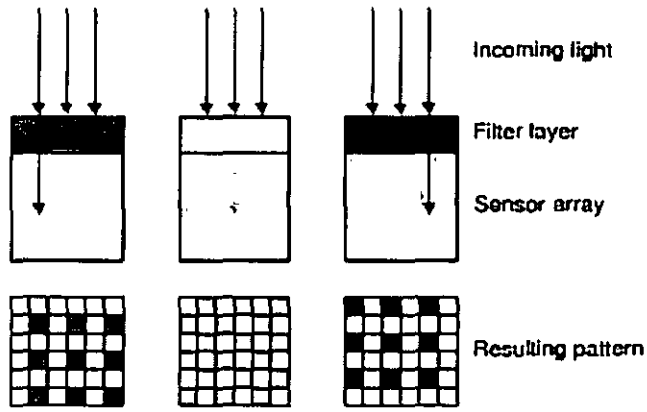

Figure 2.13 Bayer's mask filter (Bayer, 1976)

CCD is known to have better quantum efficiency than photographic film. They commonly respond to 70%-90% of the incident light [Peterson, 2001]. Quantum efficiency is a number used as a measurement of the device's sensitivity defined for a photosensitive device as the percentage of photons hitting the photoreactive surface that will produce an electron-hole pair.

2.8 Related Works

In vitiligo, the lesions are paler than their surrounding skins due to the lack of skin choromophores, called melanin. The works related to this research can be categorized into two main groups. The first group employs image processing techniques to identify and determine the areas of the lesions. This group can be further categorized based on the techniques they used,

1. Color Spaces Transformation
2. Statistical Model
3. Neural Networks
4. Scanning, Segmentation and Surface Estimation

The second group proposes the extraction of skin choromophores parameters from the skin image.

2.8.1 Color Spaces Transformation

Principal Component Transform is used for segmentation by S. Fischer, P. Schmid, and J. Guillot [Fischer, 1997]. The segmentation of image for the analysis of pigmented skin lesions, mostly for melanoma disease, is developed. Initially, skin RGB images are transformed using Principal Component Transform. Principal Component Transform is an image transformation technique based on Principal Component Analysis (PCA). To segment the skin lesion areas, fuzzy c-means clustering is used. The clustering method is developed using image histogram. No measurement performance is found in the paper.

Principal Component Transform is also used for segmentation by Scott E. Umbaugh [Umbaught, 1993; Umbaught 1996]. In the paper, the technique, based on the combination of Principal Component Transform and median cut segmentation, is used to segment skin tumor. The maximum detection rate is found to be 99.3%. It is also reported by Maglogiannis that the combination of PCT and median cut segmentation is superior to other segmentation methods such as thresholding, weighted function, region growing, spherical coordinates and CIE $L^*a^*b^*$ for pigmented skin lesions segmentation [Maglogiannis, 2003; Maglogiannis 2005]. The combination of PCT/Median Cut is very much promising for our problem; however in our initial study, it is found that the method is inaccurate [Nugroho, 2007].

An image processing technique for detecting skin color areas in HSV color space is proposed by Kyung-Min Cho [Cho, 2001]. First, a thresholding box is updated iteratively using a color histogram under the assumption that the area of skin color areas are comparable to that of similar background color ones. Next, the color vectors inside the thresholding box are classified into skin areas and non-skin areas (background) using cluster analysis.

A skin segmentation method based on principal component transform and 2D color histogram is proposed by Yuneho Yi [Yi, 2003]. It is seen that color segmentation based on a RGB color space is sensitive to illumination changes. Therefore, 2D color space that

is insensitive to illumination changes is needed. This is achieved by employing Principal Component Analysis to the image. The idea is based on the fact that skin colors in RGB color space are distributed in a linear fashion. Next, segmentation is performed using 2D lookup table. Lookup table method typically processes the input image pixel by pixel for segmentation. Result shows that using Principal Component Transform it is given less problem of color constancy.

Skin segmentation method based on TSL (Tint, Saturation, and Luminance) is proposed by F. Tomaz, T. Candeias and H. Shahbazkia [Tomaz, 2004]. Digital skin RGB image are transformed into TS color space using these following equations,

$$S = \sqrt{\frac{9}{5(r'^2 + g'^2)}} \tag{2.2}$$

$$T = \begin{cases} \tan^{-1}(\frac{x'}{g'}) + 0.5 & g' \neq 0 \\ 0 & g' = 0 \end{cases} \tag{2.3}$$

where

$$r' = \frac{R}{R+G+B} - 1/3 \tag{2.4}$$

$$g' = \frac{G}{R+G+B} - 1/3 \tag{2.5}$$

From experiments, It is observed that skin pixels always lie on a particular ellipse in the ST color space. Therefore, skin areas are defined as a pixel value whose value lies inside the ellipse. As presented in their paper, it is stated that the method are very fast (2.88 seconds). However, their overall performance is not very good compare to other method (No measurement performance is found in the paper).

Nanny van Geel *et. al.* use two methods involving digital image processing for vitiligo lesion areas measurement [van Geel, 2004]. In the first method, vitiligo lesion areas are copied onto transparent sheet by putting the sheet over the lesions and tracing all the

lesions contours. Then, these sheets are scanned at a predefined resolution, and analyzed using image processing method. In the second method, image segmentation techniques based on region growing are performed in CIE $L^*a^*b^*$ color space. Initially, dermatologist indicated a spot belongs to the vitiligo lesion areas. Then, the image processing algorithm will expand the areas using region growing scheme by including neighboring pixels that are similar to the color of indicated spot. Result is shown in Figure 2.14.

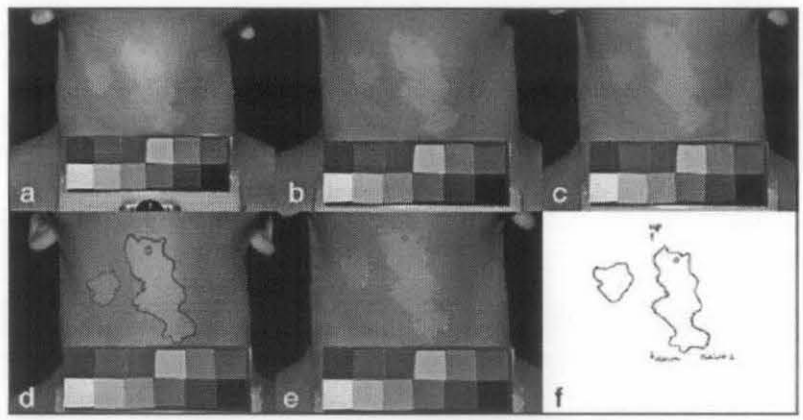

Figure 2.14 From left to right, a-c: Set of 1 lesions; d: Lesion after outlining the contours of the lesion; e: Digital image outlining; f: Lesion contour copied on a transparent sheet. [Nanny van Geel, 2004]

CIE $L^*a^*b^*$ color space is a color space which is perceptually linear with human visual system. It is widely used to measure dissimilarity between two colors. There are two steps of transform from RGB into CIE $L^*a^*b^*$. First, RGB image is transformed into CIE XYZ color space using linear transformation given as follows,

$$\begin{bmatrix} X \\ Y \\ Z \end{bmatrix} = \begin{bmatrix} 0.4124 & 0.3576 & 0.1805 \\ 0.2126 & 0.7152 & 0.0722 \\ 0.0193 & 0.1192 & 0.9505 \end{bmatrix} \times \begin{bmatrix} R \\ G \\ B \end{bmatrix} \tag{2.6}$$

Next, the resultant CIE XYZ image is transformed into CIE $L^*a^*b^*$ using the following equations,

$$
\begin{aligned}
L^* &= 116(Y/Y_n)^{1/3} - 16 \\
a^* &= 500\left[(X/X_n)^{1/3} - (Y/Y_n)^{1/3}\right] \\
b^* &= 200\left[(Y/Y_n)^{1/3} - (Z/Z_n)^{1/3}\right]
\end{aligned}
\tag{2.7}
$$

The performance of the digital image analysis is not significantly different with the measurement by the doctors. The detection rate was 78-95%. It is found that the error is increasing when the size of the lesions increases.

A skin color segmentation technique in a color space YCg'Cr' is proposed by J.J. Dios and N. Garcia [Dios, 2005]. It is found that color spaces with separated luminance and chrominance components seem to be more appropriate for skin color segmentation. Based on YCbCr, a transformed space, YCg'Cr' color space, is defined. Equation 2.8 shows the estimation of Cg' and Cr' given Cg and Cr.

$$
\begin{aligned}
Cg' &= Cg * \cos 30^\circ + Cr * \sin 30^\circ - 48 \\
Cr' &= -Cg * \sin 30^\circ + Cr * \cos 30^\circ + 80
\end{aligned}
\tag{2.8}
$$

Different decision regions defined by the threshold are tested in order to find the set that provides the best segmentation results with the training images. Two types of decision regions: maximum ([125,140] for Cg' and [136,217] for Cr') and modified mean threshold ([119,131] and [128,199] for Cg' and Cr') provide the best results. No detection rate or any other performance measurement is found in the paper.

Michael Harville *et.al* propose an image processing technique for the measurement and classification of skin color areas [Harville, 2005]. The color of an image is initially corrected using calibration target. The calibration target has 3 rows of 8 color patches set and a black background. For skin color estimation there are three steps to be taken. Firstly, the region of interest is roughly estimated using Viola-Jones detector. Secondly, the algorithm sorts the pixels by the luminance. Luminance, Y, may be computed in many ways, however it is found that $Y = R + G + B$ gives the best cross-device consistency of result. Finally, it computes the mean color of pixels ranked in the [L ..U]

Percentile in luminance, where L and U are lower and upper bounds. The best correction rate is 85%.

2.8.2 Statistical Model and Simulation

A color segmentation method for pigmented skin lesion in digital epiluminescence microscopy images is presented by P. Schmid [Schmid, 1997]. The method is based on two-dimensional histogram analysis and fuzzy c-means clustering technique. Fuzzy c-means clustering has proved to be a robust clustering technique [Lim, 1990]. Given the number of clusters, the technique computes the clusters using these two equations,

$$U_{ik} = \left(1 + \sum_{\substack{j=1 \\ j \neq i}}^{c} \left(\frac{\|x_k - v_i\|}{\|x_k - v_j\|} \right)^{2/(m-1)} \right)^{-1} \tag{2.9}$$

$$v_i = \frac{\sum_{k=1}^{n} (U_{ik})^m x_k}{\sum_{k=1}^{n} (U_{ik})^m} \tag{2.10}$$

where x_k is the k^{th} sample vector, n the number of sample vectors, c the number of classes, v_i the i^{th} class centre, U_{ik} the fuzzy membership of x_k to class i and m is the weighting exponent. $\| \cdot \|$ is any inner product norm of the form $\|v\| = v^T A v$, A being a positive definite matrix and the weighting exponent m defines the fuzziness of the membership values. The two-dimensional histogram is used to extract information about the numbers of clusters and their exact positions from the RGB images. From RGB images, the two-dimensional histogram is derived from the first and second principal components of the RGB images.

A skin detection scheme based on statistical color models is developed by M. Jones and J.M. Rehg [Jones, 2001]. The statistical color models are built using a general histogram density using a large image data base taken from World Wide Web. Firstly, they construct a general color model from the generic training set using a histogram with 256

bins per channel in RGB color space. The histogram counts are converted into a discrete probability distribution $P(\ .\ )$,

$$P(rgb) = \frac{c[rgb]}{T_C} \tag{2.11}$$

where $c[rgb]$ gives the count in the histogram bin associated with the RGB color triple rgb and T_C are the total count obtained by summing the counts in all of the bins. Secondly, they construct skin and non-skin models using the data sets. The skin pixels in the 4657 images containing skin are labeled manually and placed into the skin histogram. The 8965 images that do not contain skin are placed into the non-skin histogram. Next, the probability that a given color value belongs to skin and non-skin classes are computed.

$$P(rgb \mid skin) = \frac{s[rgb]}{T_s} \tag{2.12}$$

$$P(rgb \mid non-skin) = \frac{n[rgb]}{T_n} \tag{2.13}$$

where $s[rgb]$ is the pixel count contained in bin rgb of the skin histogram, $n[rgb]$ is the equivalent count from the non-skin histogram, and T_S and T_N are the total counts contained in the skin and non-skin histograms, respectively. Then, the skin pixel classifier is derived based on the standard likelihood ratio approach [Fukunaga, 1972]. A particular RGB value is labeled skin if,

$$\frac{P(rgb \mid skin)}{P(rgb \mid non-skin)} \geq \Theta \tag{2.14}$$

where $0 \leq \Theta \leq 1$ is a threshold which can adjusted to trade-off between correct detections and false positives. It can be also written as,

$$\Theta = \frac{c_P P(non-skin)}{c_N P(skin)} \tag{2.15}$$

where c_P and c_N are the application-dependent costs of false positives and false negatives, respectively. The performance of the skin classifier is good. The best classifier can detect 80% of skin pixels with a false positive rate of 8.5%. This work is extended by Gomez [Gomez, 2002]. Here, the performance of this statistical skin color model is tested in several color spaces. He decomposes and analyzes each component of the following color spaces; HSV, YIQ, RGB, normalized RGB, RGB-Y, Gaussian Color Model, YES, YUV, CMY, CIE XYZ, CIE L*a*b*, CIE L*u*v*, CIE xyY, CIE u'v'w', and YCrCb, and also some non-linear relations: r/g, r/b, g/b, x/y, x/z, y/z and $(\frac{r}{r+g+b}-\frac{1}{3})^2+(\frac{g}{r+g+b}-\frac{1}{3})^2$. To the latter, it is known as Wr. In addition, they also included Hue, Chroma and Luminance computed from CIE L*a*b*. Results show that the combination of H (HSV)-RY(RGB-Y) and Wr color components is found to be superior for pixel skin detection. The method is extended again by Ming-Ji Zhang [Zhang, 2004]. In their proposed method, the threshold value, Θ, of Equation 2.6 is not fixed. An algorithm which could find an optimum threshold for each image using histogram information is proposed. From experiment, their method has 87.1% of true positive and 10.3% of false negative.

Another approach using a multivariate statistical model that represents human skin colors is proposed by T. S. Caetano and D.A.C. Barone [Caetano, 2001]. The objective of their work is to discern color combination from two ethnic origins, namely Caucasian ethic origin and African ethic origin. Skin colors are modeled using a mixture of Gaussian distributions. The parameters of the model are derived iteratively using the expectation-maximization (EM) algorithm. The algorithm is reported to have detection rate of 85%. The algorithm can be extended by employing principal component analysis instead of the expectation-maximization (EM) algorithm [Fan, 2004]. The multivariate model is constructed after the data sets are transformed into their principal components. The skin model is built using the information of color combination of skin. Then, the segmentation

is performed by employing the skin model to the actual skin images. However the detection rate is low, from 2665872 test pixels only 25.1% is detected.

A novel adaptive approach is proposed for the application of hand-segmentation by X. Zhu [Zhu, 2000]. A restricted Expectation Maximization algorithm is introduced to train an adaptive Gaussian mixture model, wherein the background is modeled by four Gaussian kernels and the hand color is modeled by one Gaussian kernel. To distinguish the skin component from other Gaussian components, the authors heuristically fix the parameter of the first Gaussian in estimating the hand color. This obviously makes the algorithm not adaptive for detecting skin color from different individuals.

Skin detection method that is based on statistical model is proposed by Q. Zhu [Zhu, 2004]. First, a rough skin classification using a generic skin model is performed to define candidate areas of skin. Next, a Gaussian mixture model specific to the candidate areas of skin is derived using the standard Expectation Maximization (EM) algorithm. Finally, Support Vector Machine is used to identify the skin Gaussian from the Gaussian mixture model. From a huge training data sets (151 million skin pixels and 448 million non skin pixels) , the algorithm can achieve average detection rate of 92% for skin classification.

Different approach of Gaussian modeling is proposed by Faliang Chang [Chang, 2007]. They study the chrominance space in which the single Gaussian model fits the skin distribution of skin color best. The Fuzzy-C-means (FCM) is employed to segment the skin. From their experiments, it is found that the distribution of skin color in the normalized r-g space is the most compatible in comparison to the other color spaces.

$$r = \frac{R}{R+G+B}$$
$$g = \frac{G}{R+G+B} \qquad (2.16)$$

The correction rate is 92.3% with 38.1% of false detection rate.

Different approach of Gaussian modeling is also studied by Jong Bae-Kim *et. al.* [Kim, 2002]. He divided the algorithm into two processes: region segmentation and skin detection. In region segmentation, he combined wavelet transformation and watershed segmentation techniques. Wavelet transformation is a multi resolution method that obtains a global view of an image by examining it at various resolution levels [Liu, 1994]. This process reduces the total computation cost and it is now possible to determine the dimensions of the regions to be segmented. Watershed segmentation is an image segmentation method defined in terms of the drainage of rainfall. Regions of terrain that drain to the same points are defined to be part of the same watershed. Finally, pixels of skin color are segmented using Gaussian model. No detection rate or any other performance measurement is found in their paper.

Skin segmentation classifiers using Bayesian decision rules are proposed by Son Lam Phung *et. al.*[Phung, 2003]. Initially samples of skin pixels and non-skin pixels are collected. Secondly, a probability distribution function of skin pixels based on Bayesian rules is employed. As reported by Jones *et. al.* [Jones, 2001], this method also depends on the data collection. From their experiment, Bayesian classifier had a maximum classification rate of 89.79%. This was higher than Gaussian classifier (maximum classification rate of 88.97%) and MLP classifier (maximum classification rate of 89.54%).

2.8.3 Neural Networks

A neural network model for skin pixel detection is developed by M. J. Seow and V.K Asari [Seow, 2004]. It is observed that the skin colors are forming a nonlinear pipeline in the RGB space. It is possible to describe the skin color mathematically using the nonlinear line attractor network. A learning algorithm for a recurrent neutral network is proposed. It is found that this learning algorithm is suitable for multiple-valued pattern association using the nonlinear line attractor network. In comparison to skin probability mask (SPM), the technique performs better.

Another work that used neural network is studied by L. Mostafa and S. Abdelazeem [Mostafa, 2005]. The input image is first transformed into the normalized RGB color space.

$$r = \frac{R}{R+G+B}$$
$$g = \frac{G}{R+G+B} \qquad (2.17)$$
$$b = \frac{B}{R+G+B}$$

It is believed that normalized RGB yields the best skin detection results [Terrilon, 1999]. Neural network is used to detect skin regions. From their experiments, the input layer of the neural network is 408 neutrons and the size of hidden layer is 26 neutrons. The test set is composed of 70 images. The detection ratio was 91.43% with 7 cases of false positives.

2.8.4 Scanning, Segmentation and Surface Estimation

Digital image analysis is employed for repigmentation measurement by Bramiene R. Boersma [Boersma, 1995]. The measurements are collected from patients every 3 months up to 12 months. A video image of grafted skin areas is provided by standardized positions of the video camera and the light source. A metric scale is positioned on the skin for calibration.

A digital image analysis is proposed for accurate estimation of the vitiligo lesions by Yves Vander Haeghen [Haeghen, 2004]. First, the contours of all test lesions are traced on transparent sheet. This will take into account the original curvature of the skin. Then, the sheets are scanned at a predefined resolution and analyzed using digital image analysis software. It is claimed that the reproducibility of their method (scanning, segmentation and surface estimation) is very good with a maximum error of 2% between consecutive measurements of the same area.

2.8.5 Extraction of Skin Choromophores Information from Skin Images

Takiwaki *et. al* propose a formula to measure pigment melanin, based on the reflectance values of the red channel in RGB image [Takiwaki, 1994]. This formula is believed to be equivalent to the Melanin Index (MI) of narrow-band spectrometers. Their basic theory lies on the fact that in the red region, melanin is the predominant absorbing chromospheres.

$$A_r = 100 \times \log_{10}\left(\frac{1}{R_r}\right) \tag{2.18}$$

A_r is the absorbance index in the red channel and R_r is reflectance in the red given by the pixel intensity value of the red channel.

For practical application of skin color measurement, a skin color model is proposed by Takiwaki [Takiwaki, 1998]. The skin color model that is used to examine the relationship between the amount of skin chromospheres, namely melanin and hemoglobin, and the change CIE $L^*a^*b^*$ values is built. Result, as depicted in Figure 2.15, shows that L* color component and Melanin Index correlates almost linearly under the assumption that hemoglobin is constant.

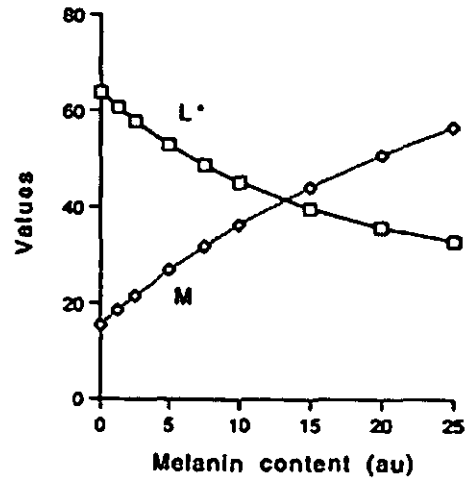

Figure 2.15 L* and Melanin (Takiwaki, 1998)

Erythema and pigment melanin in port wine stain lesions is evaluated by Jung [Jung, 2004]. The analysis converts RGB image into CIE $L^*a^*b^*$ color space and assums that the L^* image represents the inverse of the melanin distribution map and a^* image the erythema distribution map. CIE $L^*a^*b^*$ color space is a color space that is perceptually linear with human visual system. L^* represents brightness of the image, a^* represents degree of red and green, and b^* represents degree of yellow and blue.

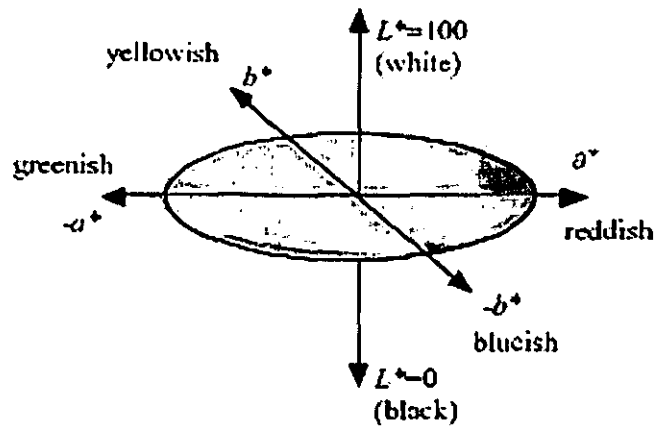

Figure 2.16 CIE L*a*b* color space, reproduced from Ohno [Ohno 2000]

A physic-based skin model based on CIE *LMS* color space for extracting histological skin parameters is proposed by Symon Cotton *et. al.* [Cotton, 1996; Cotton, 1997]. CIE *LMS*, as shown in Figure 2.17, is a color space represented by the response of the three types of cones of the human eye, named after their sensitivity at long, medium and short wavelength. Model of human skin is then constructed from the remitted and transmitted light from the dermis. Result shows that for the L primary, 86% of measured LMS values lie within the model with 78% and 82% for the M and S respectively.

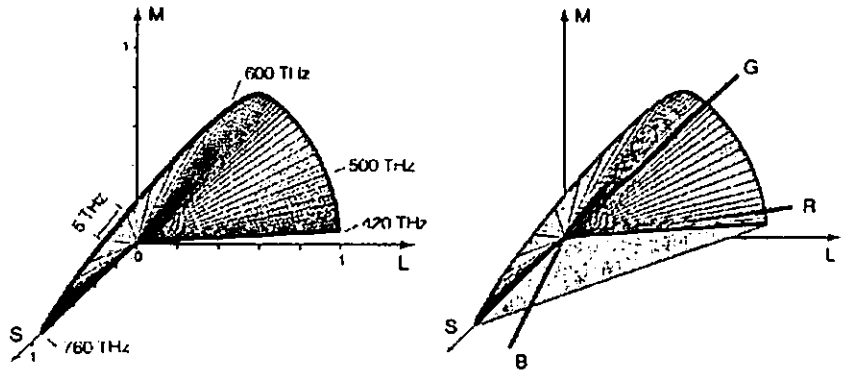

Figure 2.17 CIE LMS color space and RGB color space

The spatial distribution of melanin and haemoglobin in skin can be separated by employing linear independent component analysis of a skin color image [Tsumura, 1999]. The analysis is based on the assumptions that the spatial variations of skin image color are caused by two skin choromophores, namely melanin and haemoglobin and their quantities are mutually independent. The algorithm can be employed for e-cosmetic application [Tsumura, 2003].

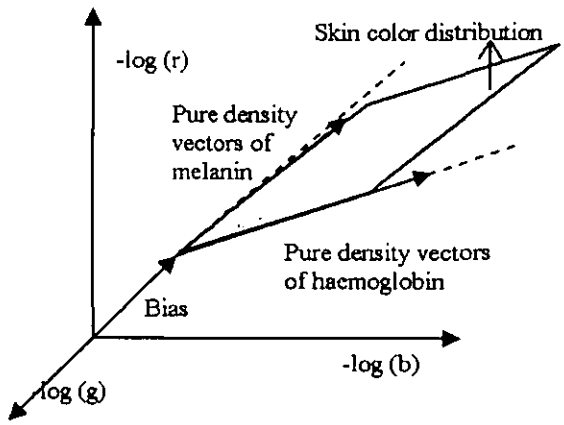

Figure 2.18 Tsumura's skin color model [Tsumura 1999]

2.9 Discussion

As mentioned earlier, vilitigo is related to melanin in human skin. Since melanin is one of the skin chromophores, Most of the technique above does not take into accounts the optical properties of skin and light in digital images and their relation to skin choromophores, namely melanin and haemoglobin. We believed to make the measurement of repigmentation areas accurate, one have to consider the optical properties of skin and light of melanin in digital image.

However, some research groups have tried to extract the parameters of skin histological from skin images. They tried to relate the skin histological parameters with properties of skin images. Since we work on vitiligo disease, we only look into the way how they extracted the information of melanin from the skin images. From this point of view, we can conclude that most of the works studied color information of skin in order to find melanin information within skin by employing different color spaces (CIE $L^*a^*b^*$ and CIE LMS). However, we found that this is not accurate since they did not relate the optic properties of skin and light of melanin in their discussions. And also in works of Jung and Takiwaki, both of them correspond the melanin with only L^* component of CIE $L^*a^*b^*$ color space. We believed this is not accurate due to the fact that in the study of the interaction of skin and light (as shown in Figure 2.12), it is found that melanin absorbs light radiation over the entire visible range.

2.10 Summary

Chapter 2 discussed information of vitiligo, interaction of light and skin, digital camera CCD and the works related to our research. It has shown that melanin is the color pigment found in skin, eyes and hair. Melanin is produced by melanocytes through processes called melanogenesis. Vitiligo, in the other hand, is a skin disorder characterized by depigmented macules that result from damage to and destruction of epidermal melanocytes. If melanocytes cannot produce melanin, the skin becomes paler or completely white in contrast to normal skin color [Roberts 2003]. Clinical

presentations of vitiligo can be categorized into generalized, acral or acrofacial, localized and segmental vitiligo. Vitiligo treatments can be categorized as three types of treatment; medical treatment, surgical and UVB/Laser treatment, as shown in Table 2.1.

The assessment of vitiligo therapeutic response is based on the degree of skin repigmentation within vitiligo areas over time by dermatologists. Physician's Global Assessment (PGA) is the current scoring systems used to evaluate treatment outcome. This evaluation however is still largely dependent on the human eye and judgment to produce the scorings. In addition, PGA score is also subjective, as there are inter and intra observer variations.

In the interaction of light and skin, it is seen that the light reflections of skin could be defined by several components, as illustrated in Figure 2.8. At incident angles close to normal about 5% of the incident light coming in contact to skin is directly reflected at the surface. This is mainly due to the change in refractive index between air ($n_D = 1.0$) and skin ($n_D = 1.5$). Most of the incident light (nearly 95%) penetrates into skin and follows a complex path until it exits back out of the skin or gets attenuated by skin choromophores, namely melanin and hemoglobin (oxy-hemoglobin and deoxy-hemoglobin) [Preece, 2004].

Digital camera is used to capture images of vitiligo lesion. An image sensor of our digital camera is CCD. CCD (Charge Coupled Device) is an integrated circuit containing an array of coupled, light sensitive capacitors. CCD is known to have better quantum efficiency than photographic film. They commonly respond to 70%-90% of the incident light [Peterson, 2001].

The related works can be categorized into two main groups. The first group is the research that did not determine skin choromophores, melanin in particular, in their analysis. The second group is research that tried to determine skin histological parameters (skin choromophores) from digital images of human skin.

Chapter 3

IMAGE AND STATISTICAL SIGNAL PROCESSING TECHNIQUES

3.1 Introduction

Image processing techniques are used to manipulate digital images. In many areas of application, image processing and computer vision systems are parts of larger system in order to solve certain tasks. In medical science, it is used to assist doctors in improving the qualitative and quantitative assessment of medical data.

In the development of the system to quantify skin repigmentation, image processing techniques and analysis are used to perform modeling, simulation, image segmentation and image statistical extraction. This chapter discusses the techniques and the mathematical formulations relevant to the research.

Image processing techniques relevant to this research are divided into these main categories; image segmentation (thresholding), morphological operators, and statistical feature extraction.

A stochastic process or random process could be seen as a mathematical model for an event that evolves in time in an unpredictable manner from the viewpoint of observers. The event may be a sequence of real-valued measurement of voltage or an image. The random process, in the context of system, changes one process to produce other process. Statistical signal processing is an area of signal processing that studies a signal based on the theory of random processes [Gray, 2004].

In this chapter, descriptions of the statistical signal processing methods that are required in the research are discussed. There are two methods that are applied in our research,

namely Principal Component Analysis (PCA) and Independent Component Analysis (ICA).

3.2 Principal Component Analysis

Principal Components Analysis (PCA) is an orthogonal linear transformation method. This linear transform has been widely used in multivariate data analysis and data compression. It could be used also to reduce multidimensional data sets into lower dimensions. PCA is defined as a method that transforms the data sets into new data sets such that the greatest variance by any projection of the data comes to lie on the first principal component of the new data sets, the second greatest variance on the second principal component of the new data sets, and so on [Anthony, 1997]. In pattern recognition theory, a data set with large variance is said to have large discriminatory power thus it could be separated [Umbaugh, 1993; Umbaugh 1996].

3.2.1 Eigenvalues and Eigenvectors

A matrix A is a system of numbers with k rows and l columns.

$$A = \begin{pmatrix} a_{11} & a_{12} & \cdots & \cdots & a_{1l} \\ \vdots & a_{22} & & & \vdots \\ \vdots & \vdots & \ddots & & \vdots \\ \vdots & \vdots & & \ddots & \vdots \\ a_{k1} & a_{k2} & & & a_{kl} \end{pmatrix} \tag{3.1}$$

Consider a $(k \times k)$ matrix A. If there exits a scalar λ and a vector γ such that,

$$A\gamma = \lambda\gamma \tag{3.2}$$

then λ is an eigenvalue and γ is an eigenvector.

It is proven that an eigenvalue λ is a root of the k-th order polynomial $|A-\lambda I|=0$, where I is an identity matrix. There are up to k eigenvalues of matrix A. For each eigenvalue, it exits a corresponding eigenvector given by equation 3.2 [Hadley, 2003].

3.2.2 Covariance Matrix

Covariance matrix is a matrix of co variances between elements of data sets [Kampen, 1981]. Covariance measures the degree of the linear relationship between variables. A large (small) value indicates high (low) redundancy.

The principal components can be derived from the covariance matrix and the correlation matrix. It is stated that the general advantage of covariance matrix is that the statistical inference is easier for covariance matrix. The second advantage of covariance matrix holds when all elements of the observations are measured in the same unit [Jolliffe, 1999]. From these reasons, we employ covariance matrix to estimate the principal components of the observed data.

Let A, B and C are the data sets. The covariance matrix, $COV(A,B,C)$ is define as

$$COV(A,B,C)=\begin{bmatrix} E[(A-\mu_A)(A-\mu_A)] & E[(A-\mu_A)(B-\mu_B)] & E[(A-\mu_A)(C-\mu_C)] \\ E[(B-\mu_B)(A-\mu_A)] & E[(B-\mu_B)(B-\mu_B)] & E[(B-\mu_B)(C-\mu_C)] \\ E[(C-\mu_C)(A-\mu_A)] & E[(C-\mu_C)(B-\mu_B)] & E[(C-\mu_C)(C-\mu_C)] \end{bmatrix} \tag{3.3}$$

μ_A, μ_B and μ_C denote means of A, B and C, respectively.

Several properties of covariance matrix:

1. Covariance matrix is a square symmetric matrix
2. The diagonal terms of covariance matrix are the variance of particular variables
3. The off-diagonal terms of covariance matrix are the covariance between variables.

3.2.3 Standardized Linear Combinations

The main objective of PCA is to reduce the dimension of the observation. The simplest way of dimension reduction is to take one element of the observed vector and discard all others. However this is not a very reasonable approach. An alternative method is to study a weighted average, namely

$$\delta^T A = \sum_{j=1}^{n} \delta_j A_j \quad \text{where} \quad \sum_{j=1}^{n} \delta_j{}^2 = 1 \tag{3.4}$$

A is the data sets, n denotes numbers of the data, and δ denotes the weighting vectors.

The weighting vectors can be optimized to investigate and detect specific features. In PCA, the aim is to maximize the variance of the projection $\delta^T A$ by choosing δ according to the following condition,

$$\max_{(\|\delta\|=1)} Var(\delta^T A) = \max_{(\|\delta\|=1)} \delta^T Var(A)\delta \tag{3.5}$$

This occurs when δ is given by the eigenvector γ corresponding to the largest eigenvalue λ of the covariance matrix $COV(A) = Var(A)$ [Hadley, 2003].

The resultant weighted vector is a projection of A into the one-dimensional space, where the components of A are weighted by the elements of γ. This is called the first principal component.

3.2.4 Properties of PCA

PCA computes the most meaningful basis to re-express a data set. However, PCA is limited to re-express the data as a linear combination of its basis vectors. This assumption

simplifies the problem by restricting the set of potential bases and formalizing the implicit assumptions of continuity in a data set [Lay, 2000].

Let A be the original data set and Y be the new representation of A, the process of PCA can be written as,

$$Y = \gamma^T (A - \mu) \tag{3.6}$$

where $COV(A) = \gamma \lambda \gamma^T$ and μ is the mean of A [Hadley, 2003].

A common measure of noise is the signal-to-noise ration (SNR) or a ratio of variances.

$$SNR = \frac{\sigma^2_{signal}}{\sigma^2_{noise}} \tag{3.7}$$

A high SNR indicates high precision data, while a low SNR indicates noise contaminated data. Let A be the original data sets with two variables x_A and y_A. As shown in Figure 3.11, we plot the data of A. The signal and noise variances, σ^2_{signal} and σ^2_{noise} respectively, are graphically represented by the two lines subtending the cloud of data.

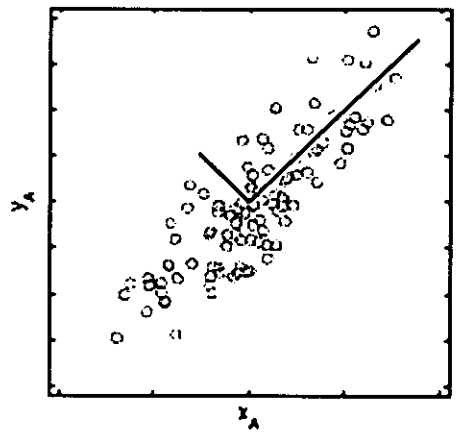

Figure 3.1 Plotted data of A

It is assumed that directions with largest variances contain the dynamics of interest. In other words, rotating the data set, A, along direction with largest variances and presumable highest SNR will maximize the signal [Lay, 2000] .

The other issue is the correlation between variables of the data sets (redundancy). Figure 3.12 might reflect the a range of possible plots between two variables, X and Y. Figure 3.12 (a) depicts a data set with no relationship or one might says X is uncorrelated with Y. On the other panel, Figure 3.12(b) depicts a highly correlated data. From this panel (b), it is assumed that it would be more meaningful to just use a single variable. One can calculate X from Y (or vice versa) using the best fit line. Employing a solely one variable would express the data more concisely and therefore reduce the number of data dimensions.

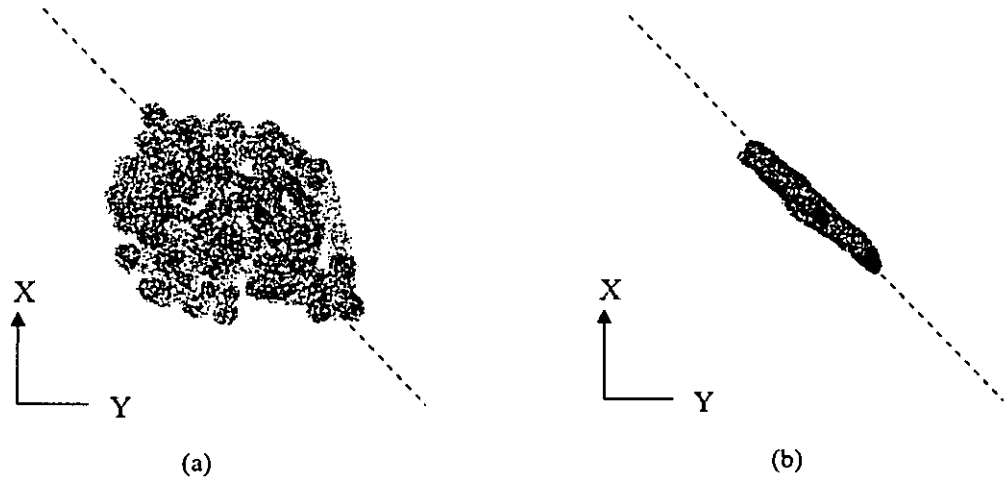

Figure 3.2 Possible redundancies in data from two separate variables (X and Y). The best fit line is indicated by the dashed line; (a) Low redundancy (b) High redundancy

3.2.5 Estimation of Principal Components

To find the principal components of an image, initially we subtract the mean value from each of image spectral bands (RGB) to obtain a zero mean variable data.

$$R = R_0 - \mu_{R_0}$$

$$G = G_0 - \mu_{G_0}$$

$$B = B_0 - \mu_{B_0} \tag{3.8}$$

where R_0, G_0, and B_0 denote image spectral band before subtraction and μ_{R_0}, μ_{G_0} and μ_{B_0} denote the mean value of image spectral bands.

Then we calculate the covariance matrix of the three dimensional color. The covariance matrix of an image in RGB data sets is defined as follow

$$COV = \begin{bmatrix} C_{RR} & C_{GR} & C_{BR} \\ C_{RG} & C_{GG} & C_{BG} \\ C_{RB} & C_{GB} & C_{BB} \end{bmatrix} \tag{3.9}$$

where

$$C_{XX} = \frac{1}{N}\sum_{i=1}^{N}(X_i - \mu_i)^2 \tag{3.10}$$

$$C_{XY} = C_{YX} = \frac{1}{N}\left[\sum_{i=1}^{N} X_i Y_i\right] - \mu_x \mu_Y \tag{3.11}$$

$$\mu_X = \frac{1}{N}\sum_{i=1}^{N} X_i \tag{3.12}$$

$X, Y \in \{R, G, B\}$, N denotes number of pixels in the image, μ denotes means value.

Then the eigenvectors are calculated from the covariance matrix by solving the following equation,

$$COV = \gamma \lambda \gamma^T \tag{3.13}$$

where is λ a diagonal matrix representing eigenvalues of covariance matrix, COV, and γ is a matrix of eigenvectors of covariance matrix, COV, arranged as a columns.

The eigenvectors are used as linear transform of original (R, G, B) values. It is reported that the resulting vectors have uncorrelated components, or in other words, the primary axis of the data has been aligned where the variance is maximal [Umbaugh, 1996]. The vectors in new space $[X_1\ X_2\ X_3]^T$ are obtained by

$$\begin{bmatrix} X_1 \\ X_2 \\ X_3 \end{bmatrix} = \begin{bmatrix} \gamma_{11} & \gamma_{12} & \gamma_{13} \\ \gamma_{21} & \gamma_{22} & \gamma_{23} \\ \gamma_{31} & \gamma_{32} & \gamma_{33} \end{bmatrix} \begin{bmatrix} R \\ G \\ B \end{bmatrix} \tag{3.14}$$

where $\begin{bmatrix} \gamma_{11} & \gamma_{12} & \gamma_{13} \\ \gamma_{21} & \gamma_{22} & \gamma_{23} \\ \gamma_{31} & \gamma_{32} & \gamma_{33} \end{bmatrix}$ are the eigenvectors of the covariance matrix. It has been experimentally determined that for skin tumor images, after the appliance of PCA, the axis with the largest variance of PCA contained approximately 91% of the total variance [Umbaugh, 1996]. Figure 3.13 shows an example of principal component transform of an image. From the appearance of the 1st principal component (as shown in panel (b)), it captures more details of the origin image in compare to the results of 2nd principal component and 3rd principal component respectively.

(a)

(b)

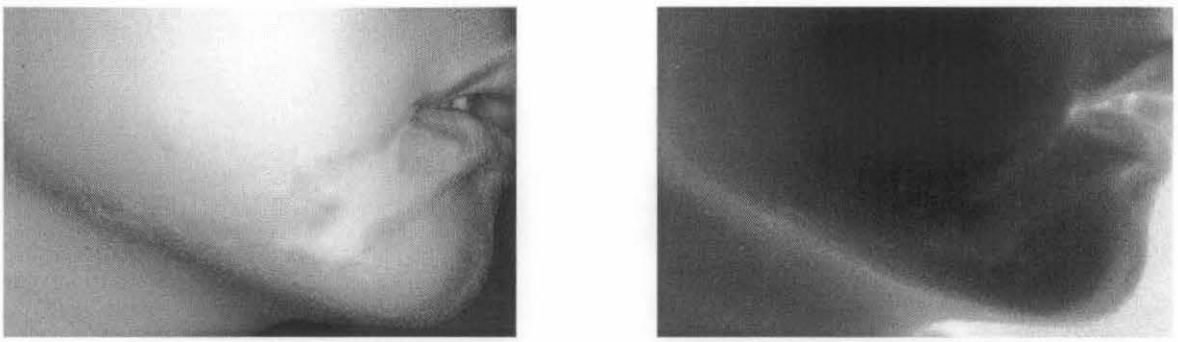

(c) (d)

Figure 3.3 An example of principal component transforms, (a) Original image, (b) the 1st principal component image of (a), (c) the 2nd principal component of image (a), (d) the 3rd principal component of image

3.3 Independent Component Analysis

Independent component analysis is a multivariate data analysis for source separation. The source separation (blind source separation) is a problem in signals processing where the source of the observed signals were mixed are unknown [Roberts, 2001].

The basic model of ICA is a discrete time model in which sources are instantaneously mixed and the resulting mixture, possibly corrupted by noise, is observed. Writing the source signals in vector form, $s(t) = [s_1(t), s_2(t), s_3(t), \ldots, s_M(t)]^T$, the N - dimensional observations, $x(t) = [x_1(t), x_2(t), x_3(t), \ldots, x_N(t)]^T$, are generated by a mixture corrupted by additive observation or sensor noise $n(t)$ as follows:

$$x(t) = f(s(t)) + n(t) \tag{3.15}$$

where f is an unknown function.

The goal of blind source separation is to invert the function f and recover the sources. The qualifier blind signifies that little is known about the quantities on the right side of

the equation 3.27. The mixing function, the noise and the sources are unknown and must be estimated. However in ICA, the analysis makes the assumption that the sources are linearly mixed by a mixing matrix A {Roberts, 2001]. Thus, observations are assumed to be generated by

$$x(t) = A(s(t)) + n(t) \tag{3.16}$$

For simplicity, it is usually assumed that s and n have mean zero.

Although the function f has been replaced with an unknown matrix A, the problem of identification of s is still under-determined, because there are unknown signals of the sources and the noises, with N known signals (the observations). In ICA, the sources are assumed to be independent. In other words, each source signal is assumed to be generated by a process unrelated to the other sources. The definition of independence will be explained in the next section.

ICA models assume the sources to be independent, assumptions about the characteristics of the noise and the source densities lead to a range of ICA models. However, the majority of ICA models are noiseless [Roberts, 2001]. This can be written as,

$$x = As \tag{3.17}$$

The aim of ICA is to recover the original sources from the observations alone. ICA seeks a separating matrix, W, which when applied to the observations, recover estimated sources, u

$$u = Wx \tag{3.18}$$

The process is depicted in Figure 3.5.

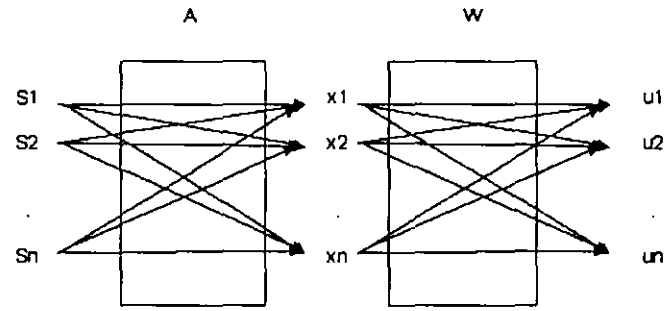

Figure 3.4 Independent Component Analysis (ICA)

3.3.1 Definition of Independence

In ICA models, the sources are assumed statistically independent. Assume that there are M sources, the statistical independence between the sources means that the multivariate probability density function of the sources can be written as the product of marginal independent distributions.

$$p(s) = \prod_{i=1}^{M} p_i(s_i) \tag{3.19}$$

If the probability density function of the estimated sources is also the product of its marginal distributions then the estimated sources are independent and the separation process has been accomplished. The definition of independence comes from information theory. The independence between the sources is measured by the mutual information, which is defined in terms of entropies.

The entropy measures the information content. Let X and Y, be random variables, the entropy of X is defined as:

$$H(X) = \Sigma P(x) \log \frac{1}{P(x)} \tag{3.20}$$

Entropy is additive for independent components

$$H(X,Y) = H(X) + H(Y) \text{ iff } P(x,y) = P(x)P(y) \tag{3.21}$$

The joint entropy X, Y is

$$H(X,Y) = \sum_{xy \in A_X A_Y} P(x,y) \log \frac{1}{P(x,y)} \tag{3.22}$$

The conditional entropy of X given Y is the average over Y of the conditional entropy of X given Y.

$$\begin{aligned} H(X \mid Y) &= \sum_{y \in A_Y} P(y) \left[\sum_{x \in A_X} P(x \mid y) \log \frac{1}{P(x \mid y)} \right] \\ H(X \mid Y) &= \sum_{xy \in A_X A_Y} P(x,y) \log \frac{1}{P(x \mid y)} \end{aligned} \tag{3.23}$$

The mutual information between X and Y is

$$\begin{aligned} I(X;Y) &= H(X) - H(X \mid Y) \\ I(X;Y) &= I(Y;X) \\ I(X;Y) &\geq 0 \end{aligned} \tag{3.24}$$

The mutual information measures the average amount of information that X conveys about Y; or vice versa. It will always positive and will only equal zero when the components are independent.

3.4 Fast ICA

FastICA is ICA technique developed by Aapo Hyvarinen [Hyvarinen, 1997; Hvyarinen, 1999, Hyvarinen, 2000]. In this method, a simple principle of ICA estimation is used: the independent components are found as the projections that maximize non-Gaussianity.

3.4.1 Whitening

As depicted in Figure 3.14, the goal ICA is to find linear transformation, W, of the dependent signals, x, that makes the output, u, independent as possible. However, due

to the complexities of ICA algorithm, it is important to pre-process the dependent signal, x, in order to simplify the ICA algorithm [Hvyarinen, 1999].

The preprocessing used is called whitening. Whitening transforms the signals, x, linearly to the new vector, $\tilde{x}$, whose components are uncorrelated and their variances equal unity. In other words, the covariance matrix of $\tilde{x}$ equals the identity matrix:

$$E\{\tilde{x}\tilde{x}^T\} = 1 \tag{3.25}$$

One popular method for whitening is to use the eigenvalue decomposition (EVD) of the covariance matrix $\tilde{x}\tilde{x}^T = \gamma\lambda\gamma^T$, where γ is the orthogonal matrix of eigenvectors of $\tilde{x}\tilde{x}^T$ and λ is the diagonal matrix of its eigenvalues. Whitening can be done by,

$$\tilde{x} = \gamma\lambda^{-\frac{1}{2}}\gamma^T x \tag{3.26}$$

where the matrix $\lambda^{-\frac{1}{2}}$ is computed as $\lambda^{-\frac{1}{2}} = diag(\lambda_1^{-\frac{1}{2}},...,\lambda_n^{-\frac{1}{2}})$. Whitening transforms the mixing matrix, A, into a new one, $\tilde{A}$.

$$\tilde{x} = \gamma\lambda^{-\frac{1}{2}}\gamma^T x = \gamma\lambda^{-\frac{1}{2}}\gamma^T As = \tilde{A}s \tag{3.27}$$

Whitening reduces the number of parameters to be estimated. Instead of having to estimate the n^2 parameters that are the elements of the original mixing matrix, A, it is now reduced to $n(n-1)/2$.

3.4.2 Basic Intuitive of Fast ICA

The basic intuitive of ICA lies on the Central Limit Theory. Central Limit Theory stated,

Let $x_1, x_2, x_3, \ldots$ be a sequence of random variables which are defined on the same probability space, share the same probability distribution and are independent. The

convolution of all density functions of the random variables tends to be the normal density function (Gaussian distribution) as the number of density functions increases, under the conditions stated above.

Let us assume that the whitened data, $\tilde{x}$, is distributed according to the ICA data model:

$$\tilde{x} = \tilde{A}s \tag{3.28}$$

Estimating the independent component, s, can be accomplished by finding the right linear combinations of the mixture variables. Thus, to estimate one of the independent components, it is possible to consider a linear combination of the $\tilde{x}_i$. Let us denote,

$$a = w^T\tilde{x} = \sum_i w_i\tilde{x}_i \tag{3.29}$$

where w is a vector to be determined. If w were one of the rows of the inverse $\tilde{A}$, this linear combination would actually equal to one of the independent component.

By defining $q = \tilde{A}^T w$, Equation 3.38 can be re-written as,

$$a = w^T\tilde{x} = w^T\tilde{A}s = q^T s \tag{3.30}$$

Thus a is a linear combination of s_i with weights given by q_i. Central Limit Theory ensures that the sum of even two independent random variables is more Gaussian than the original variables, $q^T s$ is more Gaussian than any of the s_i and become least Gaussian when it equals to one of the s_i. Therefore, taking w as a vector that maximizes the non-Gaussianity of $w^T\tilde{x}$, this vector will correspond to a q which has only one nonzero component. In other words, $w^T\tilde{x} = q^T s$ equals one of the independent components as shown in Figure 3.15.

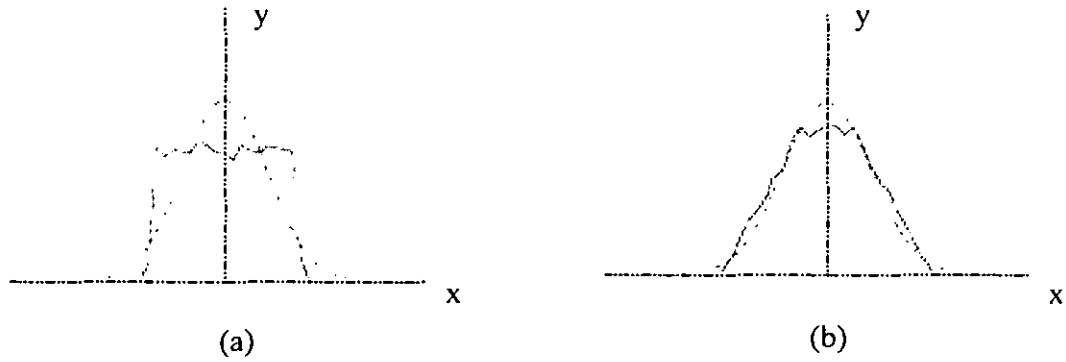

Figure 3.5 (a) the estimated density of one uniform independent component with the Gaussian density (dashed curve) given for comparison. (b) the marginal density of the mixed signal. It is closer to the Gaussian density (dashed curve) than the density of the independent component.

3.4.3 Measuring Non Gaussian

To use non-Gaussianity in ICA estimation, it is necessary to have quantification tool of non-Gaussianity of a random variable. In this particular technique, negentropy is used to measure the non-Gaussianity. Negentropy is based on the information-theoretic quantify of entropy. The entropy of a random variable can be interpreted as the degree of information that the observation of the variable gives.

A fundamental result of information theory is that a Gaussian variable has the largest entropy among all variables of equal variance. The Gaussian distribution is the least structured of all distribution [Hyvarinen, 1997; Hyvarinen, 1999]. Negentropy J is defined as,

$$J(x) = H(x_{gauss}) - H(x) \tag{3.31}$$

where x_{gauss} is a Gaussian random variable of the same covariance matrix as x. Due to the above-mentioned properties, negentropy is always non-negative, and it is zero if and only if x has a Gaussian distribution.

The advantage of using negentropy, as a measure of non-Gaussianity is that it is well justified by statistical theory. However, negentropy is very difficult to compute. Therefore, a simpler approximation of negentropy is used.

3.4.4 Approximation of Negentropy

General nonquadratic functions to generalize the higher order cumulant are proposed by Hvyarinen [Hyvarinen, 1998]. This is used to approximate negentropy. In general, the approximation of negentropy, $J(x)$, can be written as,

$$J(x) \approx k_1 (E\{G^1(x)\})^2 + k_2 \left(E\{G^2(x)\} - E\{G^2(v)\} \right)^2 \tag{3.32}$$

where G^1 is odd and G^2 is even nonquadratic functions, k_1 and k_2 are positive constants, and v is a Gaussian variable of zero mean and unit variance. The variable x is assumed to have zero mean and unit variance. It is reported by Roberts that even this approximation is not very accurate, it can be used to construct a measure of non-Gaussianity that is consistent in the sense that it is always non-negative, and equal to zero if x has a Gaussian distribution [Roberts, 2001]. If we use only one nonquadratic function, G, Equation 3.42 becomes,

$$J(x) \propto \left[E\{G(x)\} - E\{G(v)\} \right]^2 \tag{3.33}$$

for practically any nonquadratic function G.

The performance of the approximation of negentropy as shown in Equation 3.43 depends on the nonquadratic function G. By choosing G, it will produce a good approximation of negentropy. In particular, choosing G that does not grow too fast, one obtains robust estimators. The following choices of G have proved very useful:

$$
\begin{aligned}
G_1(u) &= \tanh(a_1 u) \\
G_2(u) &= u \exp(-u^2/2) \\
G_3(u) &= u^3
\end{aligned}
\tag{3.34}
$$

where $1 \le a_1 \le 2$ is some suitable constant [Hyvarinen, 1999].

3.4.5 Fixed-Point Algorithm

Fast ICA is based on fixed-point iteration scheme for finding a maximum of the non-Gaussianity of $w^T\tilde{x}$. The fixed-point iteration scheme is derived from Newton iteration method.

The maxima of $w^T\tilde{x}$ are obtained at certain optima of $E\{G(w^T\tilde{x})\}$. According to the Kuhn-Tucker conditions, the optima of $E\{G(w^T\tilde{x})\}$ under the constraint $\|w\|^2 = 1$ are obtained at points where,

$$E\{\tilde{x}G(w^T\tilde{x})\} + \beta w = 0 \tag{3.35}$$

where β is some constant.

To solve Equation 3.44 using Newton's method, firstly, we obtain its Jacobian matrix, $JF(w)$, as

$$JF(w) = E\{\tilde{x}\tilde{x}^T G'(w^T\tilde{x})\} + \beta I \tag{3.36}$$

Secondly, to simply the inversion of the matrix, first term of Equation 3.45 is estimated first. Since the data is sphered, the approximation can be written as,

$$E\{\tilde{x}\tilde{x}^T G'(w^T\tilde{x})\} \approx E\{\tilde{x}\tilde{x}^T\}E\{G'(w^T\tilde{x})\} = E\{G'(w^T\tilde{x})\}I \tag{3.37}$$

Thus the Jacobian matrix becomes diagonal, and can be inverted. From Equation 3.44, the approximation of Newton's iteration becomes,

$$w \leftarrow w - \frac{\left[E\{\tilde{x}G(w^T\tilde{x})\} + \beta\tilde{x}\right]}{\left[E\{G'(w^T\tilde{x})\} + \beta\right]} \tag{3.38}$$

Equation 3.47 can be simplified as follows,

$$w \leftarrow E\{\tilde{x}G(w^T\tilde{x}) - E\{G'(w^T\tilde{x})\}w\} \tag{3.39}$$

This is the basic fixed-point iteration in Fast ICA.

3.4.6 Estimation of Independent Component

From Section 3.7.4, it stated that the performance of the approximation of negentropy depends on the performance of the nonquadratic function, G.

The basic steps of the Fast ICA is described as follows,

1. Pre-processing the input data, x, into the whitened data $\tilde{x}$.
2. Initialing the weight vector w of unit norm.
3. Let $w \leftarrow E\{\tilde{x}G(w^T\tilde{x}) - E\{G'(w^T\tilde{x})\}w\}$, where G is defined in
4. Let $w \leftarrow {}^{w}\!/\!_{\|w\|}$.
5. If not converged, go back to step (3).

Convergence means that the old and new values of w point in the same direction. In other words, their dot-product is almost equal to 1. It is not necessary that the vector converge to a single point, since w and $-w$ define the same direction.

3.4.7 Properties of Fast ICA

The Fast ICA algorithm and the underlying non-Gaussianity measures have a number of desirable properties as follows,

1. The convergence is cubic, or at least quadratic, under the assumption of the ICA dara model [Hyvarinen, 1999].
2. There are no step size parameters to choose.
3. The algorithm finds directly independent component of any-Gaussian distribution using any nonquadratic function G.
4. The performance of the algorithm can be optimized by choosing a suitable nonquadratic function G. In particular, it possible to obtain robust algorithm [Hyvarinen, 1997].
5. The independent components are estimated one by one which is roughly equivalent to projection pursuit [Hyvarinen, 1999].

3.5 Morphology

Mathematical morphology relates to the structure of objects [Scultze, 1994]. In morphology, image filtering and geometrical analysis are delineated by structuring elements. Dilation and erosion are the two fundamental operations which define the algebra of mathematical morphology. These two operations are applied in different combination to perform more sophisticated operations, such as opening and closing.

3.5.1 Dilation

Dilation allows object to grow and contributing in filling in small holes and connecting objects. Dilation is a morphological transformation that combines two sets by using vector addition of set elements. Dilation is based on the classical operation of Minkowski addition of integral geometry. For any two sets A and B, Minkowski addition is defined as

$$A \times B = \{a + b : a \in A, b \in B\} \tag{3.40}$$

In image algebra, Equation 3.14 can be expressed as,

$$\text{Dilation of } A \text{ by } B = A \oplus B = \bigcup_{b \in B} (A + b) \tag{3.41}$$

When performing a dilation of A by B, it is assumed that A is the set to be analyzed and B is the measuring stick, called a structuring element.

The process of dilation can be explained as follows:

1. Positioning of the origin of the structuring element over the first pixel of the image being dilated.
2. Computation of the sum of each corresponding pair of pixel values in the structuring element and the underlying image.
3. Substituting the corresponding pixel in the output image with the result of the sum.
4. Repetition of this process for each pixel in the underlying image.

Figure 3.8 shows an example of a 3-by-3 matrix of structuring element. Figure 3.9 shows the effect of dilation using the 3-by-3 structuring element.

1	1	1
1	1	1
1	1	1

Figure 3.6 3×3 square structuring element

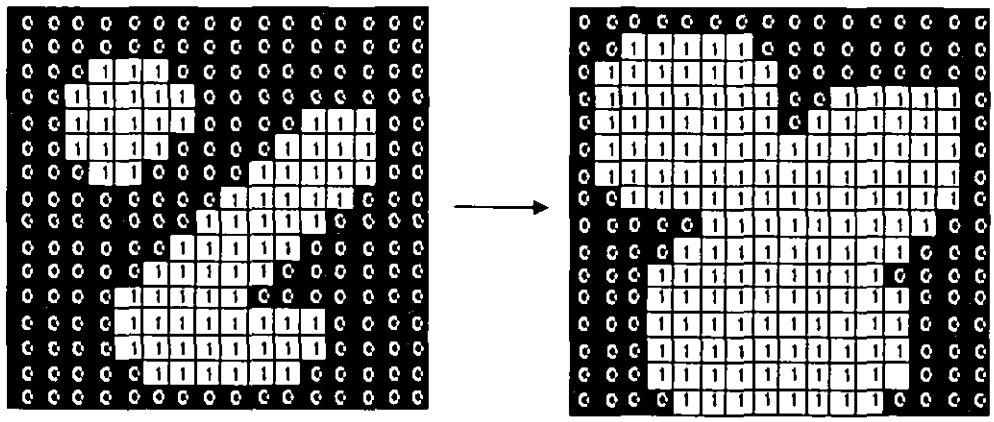

Figure 3.7 Effect of a dilation using 3×3 square structuring element

3.5.2 Erosion

Erosion is a process of shrinking objects by eroding their boundaries [Nixon 2002]. It is a morphological transformation that combines two sets by using vector subtraction of set elements. Erosion is based on the classical operation of Minkowski substraction of integral geometry. For any two sets A and B, Minkowski substraction is defined as,

$$A/B = (A' \times B^*)' \tag{3.42}$$

B^* denotes the reflection of B across the origin, while A' denotes the complement of A. In image algebra, Equation 3.16 can be expressed as,

$$\text{Erosion of } A \text{ by } B = A \otimes B = \bigcap_{b \in B} (A - b) \tag{3.43}$$

The process of erosion can be explained as follows:

1. Positioning the origin of the structuring element over the first pixel of the image.
2. Computation of the subtraction of each corresponding pair of pixel values in the structuring element and the underlying image.
3. Substituting the corresponding pixel in the output image with the result.
4. Repetition of this process for each pixel in the underlying image.

Figure 3.10 shows the effect of erosion using the 3-by-3 structuring element (Figure 3.8).

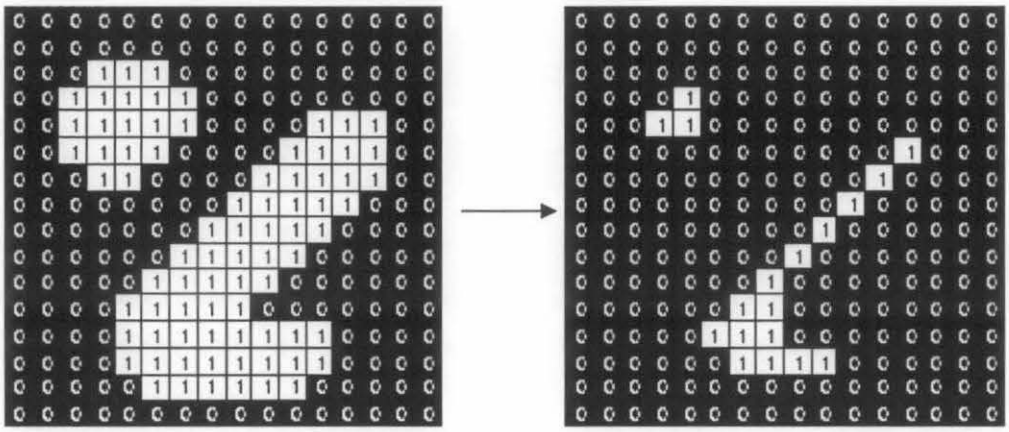

Figure 3.8 Effect of an erosion using 3×3 square structuring element

3.5.3 Opening

Opening is a morphological operation of erosion followed by dilation. Opening smoothes the contours of an object, break narrow isthmuses and eliminates thin protrusions. Thin objects can be eliminated because they are erased during erosion and are unable to be regenerated by dilation.

In image algebra, opening of an image A by structuring element B, denoted $A \circ B$, is defined as follows,

$$\text{Opening of } A \text{ by } B = A \circ B = (A \otimes B) \oplus B \tag{3.44}$$

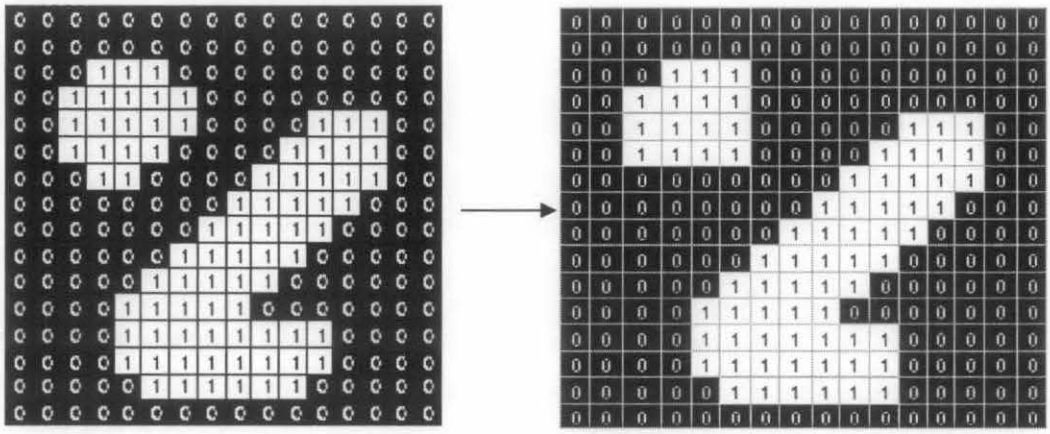

Figure 3.9 Effect of an opening using 3×3 square structuring element

3.5.4 Closing

Closing is a morphological operation of dilation followed by erosion. Closing results in removing small black areas as objects that are closer than the minimum allowable space will grow together. Closing tends to smooth contours; however it generally fuses narrow breaks and long thin gulfs.

In image algebra, closing of an image A by structuring element B, denoted $A \bullet B$, is defined as follows,

$$\text{Closing of } A \text{ by } B = A \bullet B = (A \oplus B) \otimes B \tag{3.45}$$

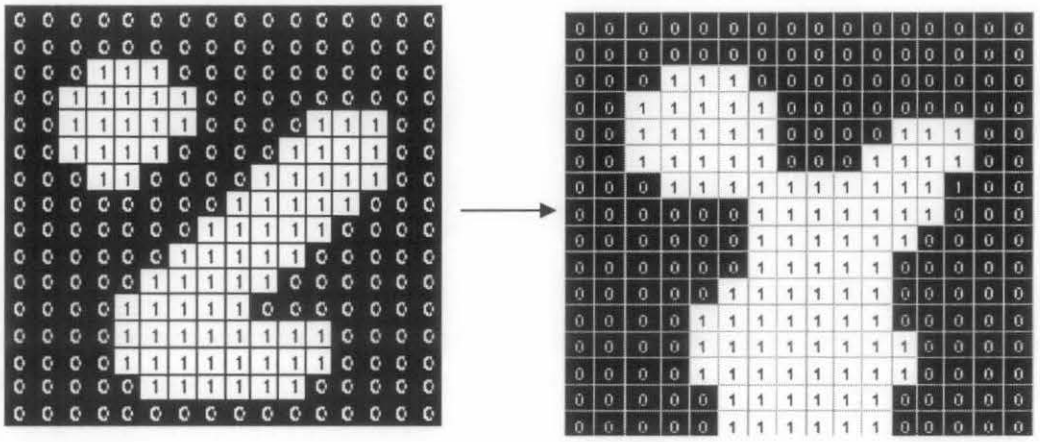

Figure 3.10 Effect of a closing using 3×3 square structuring element

3.6 Thresholding Techniques

Thresholding is one of the simplest and most widely used image segmentation techniques. The goal of thresholding is to segment an image into regions of interest and to remove all other regions deemed inessential. There are many methods of thresholding. The simplest method uses a single threshold in order to discern foreground and background.

3.6.1 Global Tresholding

The global thresholding technique is used to isolate objects of interest having values different from the background. Each pixel is classified as either belonging to an object of an interest or to background. This is accomplished by assigning to a pixel the value 1 if the source image value is within a given threshold range and 0 otherwise [Rosenfeld, 1982].

The global thresholding is straightforward. Let a be the input image and $[h,k]$ be a given threshold range. The threshold image, b, is given by

$$b(x,y) = \begin{cases} 1 & for\ h \le a(x,y) \le k \\ 0 & else \end{cases} \tag{3.46}$$

where (x,y) represents spatial coordinates of pixels of image.

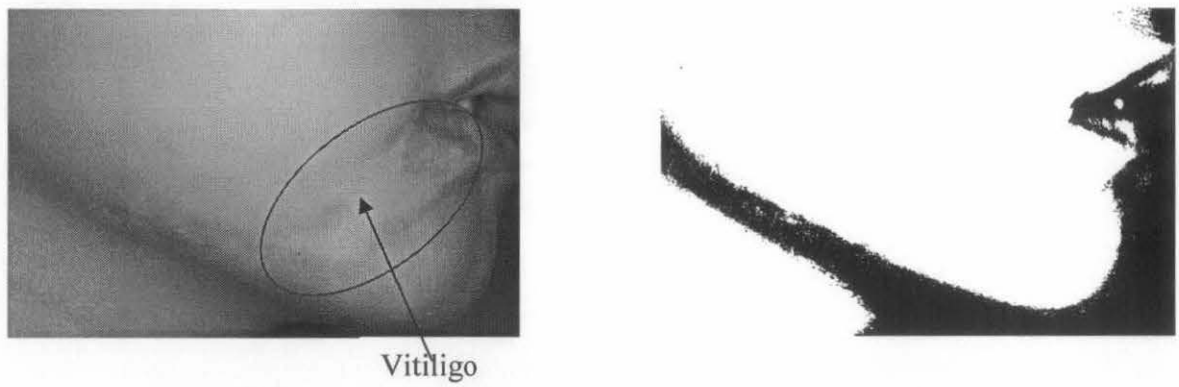

(a) (b)

Figure 3.11 (a) Original image; (b) Global thresholding with fix threshold value, 100

Global thresholding is effective in isolating objects of uniform value placed against background of different values. Problems occur when the object and the background assume a broad range of values. Figure 3.1 shows that the lesion areas can not be captured using global thresholding due to its broad range of values.

3.6.2 Semi Tresholding

Semithresholding is a useful variation of global thresholding [Rosenfeld, 1982]. Pixels whose values lie within a given threshold range retain their original values. Pixels with values lying outside of the threshold range are set to 0. For a source image a and the threshold range $[h,k]$, the semi-thresholded image b is given by,

$$b(x,y) = \begin{cases} a(x,y)\ for\ h \le a(x,y) \le k \\ 0 \quad else \end{cases} \tag{3.47}$$

where (x, y) represents spatial coordinates of pixels of image. Figure 3.2 shows the result of semi thresholding. It can be seen that the method can not captured lesion areas due to its broad range of values.

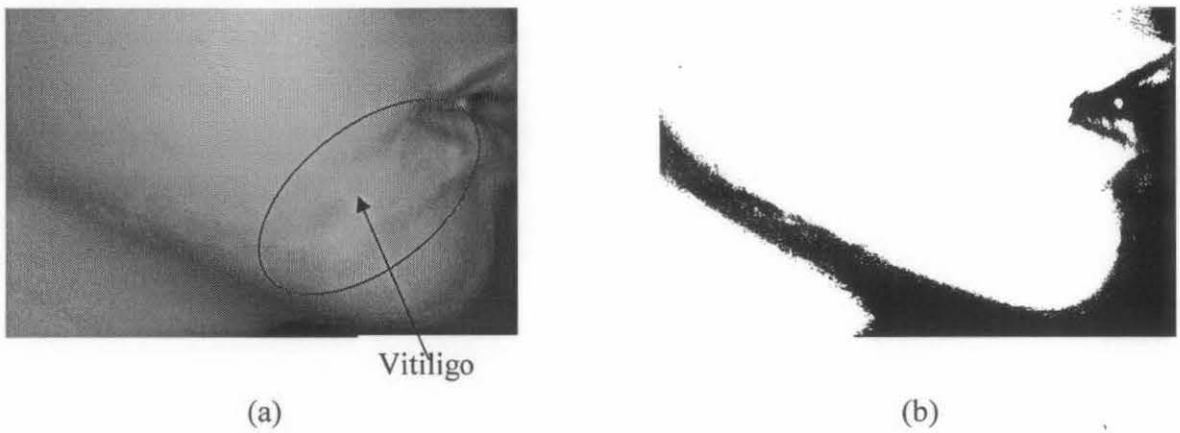

Figure 3.12 (a) Original image; (b) Semi thresholded image

3.6.3 Multilevel Thresholding

Global thresholding and semi thresholding techniques divide an image based on the assumption that the image contains only two types of regions. However, it is possible that an image has more than two regions of our interest. Multilevel thresholding is an extension of the two earlier thresholding techniques that allows for segmentation of pixels into multiple cases [Rosenfeld, 1982].

For example, if the image histogram contains four peaks, then it is possible to segment the image using three thresholds. These thresholds will divide the value sets into four ranges, each of which can be associated with a unique value in the resulting image.

Let a be the input image and $k_1, k_2, ..., k_n$ be given threshold values satisfying $k_1 > k_2 > ... > k_n$. The threshold image, b, is given by,

$$b(x,y)=\begin{cases} v_1 & if \quad k_1 < a(x,y) \\ v_2 & if \quad k_2 < a(x,y) \le k_1 \\ v_3 & if \quad k_3 < a(x,y) \le k_2 \\ v_n & if \quad a(x,y) \le k_3 \end{cases} \tag{3.48}$$

where (x,y) represents spatial coordinates of pixels of image.

3.6.4 Variable Thresholding

No single threshold value produces good segmentation results. Variable thresholding allows different threshold values to be applied to different regions of an input image.

For example, objects may contrast with the background throughout an image, but due to uneven illumination, objects and background may have lower values on one side of the image than on the other. To overcome this problem, this image may be subdivided first into smaller regions. Thresholds are then established for each region and thresholding is applied to each subimage corresponding to a region [Rosenfeld, 1982].

The exact method can be written as follows. Let a be the input image and let d denotes the region threshold value associated with each point in a. The threshold image, b, is given by,

$$b(x,y)=\begin{cases} 1 & if\ a(x,y) \ge d(x,y) \\ 0 & if\ a(x,y) < d(x,y) \end{cases} \tag{3.49}$$

where (x,y) represents spatial coordinates of pixels of image.

Variable thresholding is effective for images with locally bimodal histograms. This technique will produce the desired results if the objects are relatively small and are not clustered too close together. The subimages should also be large enough to ensure that they contain both background and object pixels [Ritter, 2001].

3.6.5 Threshold Selection Using Mean and Standard Deviation

This thresholding technique is an automatic thresholding technique. Proposed in [Hamadani, 1981], the threshold value of an image is derived from a linear combination, $k_1\mu + k_2\sigma$, of the mean and standard deviation of the image.

Let a be the input image, μ and σ, the mean and standard deviation of a are given by

$$\mu = \frac{1}{xy}\sum_{i=1}^{x}\sum_{j=1}^{y} a(i,j) \tag{3.50}$$

and

$$\sigma = \sqrt{\frac{1}{xy}\sum_{i=1}^{x}\sum_{j=1}^{y}(a(i,j)-\mu)^2} \quad , \tag{3.51}$$

respectively. The threshold level τ is set at

$$\tau = k_1\mu + k_2\sigma \tag{3.52}$$

where the constants k_1 and k_2 are image type dependent.

Figure 3.3 shows that the threshold selection using Hamadani's method can not capture the lesion areas.

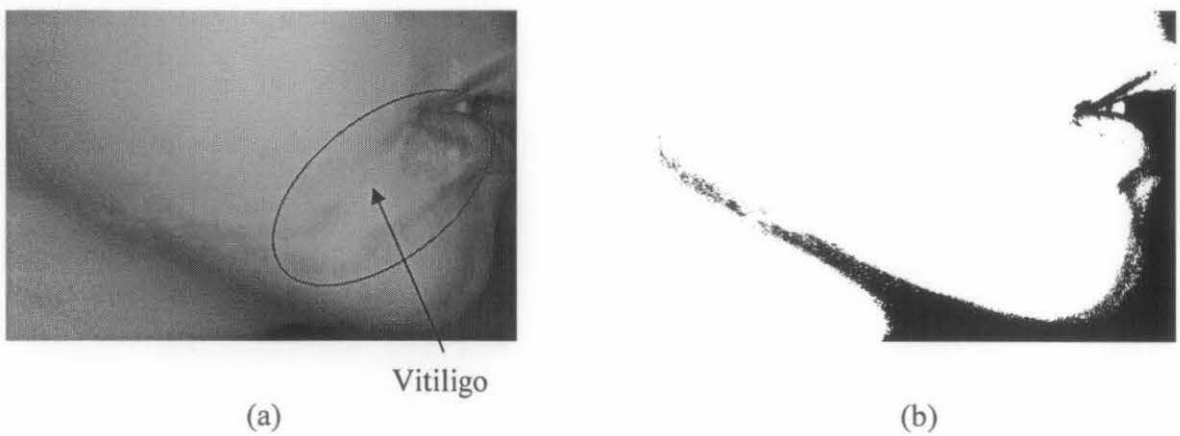

Figure 3.13 (a) Original image; (b) Thresholded image using Hamadani's method.

3.6.6 Threshold Selection by Maximizing Between-Class Variance

In this section, thresholding technique proposed by [Otsu, 1979] is presented. Otsu uses between-class variance as the measure of separability between classes. Its definition, which follows bellow, utilizes histogram information derived from the input image.

Let a be an input image and let $\bar{h}$ be the normalized histogram of a. The pixels of a are partitioned into k classes $C_0, C_1, ..., C_{k-1}$. The probability of class occurrence $\Pr(C_i)$ are given by,

$$\Pr(C_0) = \omega_0 = \sum_{j=0}^{\tau_1} \bar{h}(j) = \varpi(\tau_1)$$

$$\Pr(C_i) = \omega_i = \sum_{j=\tau_{i+1}}^{\tau_{i+1}} \bar{h}(j) = \varpi(\tau_{i+1}) - \varpi(\tau_1)$$

$$\Pr(C_{k-1}) = \omega_{k-1} = \sum_{j=\tau_{k-1}+1}^{l-1} \bar{h}(j) = 1 - \varpi(\tau_{k-1}) \tag{3.53}$$

where $\omega(\tau_1) = \sum_{j=0}^{\tau_1} \bar{h}(j)$ is the 0^{th}-order cumulative moment of the histogram evaluated up to the τ_ith level. The class mean levels are given by,

$$\mu_0 = \sum_{j=0}^{\tau_1} \frac{j.\bar{h}(j)}{\omega_0} = \frac{\mu(\tau_1)}{\omega(\tau_1)}$$

$$\mu_i = \sum_{j=\tau_1+1}^{\tau_{i+1}} \frac{j.\bar{h}(j)}{\omega_i} = \frac{\mu(\tau_{i+1}) - \mu(\tau_i)}{\omega(\tau_{i+1}) - \omega(\tau_i)}$$

$$\mu_{k-1} = \sum_{j=\tau_{k-1}+1}^{l-1} \frac{j.\bar{h}(j)}{\omega_{k-1}} = \frac{\mu_r - \mu(\tau_{k-1})}{1 - \omega(\tau_{k-1})} \tag{3.54}$$

where $\mu(\tau_1) = \sum_{j=0}^{\tau_1} j.\bar{h}(j)$ is the 1^{st} order cumulative moment of the histogram up to the τ_ith level and $\mu = \sum_{j=0}^{l-1} j.\bar{h}(j)$ is the total mean level of a.

In order to evaluate the threshold value, the between class variance is used as discriminant measure of class separability. The between-class variance, σ_b^2, is defined as

$$\sigma_b^2 = \omega_0\mu_0^2 + \omega_1\mu_1^2 + ... + \omega_{k-1}\mu_{k-1}^2 - \mu^2 \tag{3.55}$$

The threshold value, τ, is defined as the threshold value which optimize the between-class variance. Figure 3.4 shows the result of Otsu's method and Figure 3.5 shows the threshold value computed using Otsu's method. It can be seen that the method can not capture the lesion areas.

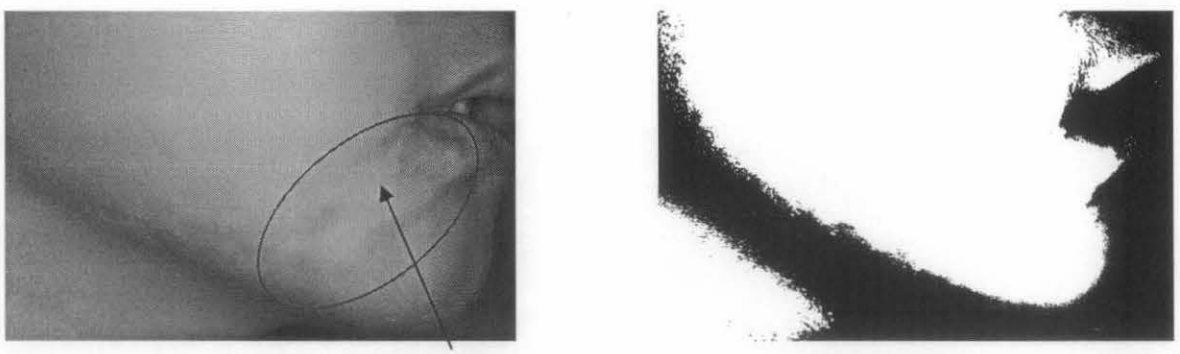

(a) (b)

Figure 3.14 (a) Original image; (b) Thresholded image using Otsu's method

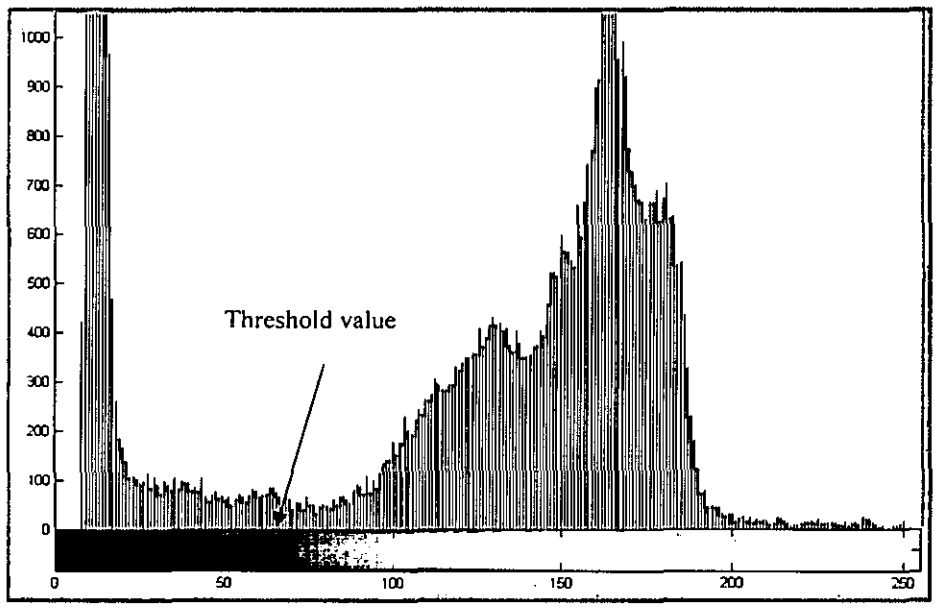

Figure 3.15 Histogram of original image; the threshold value is defined as a value that maximize the between-class variance

3.6.7 Threshold Selection Based on Median Cut

Median cut was developed for color image quantification by Paul Heckbert [Heckbert, 1980. However in some recent studies by S.E. Umbaugh and I. Maglogiannis, this technique, combined with Principal Component Transform, is proven to perform well for skin image segmentation [Umbaugh, 1993; Umbaugh, 1996; Maglogiannis, 2003; Maglogiannis, 2005].

Median cut is used to segment skin lesion from health skin in skin image. In this technique, there are three steps to be taken. First, two samples, each representing the skin lesion and healthy skin segment are obtained. Next, Euclidean distance of every pixel to these two samples is measured. The Euclidean distance, D_E, for two-dimensional point, $p(x,y)$ and $q(x,y)$, is defined as,

$$D_E = \sqrt{(p(x)-q(x))^2 + (p(y)-q(y))^2} \tag{3.56}$$

Finally, each pixel is mapped to its closest segments. In other words, the threshold value is defined as a valued whose Euclidean distance is equal both from healthy skin reference and skin lesion reference as depicted in Figure 3.6. Figure 3.7 however shows that median cut method is not able to capture lesion areas.

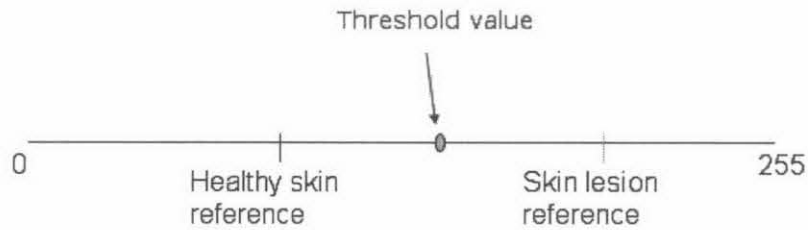

Figure 3.16 Threshold value is defined as a median value between skin lesion reference and healthy skin reference

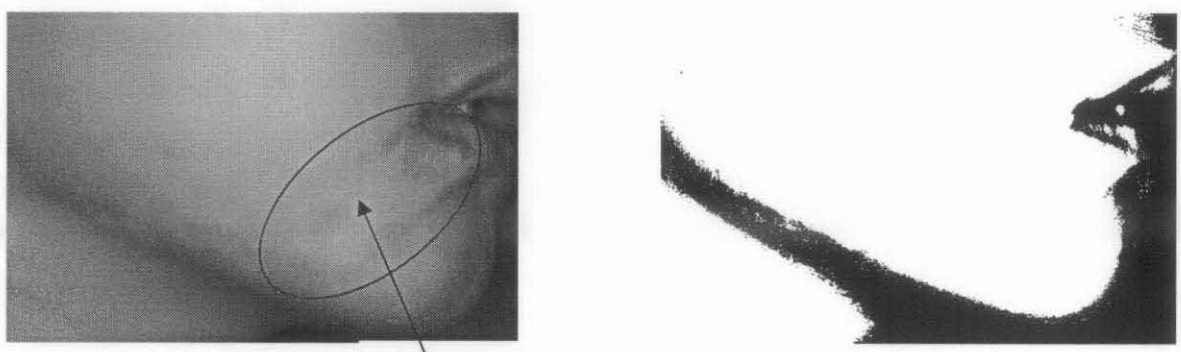

Figure 3.17 (a) Original image, (b) Thresholded image using median cut thresholding

3.7 Summary

Chapter 3 discussed image and statistical signal processing techniques that are used in our research work. There are two statistical signal processing methods that are employed in our research, Principal Component Analysis and Independent Component Analysis.

Principal Component Analysis (PCA) has been widely used in multivariate data analysis, data compression and reduction of multidimensional data sets into lower dimensions. PCA is defined as an orthogonal linear transformation that transforms the data sets into new data sets such that the greatest variance by any projection of the data comes to lie on the first principal component of the new data sets, the second greatest variance on the second principal component of the new data sets, and so on [Anthony, 1997]. The goal of PCA is to reduce the dimension of the observation (data). However, PCA is limited to re-express the observation (data) as a linear combination of its basis vectors. This assumption simplifies the problem by restricting the set of potential bases and formalizing the implicit assumptions of continuity in a data set [Lay, 2000].

Independent Component Analysis (ICA) is a multivariate data analysis for blind source separation. The blind source separation is a problem in signal processing where the sources of the observed signals are unknown. ICA assumed that the observed signals are generated by mixing the original sources with an unknown mixing matrix (Figure 3.14). ICA accomplishes the separation of the original sources by relying on the assumptions that the sources are statistically independent. The statistical independence between the sources means that the multivariate probability density function of the sources can be written as the product of marginal independent distributions (Equation 3.29. There are many methods of ICA estimations. In our research work, we use ICA estimation developed by Hyvarinen [Hyvarinen, 1999]. In this method, the independent sources are found as the the projections that maximize non-Gaussianity. In this particular technique, negentropy is used to measure the non-Gaussianity. Negentropy is based on the information-theoretic quantify of entropy (Equation 3.41). The advantage of using negentropy, as a measure of non-Gaussianity is that it is well justified by statistical theory. However, negentropy is very difficult to compute. Therefore, a simpler approximation of negentropy is used. The performance of the approximation of negentropy (Equation 3.43) depends on the nonquadratic function we use. Newton iterative method is then used to find the independent components.

Morphology operation is a mathematical operation that relates to the structure of objects. Dilation and erosion are the two fundamental operations which define the algebra of image morphology. Opening is made up of erosion followed by dilation. Due to its characteristic, opening can be used to smooth the contours of an image.

Thresholding is the most widely used image segmentation techniques. The goal of thresholding is to segment an image into regions of interest and to remove all other regions deemed inessential. In our research work, we used two methods of thresholding, a threshold selection method by maximizing between-class variance [Otsu, 1979] and a threshold selection method by median cut [Heckbert, 1980]. These two methods are used for different purposes. Otsu's method is used to segment the reference from the skin image whilst the median cut thresholding is used to segment vitiligo lesion areas after Principal Component Analysis and Independent Component Analysis.

Chapter 4

DEVELOPMENT OF THE VITILIGO MONITORING SYSTEM

4.1 Introduction

Visual signs play an important role in enabling dermatologists make accurate diagnosis. Visual descriptors of vitiligo lesion areas and normal skin lie on the fact that the vitiligo lesion areas are paler in contrast to normal skin. In addition, it is found that the appearance of skin due to repigmentation is similar to the appearance of normal skin.

In this chapter, the development of the vitiligo monitoring system is discussed. The performance and the limitation of the system are also studied. Digital color skin images are analyzed under several assumptions based on skin optic properties. The image processing analysis algorithm to be used in the system is based on principal component analysis (PCA) and independent component analysis (ICA). PCA and ICA are used to transform digital color skin images into skin images that represent skin areas due to melanin and hemoglobin only. The transformed skin images will enable the determination of melanin areas within skin image. The determination and quantification of repigmentation is investigated to enable treatment efficacy over a shorter time frame. The difference in the vitiligo surface areas before and after treatment will be expressed as a percentage of repigmentation in each vitiligo lesion. This percentage will represent the repigmentation progression of a particular body region

To measure the performance and the limitation of the developed system, the image processing analysis is employed in the controlled environment. The controlled environment comprises skin color models of healthy skin, vitiligo lesion, skin areas due to repigmentation and added noise.

4.2 Flow Chart of the Vitiligo Monitoring System

As depicted in Figure 4.1, the flow chart of the image processing analysis system comprises pre-processing, ICA estimation, image segmentation and repigmentation measurement. Each process in the flow chart diagram is elaborated in following sections.

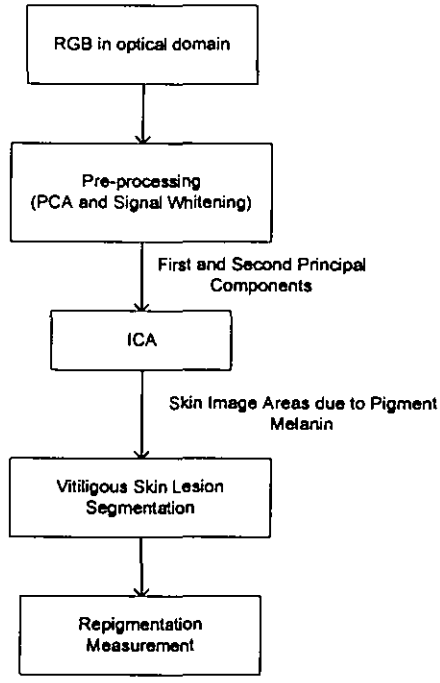

Figure 4.1 Flow chart of the algorithm

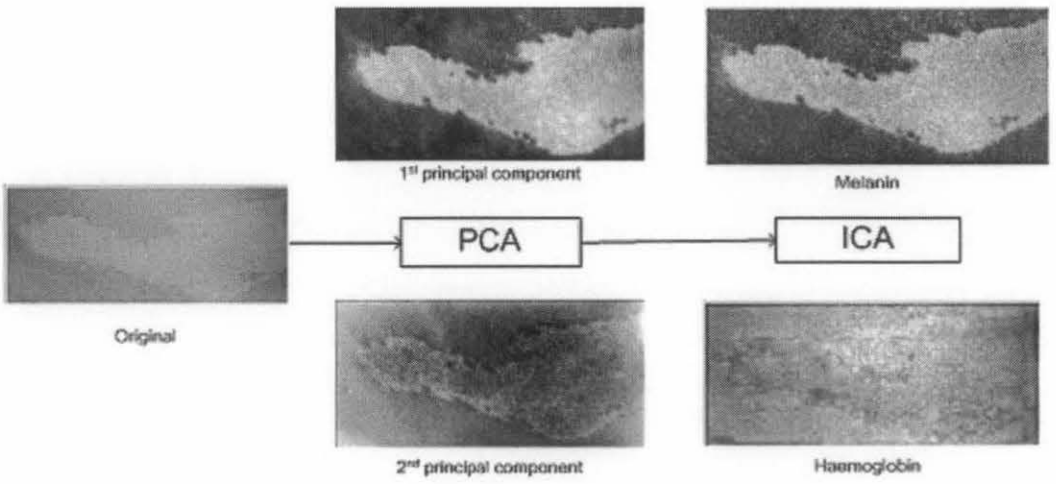

Figure 4.2 The process of the developed system

4.2.1 RGB Data Set

In the case of skin surface, a small portion of the incident light will be reflected because of the difference in the index of reaction between the air and skin surface. It has been found that the surface reflectance is typically between 4% -7% over the entire spectrum from 250 -3000 nm [Perish 1982]. Most of the incident light penetrates into the skin and follows a complex path until it exits back out of the skin or gets attenuated by skin choromophores.

Skin choromophores absorb electromagnetic energy of the light. As shown in Figure 4.2, the primary choromophores in skin are pigment melanin, and haemoglobin (oxy-haemoglobin and deoxy-haemoglobin).

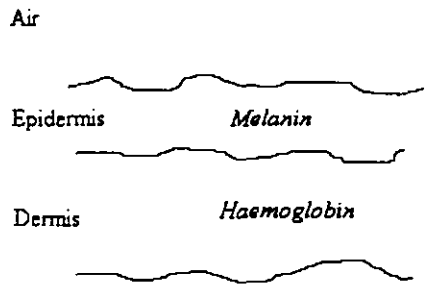

Figure 4.3 Skin Choromophores

Due to above process, information about skin choromophores can be extracted from the reflected light coming from skin. This reflected light is recorded by CCD sensor of a camera and forms a digital color image (section 2.7.2). The digital color image is created by combining three different spectral bands, namely, Red, Green and Blue (RGB).

4.2.2 Skin Image Model

The spatial distribution of melanin and haemoglobin in skin could be separated by employing linear independent component analysis of a skin color image [Tsumura 1999]. The analysis is based on the skin color model with three assumptions. Firstly, it is assumed linearity in the optical density domain of RGB channels. The second and third assumptions state that the spatial variations of skin image color are caused by two skin choromophores, namely melanin and haemoglobin and their quantities are mutually independent, as shown in Figure 4.2. Figure 4.3 shows the skin model developed by Tsumura.

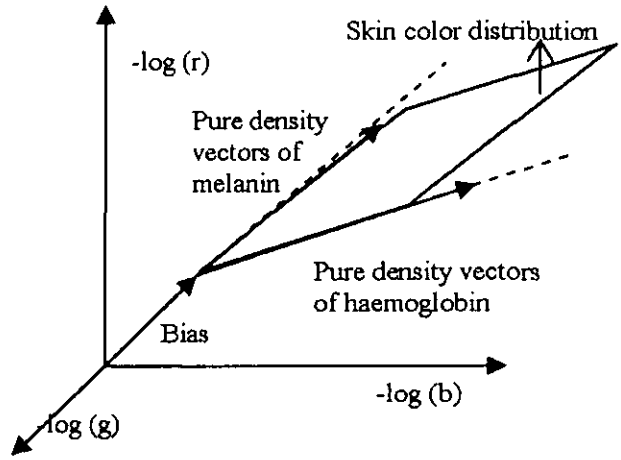

Figure 4.4 Skin color model (reproduced from Tsumura, 1999)

4.2.3 Principal Component Analysis

Figure 4.3 shows that skin color distribution lies on a two-dimensional melanin-haemoglobin color subspace. In order to determine repigmentation (due to pigment melanin) it is necessary to perform a conversion from RGB skin image to this two-dimensional color subspace. Using PCA (section 3.5) as a dimensional reduction tool, a two-dimensional subspace can be formed using the PCA first and second principal components. It is reported that the values of the RGB skin image can be adequately represented by using two principal components with an accuracy of 99.3 % [Tsumura 1999]. In addition, it is also necessary to make the two-dimensional subspace zero mean and unit variance in order to get stronger independence condition. The stronger independence condition will make the results of independent component analysis (ICA) more accurate [Hyvarinen, 1998]. The two dimensional subspace zero mean is the two-dimensional subspace after subtracting the mean value from the data sets (section 3.9.1).

4.2.4 Independent Component Analysis

Skin color distribution can be expressed as functions of pure density vector of melanin and haemoglobin. Let $s_1(x, y)$ and $s_2(x, y)$ represent the quantities of the two color

pigments on image coordinate, (x, y), that are independent variables. The color vectors of the two pigments per unit quantity are denoted a_1 and a_2, respectively. It is also assumed that the compound color vector $v(x, y)$ can be calculated using linear combination of the color vectors as follows

$$v(x, y) = a_1 s_1(x, y) + a_2 s_2(x, y) \tag{4.1}$$

This equation can be written as:

$$v(x, y) = As(x, y) \tag{4.2}$$

$$A = [a_1 a_2] \tag{4.3}$$

Equation 4.3 is known as linear Independent Component Analysis (ICA), where A is a mixing matrix and s contains the independent components.

As depicted in Figure 4.4, the goal of ICA is to find a linear transformation W of the dependent sensor signals v that makes the output independent as possible [Hvyarinen 2000] (Equation 4.4).

$$u = Wv, \quad u >> s \tag{4.4}$$

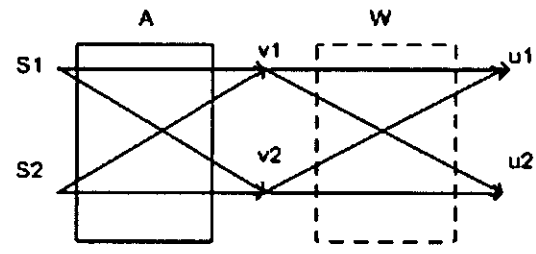

Figure 4.5: ICA model for color skin image

In this work, matrix W is estimated using a method developed by Hyvarinen [Hyvarinen 1999, 2000]. From this process, the two independent components of the skin image can

be extracted. One is the image of skin areas due to melanin and the other is the image of skin areas do to hemoglobin only.

4.2.5 Image Segmentation

Image segmentation method is performed on the image that represents skin areas due to melanin. The objective of the segmentation process is to separate vitiligo skin lesion from healthy skin. As detailed in Section 3.5, we employed thresholding based image segmentation technique.

Thresholding segments an image into regions of interest and to remove all other regions deemed inessential. There are many thresholding based segmentation techniques. In this particular research, we employ thresholding technique based on median cut algorithm (section 3.5.7).

4.2.6 Repigmentation Measurement

Repigmentation skin is having similar color with normal skin and found to be too small to be easily determined. In the developed system, the difference in the vitiligo surface areas between skin images before and after treatment will be expressed as a percentage of repigmentation in each vitiligo lesion. This percentage will represent the repigmentation progression of a particular body region.

The dermatologists choose the vitiligo surface areas and the details position and locations of the lesions are recorded by the clinicians. This is to ensure the accuracy of the measurement by the developed system.

The calculation is explained as follows. Let $a(K,L)$ be the logical image where vitiligo lesion and normal skin areas are represented by 1 and 0, respectively. $a(K,L)$ is defined as an processed image of the image segmentation of the developed system.

The vitiligo surface areas, *Area*, is measured as follows,

$$Area = \sum_{i=0}^{K} \sum_{j=0}^{L} a(i,j) \tag{4.4.5}$$

4.3 Reference model

4.3.1 Introduction

Reference model images are simulated images that represent healthy skin and vitiligo skin images. These images are modeled based on the distribution of color combinations in the three spectral bands, namely Red, Green and Blue.

4.3.2 Distribution Model

The distribution models are developed using samples of skin color taken from historical data of 4 patients. These samples are chosen together with dermatologists to obtain valid reference model images. The distribution of each spectral value is modeled using Gaussian distribution.

$$f(x;\mu,\sigma) = \frac{1}{\sigma\sqrt{2\pi}} e^{-\frac{(x-\mu)^2}{2\sigma^2}} \tag{4.6}$$

where σ is the standard deviation and μ is the mean value.

The Gaussian distribution model is chosen based on studies of skin modeling by Caetano, Zhu and Chang. [Caetano, 2001; Zhu, 2000; Chang, 2004]. In their works, it is reported that the skin color distribution can be modeled by Gaussian distributions.

To employ reliable statistical parameters of normal distribution (mean and standard deviation), a good estimator is needed. In this work, an estimator called Minimum Variance Unbiased Estimator (MVUE) is used [Keener, 2006]. MVUE is commonly used to estimate the parameters of normal distribution.

$$\bar{x} = \sum_{i=1}^{n} \frac{x_i}{n} \tag{4.7}$$

$$\sigma = \sqrt{\left(\frac{1}{n-1} \sum_{i=1}^{n} (x - \bar{x})^2 \right)} \tag{4.8}$$

Equation 4.10 is used to measure the mean value of the distribution whilst Equation 4.11 estimates the standard deviation parameter.

4.3.3 Healthy Skin Model

Healthy skin model is a simulated healthy skin images. The simulated images are produced by the distribution model of healthy skin.

To develop the distribution model, we take approximately 60000 pixels of healthy skin taken from 4 patients. Together with dermatologist, we grab samples of healthy skin from patients. These samples have approximately 60000 pixels. Figure 4.6, 4.7 and 4.8 show the distribution of the intensity value in the three different spectral bands. Parameters of Gaussian distribution are then estimated.

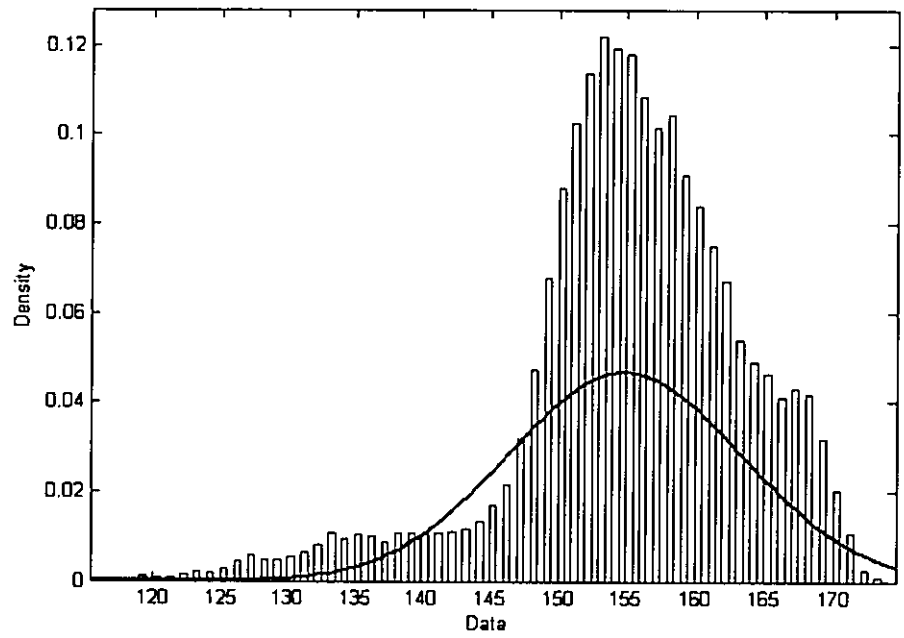

Figure 4.6 Intensity distribution of red spectral band in healthy skin

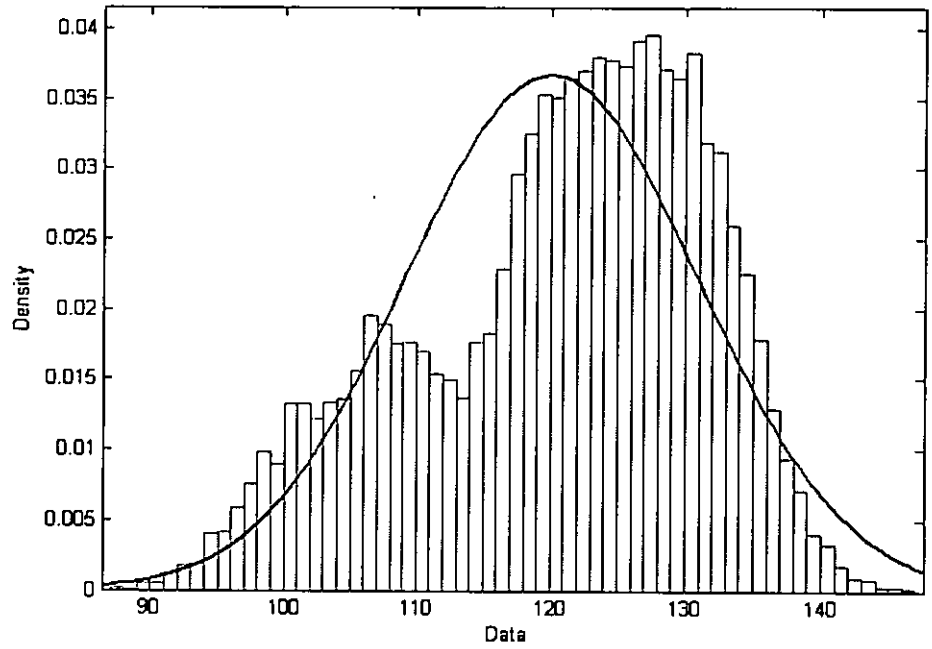

Figure 4.7 Intensity distribution of green spectral band in healthy skin

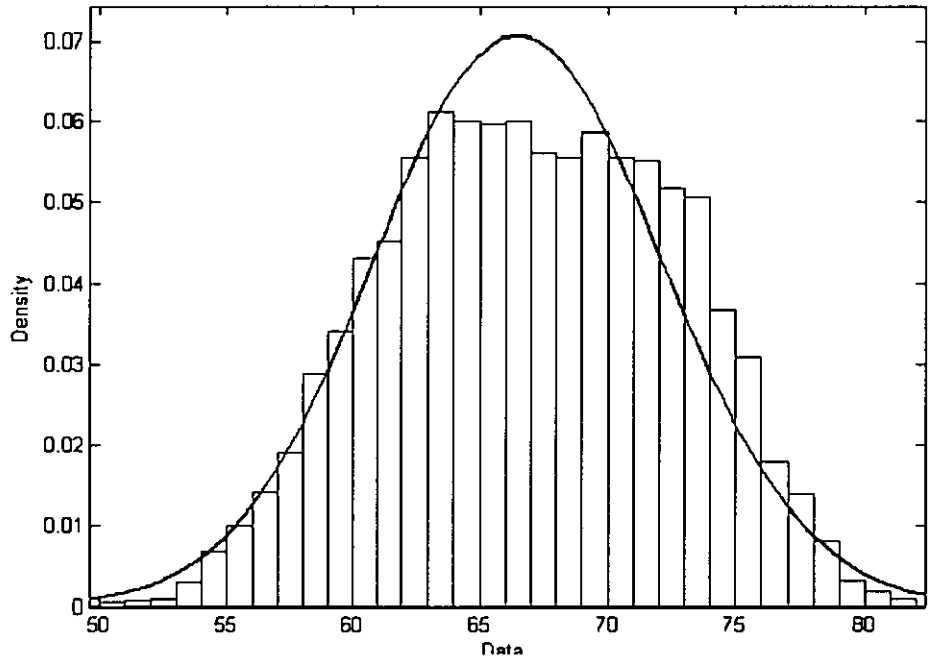

Figure 4.8 Intensity distribution of blue spectral band in healthy skin

Table 4.1 shows the parameters of Gaussian distribution using Minimum Variance Unbiased Estimator (MVUE).

Table 4.1 The Estimated Parameters of Gaussian Distribution

	Mean	Standard Deviation
Red	154.869	8.54991
Green	120.025	10.8663
Blue	66.476	5.63958

Using these estimated parameters, we can now generate a sample of healthy skin image. Figure 4.8 shows an example of 20-by-20 pixels of generated healthy skin using the healthy skin model function.

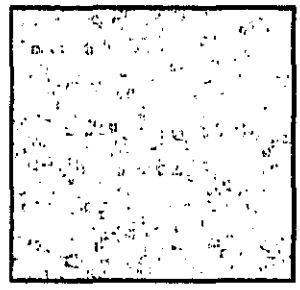

Figure 4.9 Generated Skin

4.3.4 Vitiligo Lesion Model

Vitiligo lesion model is a simulated vitiligo skin images. The simulated images are produced by the distribution model of vitiligo lesion.

To develop the distribution model, we take approximately 40000 pixels of healthy skin taken from 4 patients. Together with dermatologist, we grab samples of healthy skin from patients. These samples have approximately 40000 pixels. Figure 4.10, 4.11 and 4.12 show the distribution of the intensity value in the three different spectral bands. Parameters of Gaussian distribution are then estimated.

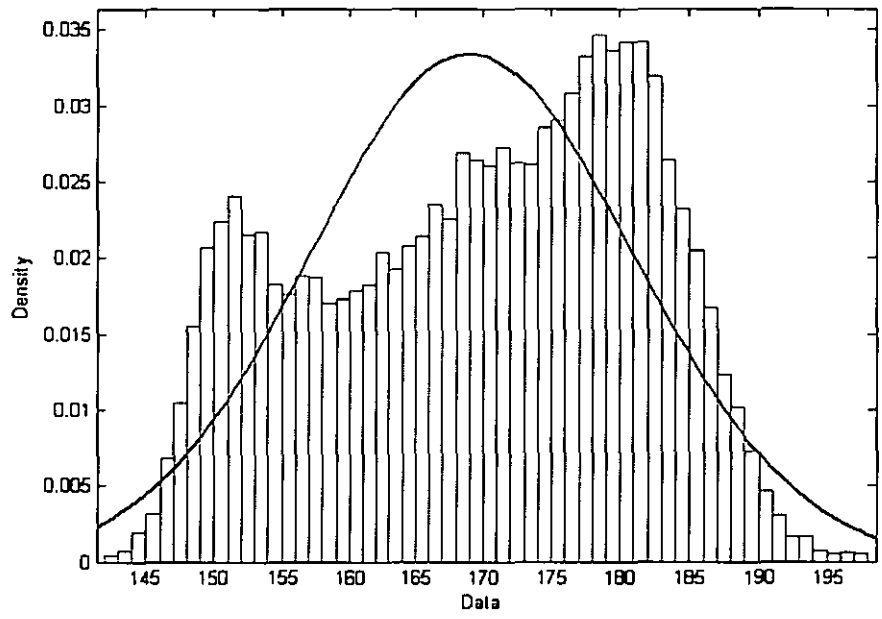

Figure 4.10: Vitiligo lesion distribution in red spectral band

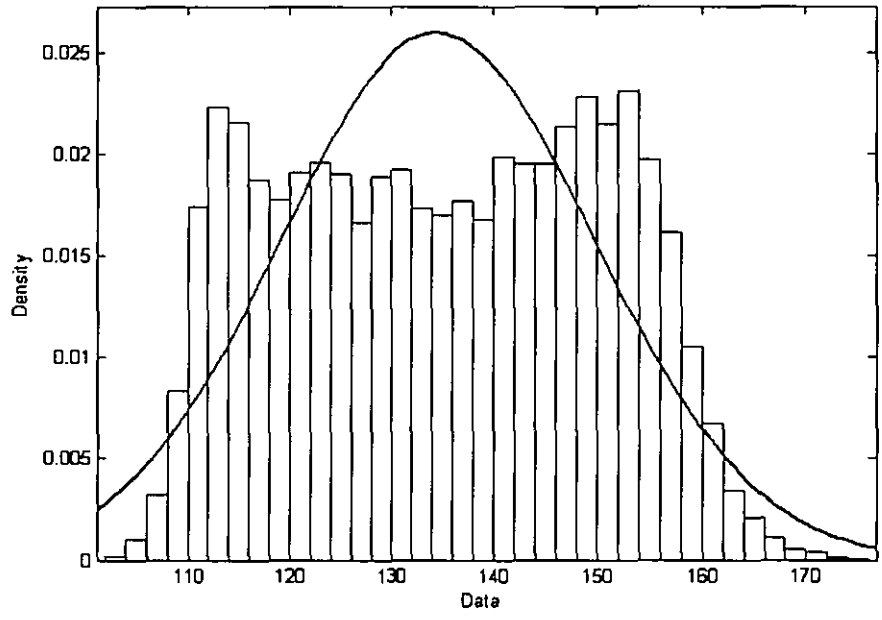

Figure 4.11 Vitiligo lesion distribution in green spectral band

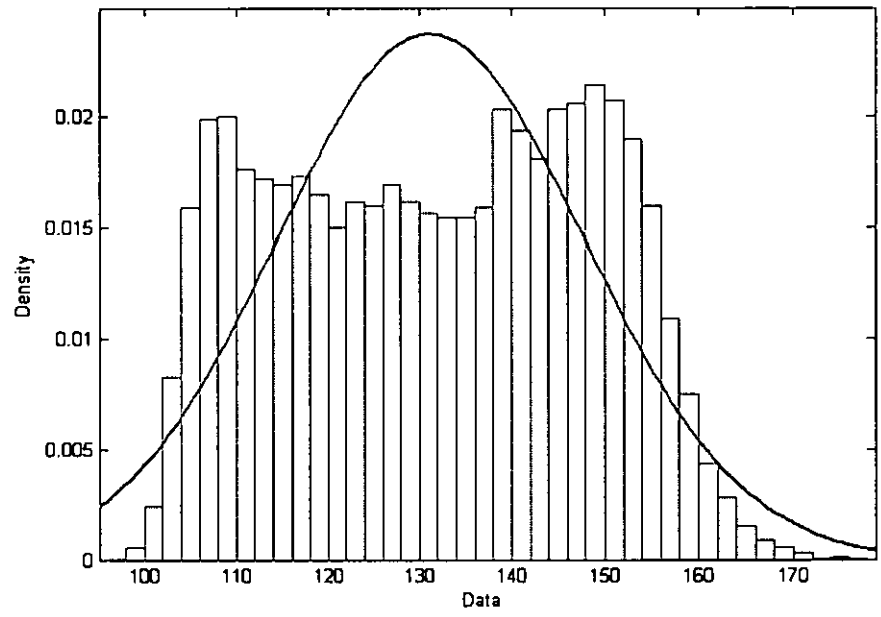

Figure 4.12 Vitiligo lesion distribution in blue spectral band

Table 4.2 shows the parameters of Gaussian distributions for Red, Green and Blue spectral bands respectively using Minimum Variance Unbiased Estimator (MVUE).

Table 4.2 The Estimated Parameters of Gaussian Distribution

	Mean	Standard Deviation
Red	169.016	11.9486
Green	134.417	15.3538
Blue	131.124	16.8001

Figure 4.12 shows an example of 20-by20 pixels of generated vitiligo lesion image using the vitiligo lesion model function.

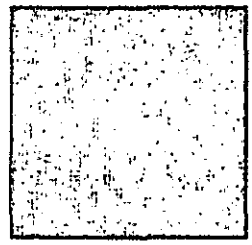

Figure 4.13 Generated vitiligo lesion image

4.3.5 Reference Model Images

There are four reference images used in the development of the system, namely reference image A, B, C and D. Each reference image consists of 200-by-200 pixels. The size is constructed based on the advice from the doctor and the size of vitiligo lesions found on the data.

Reference image A (Figure 4.14(a)) is constructed to model a skin image having vitiligo lesion. In this model the size of image A is 200-by-200 pixels whilst the vitiligo lesion areas are having 40-by-50 pixels.

Reference image B (Figure 4.14(b)) is created similar to reference image A. However, in its vitiligo lesion areas we add three areas which represent skin areas due to repigmentation. The size of each repigmentation areas is 5-by-5 pixels.

Reference image C (Figure 4.14(c)) and reference image D (Figure 4.14(d)) are created similar to reference image B. The differences of these reference images are on the size of the skin areas due to repigmentation. In reference image C, the size of the repigmentation areas is 3-by-3 pixels whilst in the reference image D, the size is reduced into 1-by-1 pixel. (Figure

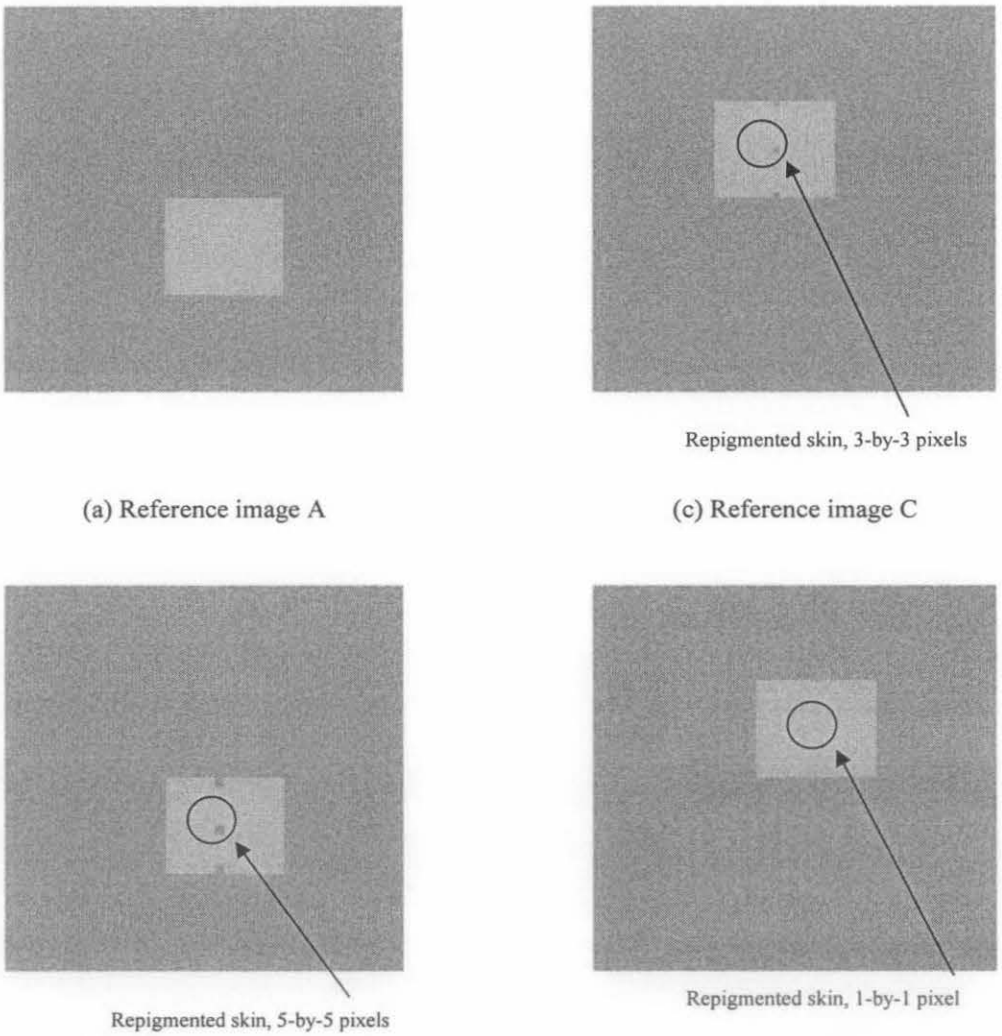

(a) Reference image A

(c) Reference image C

(b) Reference image B

(d) Reference image D

Figure 4.14 Reference images; (a) Skin image with vitiligo lesion, (b) Image of vitiligo lesion with repigmented skin (5-by-5 pixels), (c) Image of vitiligo lesion with repigmented skin (3-by-3 pixels), (d) Image of vitiligo lesion with repigmented skin (1-by-1 pixel)

4.3.6 Noise Generator

Noise generator is a function that generates noises. The noise generator is used to add controlled noises to the reference model images. Developed based on white Gaussian noise, the generator is developed in order to measure the performance of the developed system before applying it to the real data.

The limitation of the developed system is analyzed by employing the developed system to the reference images added by noise. Let I be the reference image and n is the noise. The reference image, R, after being added by noise can be written as,

$$R = I + n \tag{4.9}$$

where n is considered to be a white Gaussian noise defined as follows,

$$n(i;\mu,\sigma) = \frac{1}{\sigma\sqrt{2\pi}} e^{-\frac{(i-\mu)^2}{2\sigma^2}} \tag{4.10}$$

The added noise is controlled by the SNR (signal-to-noise ratio). SNR is the power ratio between a signal and the background noise.

$$SNR(dB) = 10\log\left(\frac{P_{signal}}{P_{noise}}\right) = 20\log\left(\frac{A_{signal}}{A_{noise}}\right) \tag{4.11}$$

where P is power and A is the RMS (root mean square) value. The connection of RMS value and standard deviation of a data set x can be written as,

$$\begin{aligned} A &= x_{RMS} \\ x_{RMS}^2 &= \mu_x^2 + \sigma_x^2 \end{aligned} \tag{4.12}$$

where x_{RMS} is the RMS value of x, μ_x is the mean value of x, and σ_x is the standard deviation of x. Equation 4.12 can be written as follows;

$$SNR(dB) = 20\log\left(\sqrt{\frac{\mu_{signal}^2 + \sigma_{signal}^2}{\mu_{noise}^2 + \sigma_{noise}^2}}\right) \tag{4.13}$$

If x is a zero mean data set, the RMS value of x is equal to the standard deviation. Equation 4.13 can be written as;

$$SNR(dB) = 20\log\left(\sqrt{\frac{\sigma_{signal}^2}{\sigma_{noise}^2}}\right) = 20\log\left(\sqrt{\left(\frac{\sigma_{signal}}{\sigma_{noise}}\right)^2}\right) = 20\log\left(\frac{\sigma_{signal}}{\sigma_{noise}}\right) \tag{4.14}$$

Using equation 4.14, we can generate Gaussian noise based on the signal-to-noise ratio that we want to have.

$$\sigma_{noise} = \left(\frac{\sigma_{signal}}{10^{\frac{SNR(dB)}{20}}}\right) \tag{4.15}$$

Using equation 4.14, noise, n of equation 4.10, can be calculated. Then from equation 4.9, image with noise, R, can be constructed.

4.3.7 Accuracy Measurement Result

Employing the developed system to all of the reference images, the developed system has been able to discern vitiligo lesion, the healthy skin and the skin repigmentation areas as shown in Figure 4.14, Figure 4.15, Figure 4.16 and Figure 4.17. Moreover, it can detected skin repigmentation areas whose size are only 1-by-1 pixels as depicted in Figure 4.18

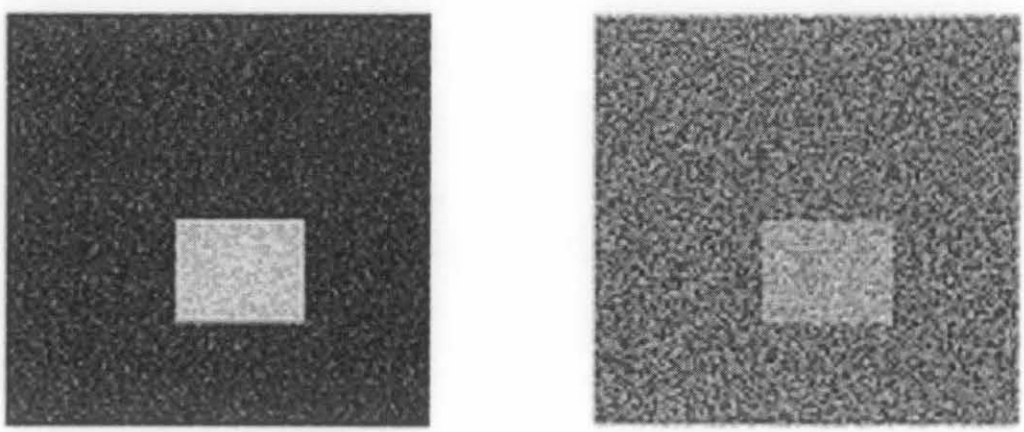

(a) (b)

Figure 4.15 The result of reference image A; (a) Skin areas due to melanin, (b) Skin areas due to haemoglobin

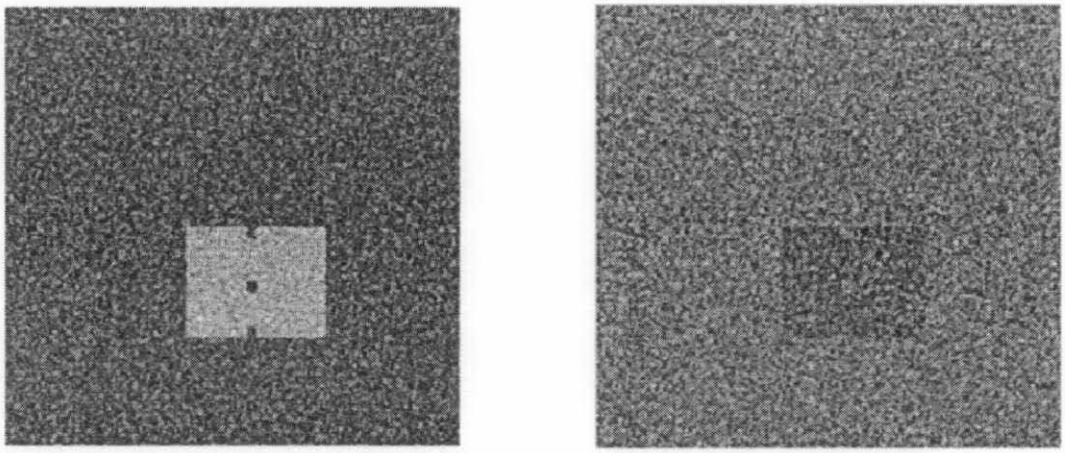

(a) (b)

Figure 4.16 The result of reference image B; (a) Skin areas due to melanin (b) Skin areas due to haemoglobin

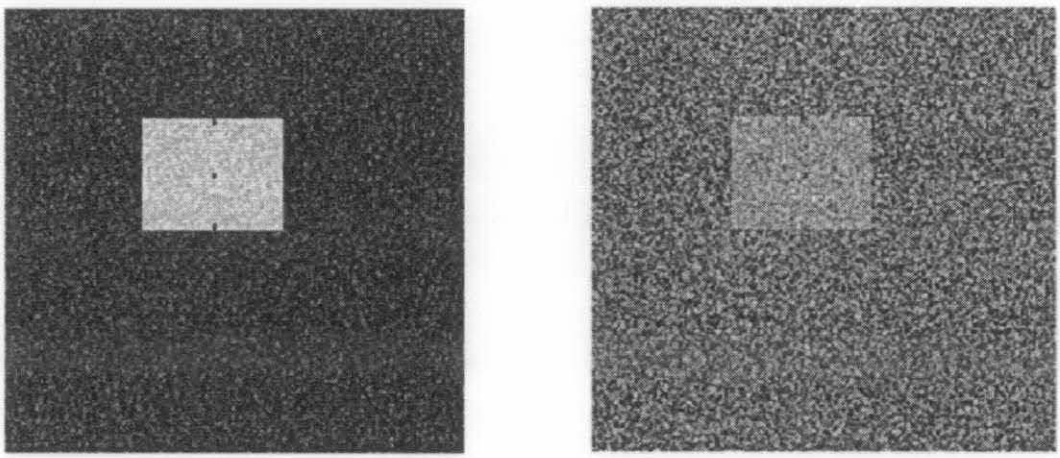

(a) (b)

Figure 4.17 The result of reference image C; (a) Skin areas due to melanin (b) Skin areas due to haemoglobin

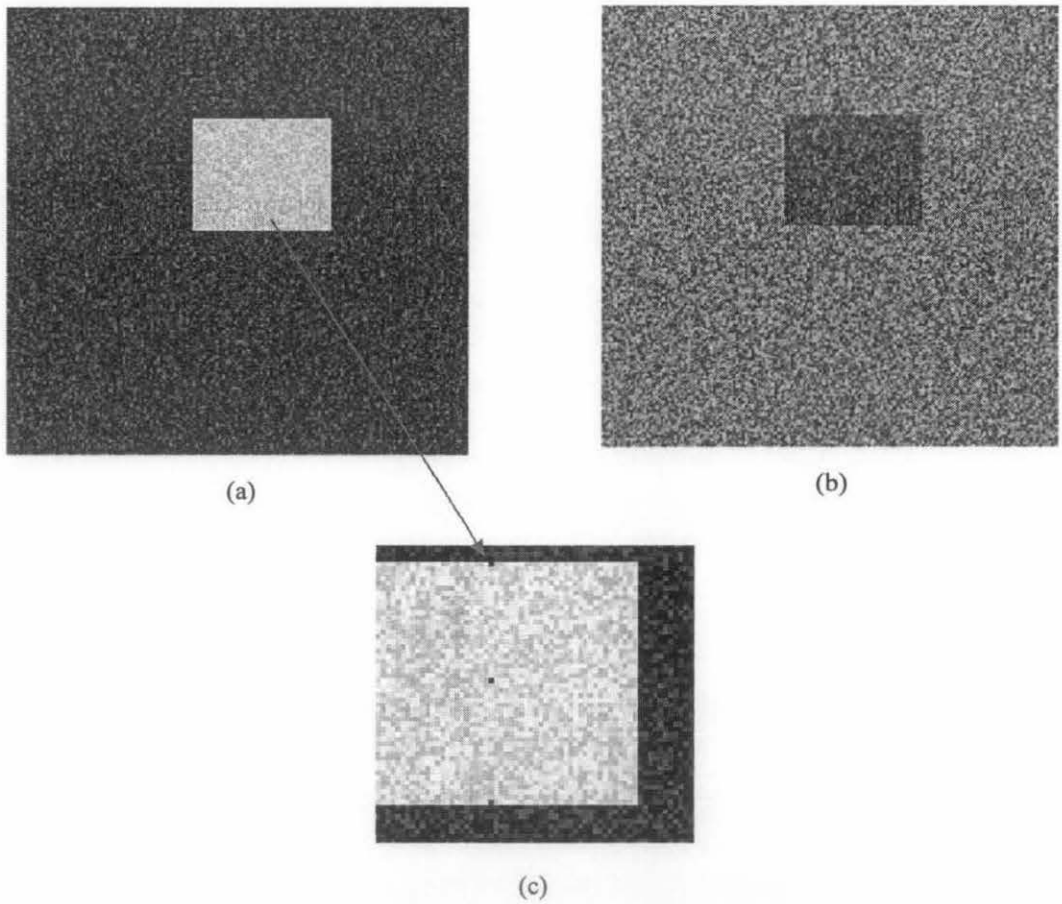

Figure 4.18 The result of the reference image D; (a) Skin areas due to melanin , (b) Skin areas due to haemoglobin, (c) Close-up of repigmentation areas

4.3.8 Noise Limitation Measurement Result

In this section, we test the limitation of the developed system by adding noise to the reference images. The range of SNR used for the test is from 20 dB to 1 dB. From the test, it is found that the developed vitiligo monitoring system can discern the vitiligo lesion, healthy skin and skin repigmentation areas of reference image A, B and C even though the SNR is 1 dB, as shown in Figures 4.19, 4.20 and 4.21.

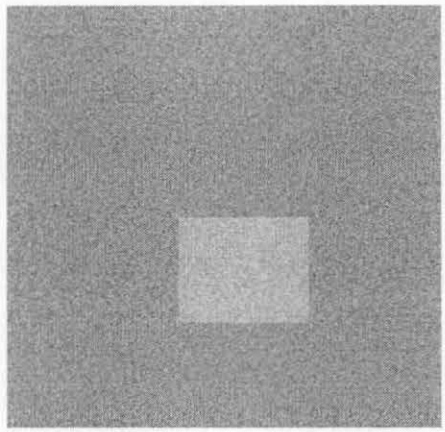

(a)

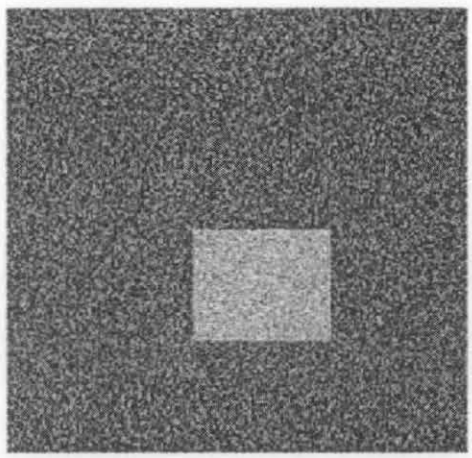

(b)

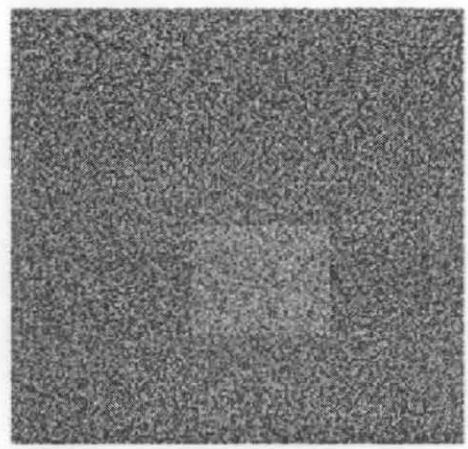

(c)

Figure 4.19 The result of (a) reference image A with noise (SNR=1 dB); (b) Skin areas due to melanin- We can easily determine vitiligo areas- (c) Skin areas due to haemoglobin

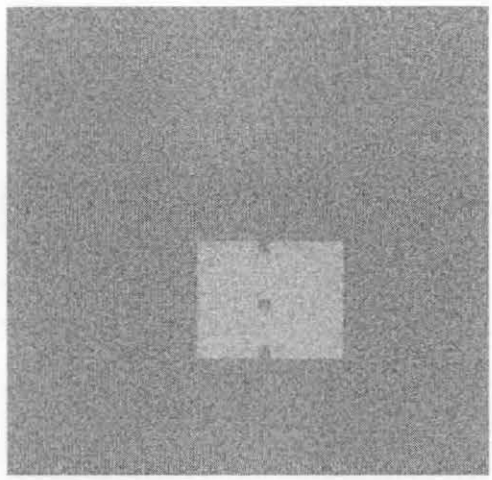

(a)

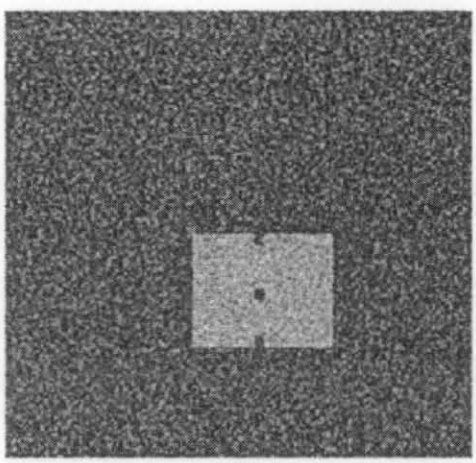

(b)

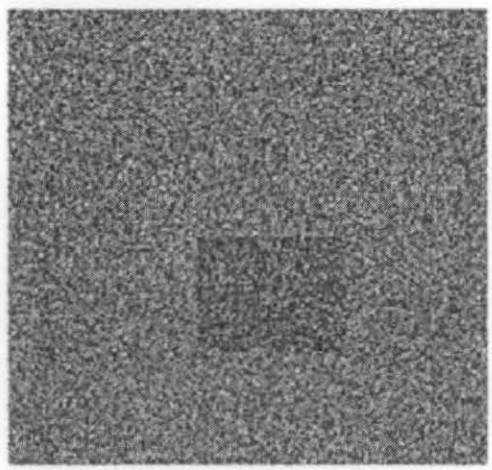

(c)

Figure 4.20 The result of (a) reference image B with noise (SNR=1 dB) ; (b) Skin areas due to melanin- It ican discern the 5-by-5 pixels, skin repigmentation areas in vitiligo lesion; (c) Skin areas due to haemoglobin

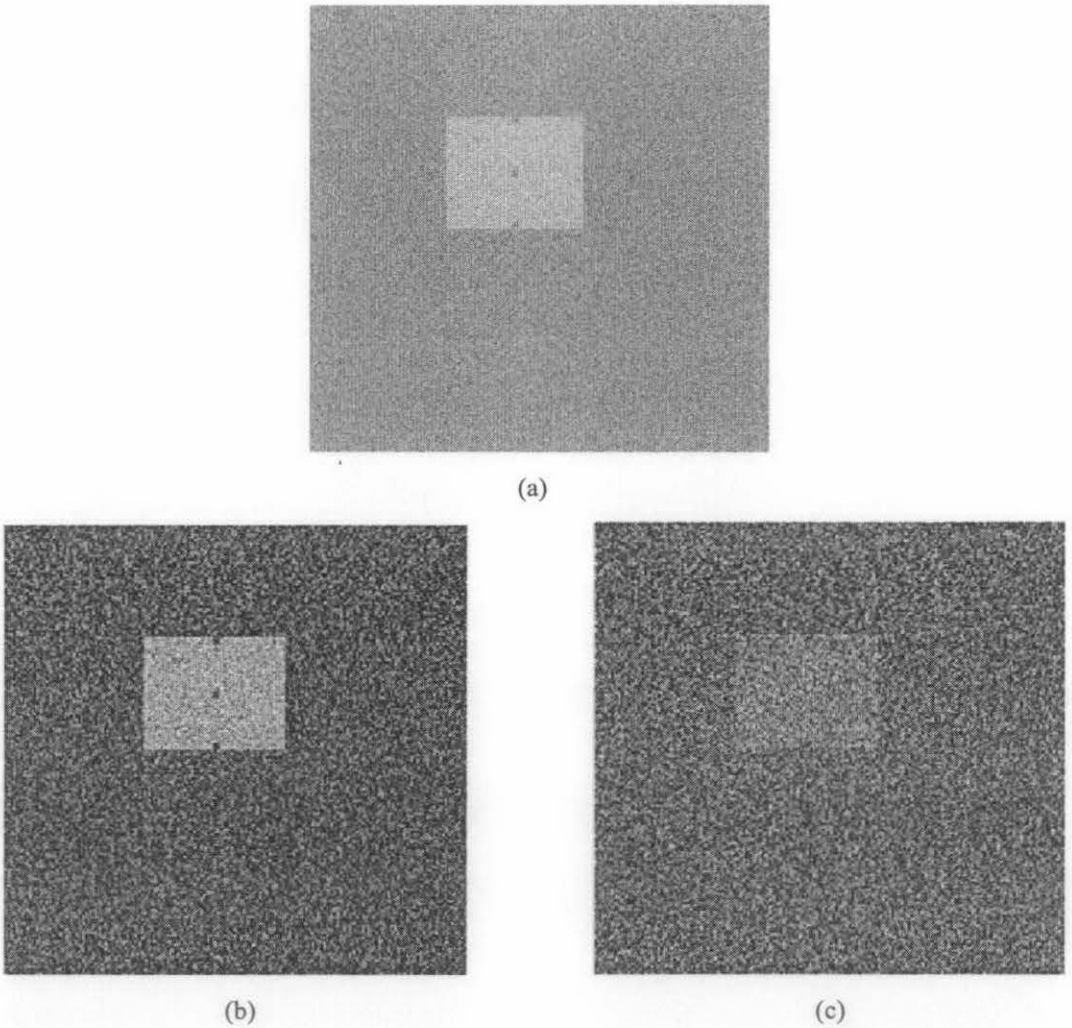

Figure 4.21 The result of (a) reference image C with noise (SNR=1 dB); (b) Skin areas due to melanin- It can determine the 3-by-3 pixels, skin repigmentation areas, in vitiligo lesion; (c) Skin areas due to haemoglobin

However, for reference image D, it is found that if the SNR value less than 15 dB, the repigmentation areas located on the border of lesions and skin are starting to be blurring. Figure 4.23 shows the reference image D with SNR of 15 dB. It can be seen that the repigmentation areas located on the border are still discernable. Figures 4.22 and 4.23 show reference images D with SNR of 14 dB and 13 dB, respectively. The repigmentation areas located on the border are not visible.

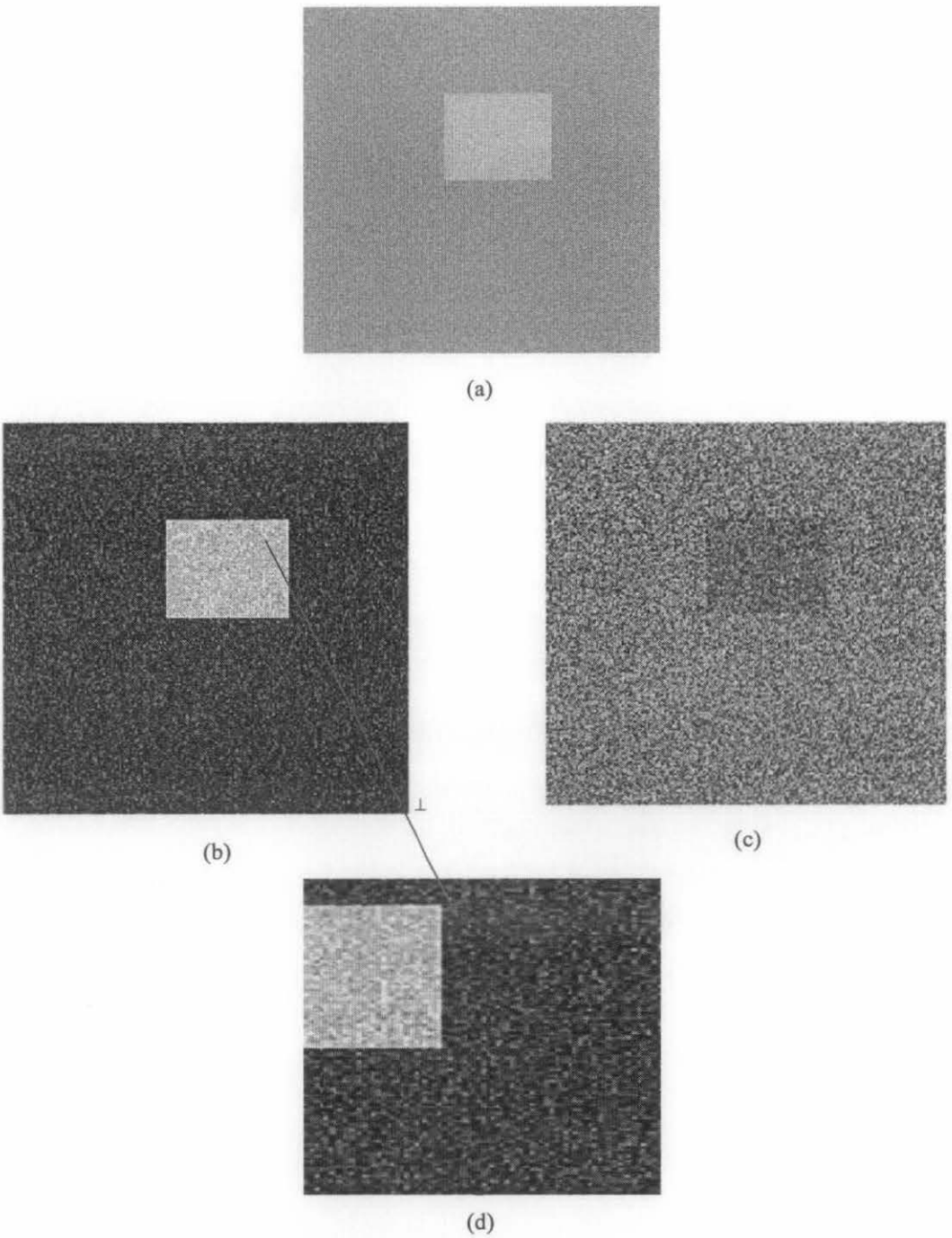

Figure 4.22 The result of (a) reference image D with noise (SNR=15 dB); (b) Skin areas due to melanin; (c) Skin areas due to haemoglobin; (d) Closed up of skin repigmentation areas- The repigmentation areas located on the border are still discrenable.

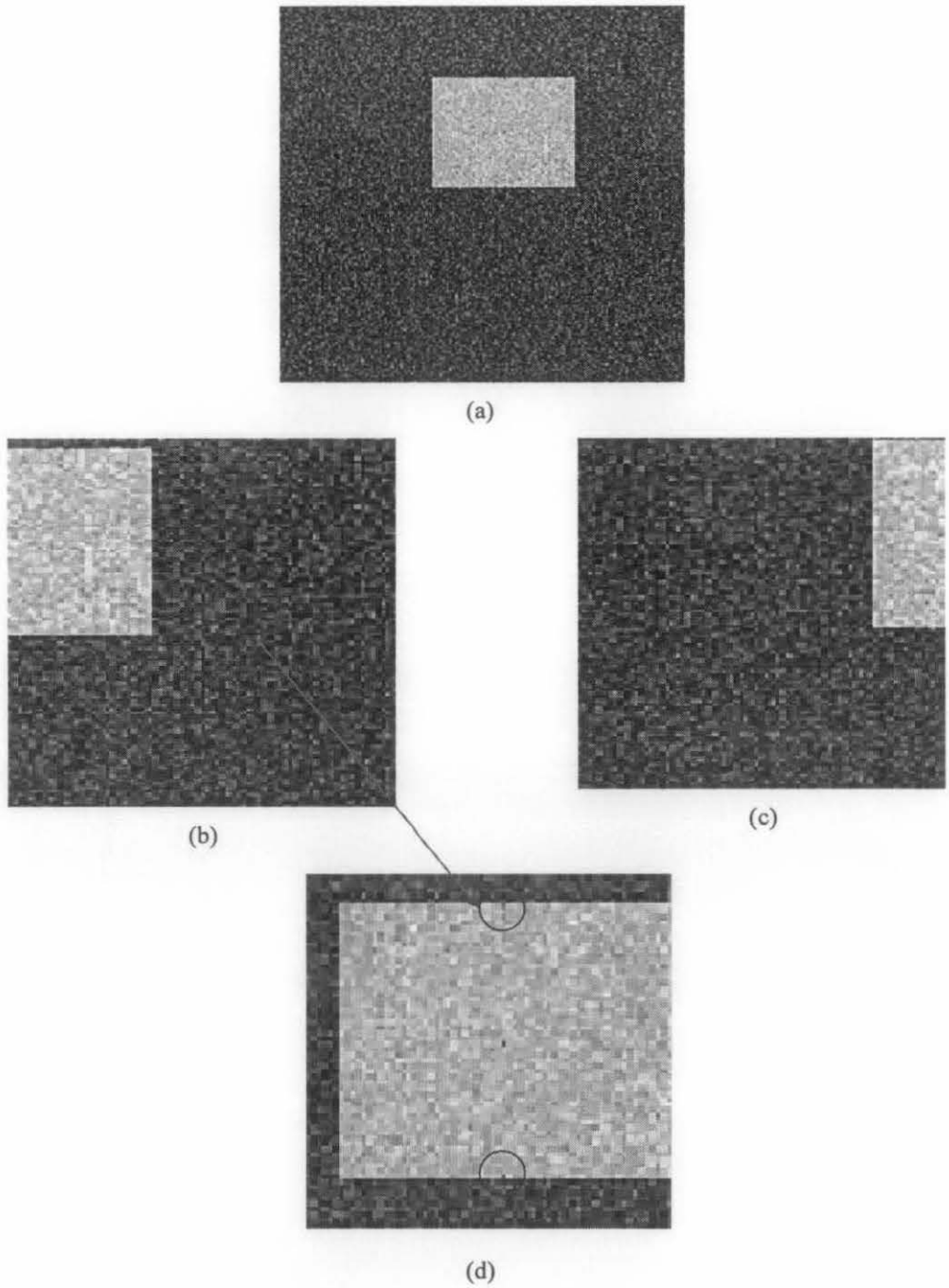

Figure 4.23 The result of (a) reference image D with noise (SNR=14 dB); (b) Skin areas due to melanin- (c) Skin areas due to haemoglobin; (d) Closed up of skin repigmentation areas, the repigmentation areas on the border are not visible.

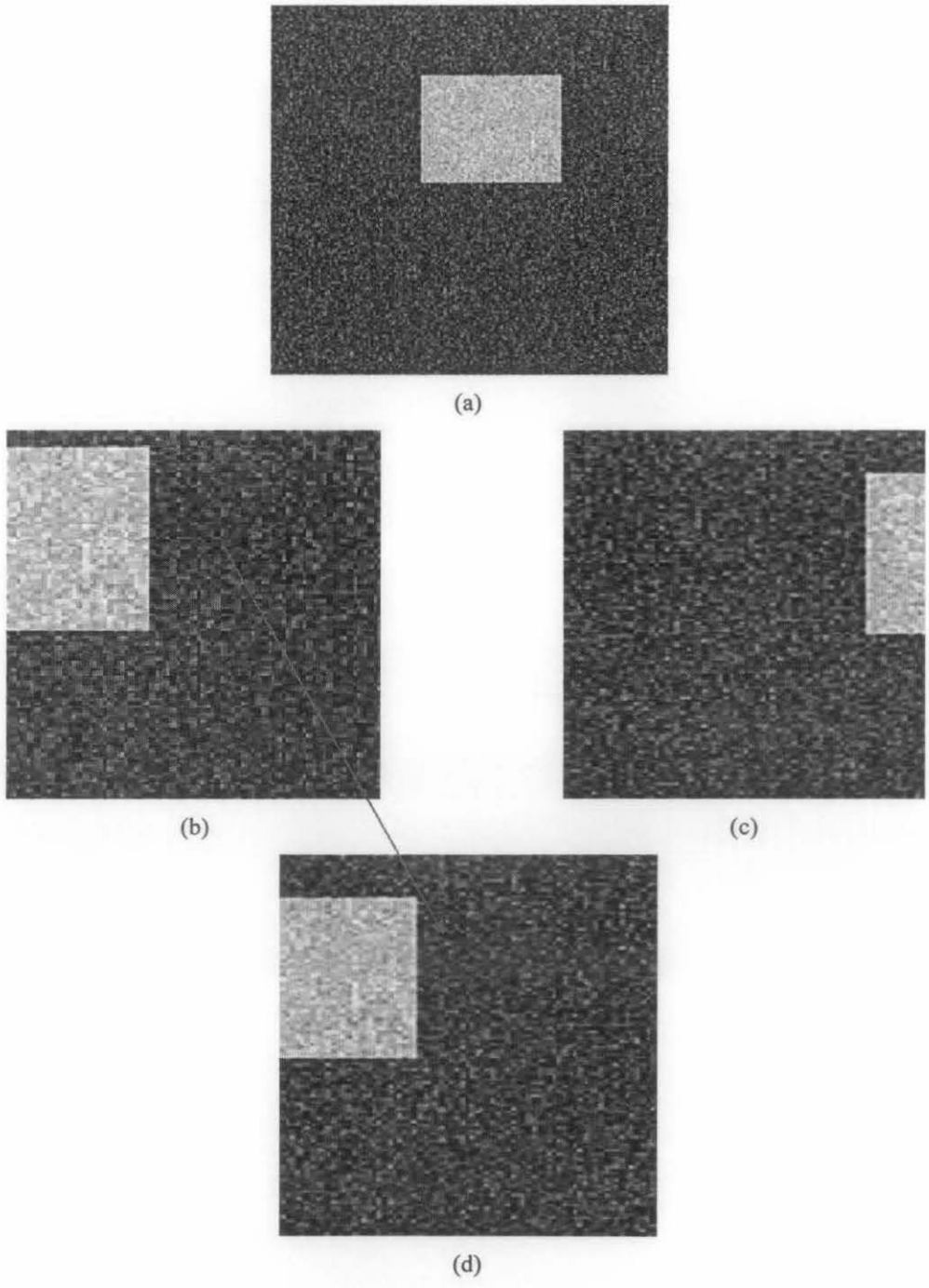

Figure 4.24 The result of (a) reference image D with noise (13 dB); (b) Skin areas due to melanin- (c) Skin areas due to haemoglobin; (d) Closed up of skin repigmentation areas, the repigmentation areas on the border are not visible.

The repigmentation area located in the center of the lesion area starts to fade away when the SNR value is less than 10 dB. Figure 4.25 (SNR = 10dB) shows the lesion is starting to be blurring. Figures 4.26 (SNR = 9dB) and 4.27 (SNR = 8dB) show the lesions are not visible again.

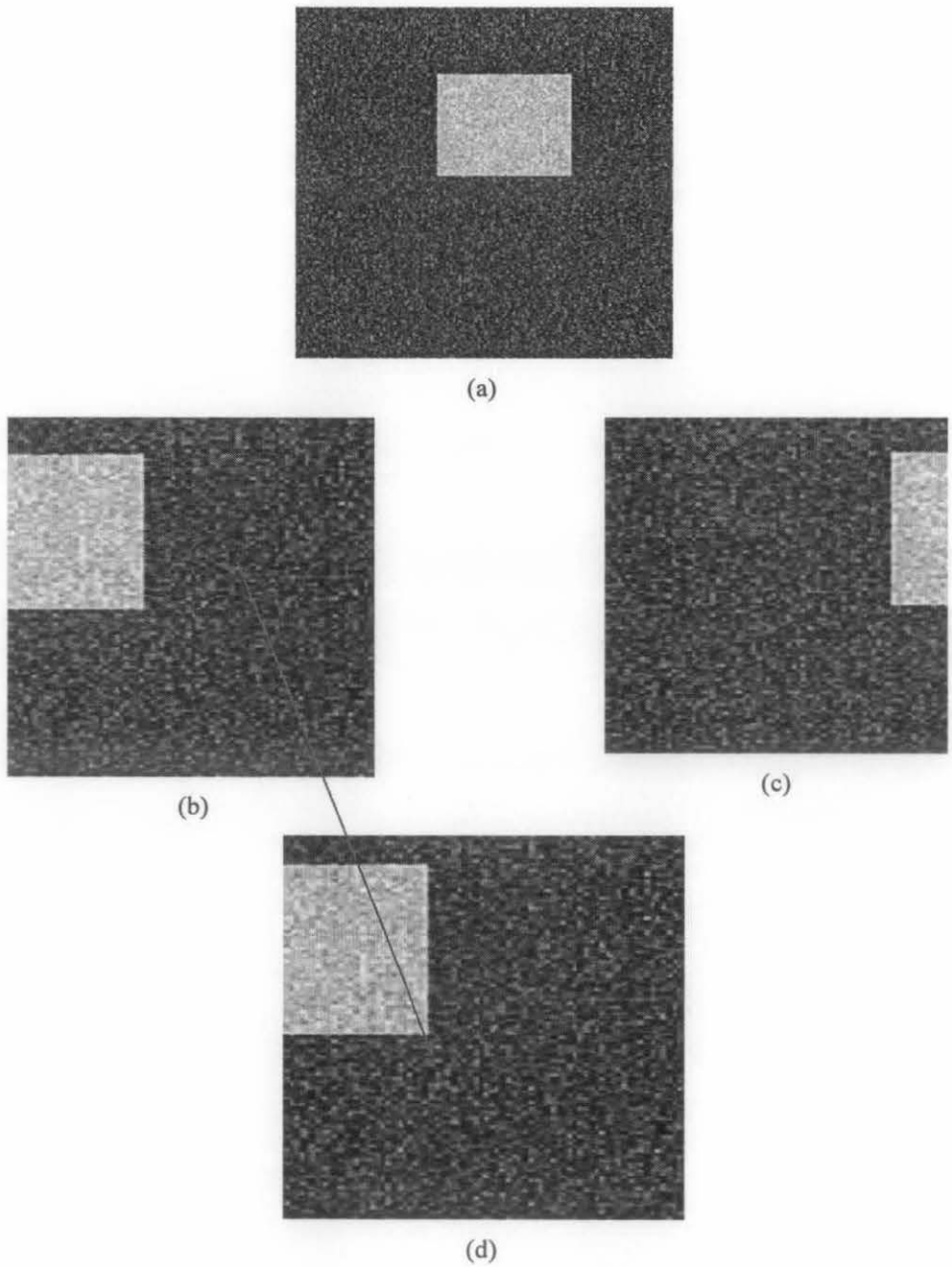

Figure 4.25 The result of (a) reference image D with noise (10 dB); (b) Skin areas due to melanin- (c) Skin areas due to haemoglobin; (d) Closed up of skin repigmentation areas, the repigmentation areas in the center of the lesion starts to fade away.

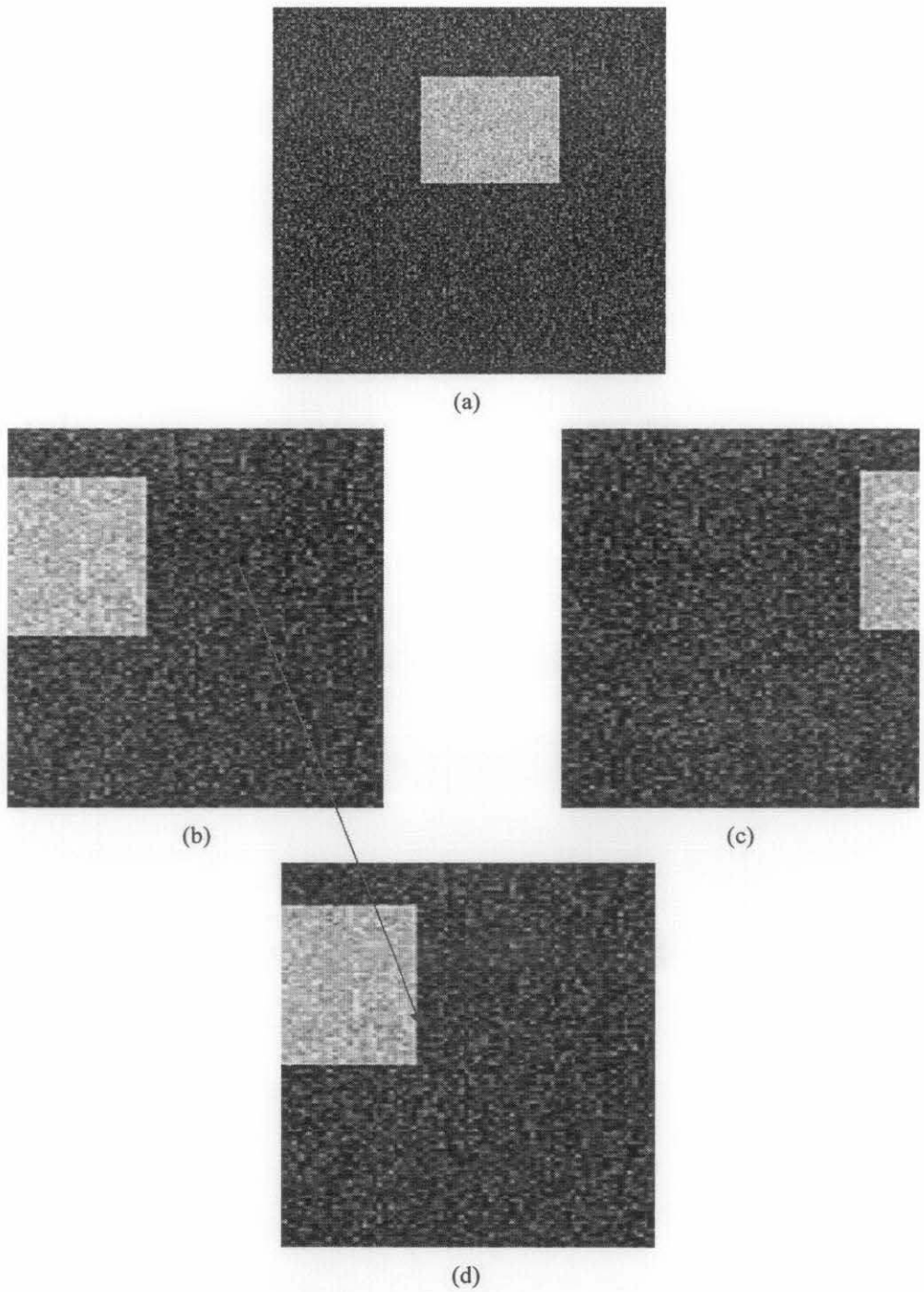

Figure 4.26 The result of (a) reference image D with noise (9 dB); (b) Skin areas due to melanin- (c) Skin areas due to haemoglobin; (d) Closed up of skin repigmentation areas, the repigmentation area in the center of the lesion is not visible again.

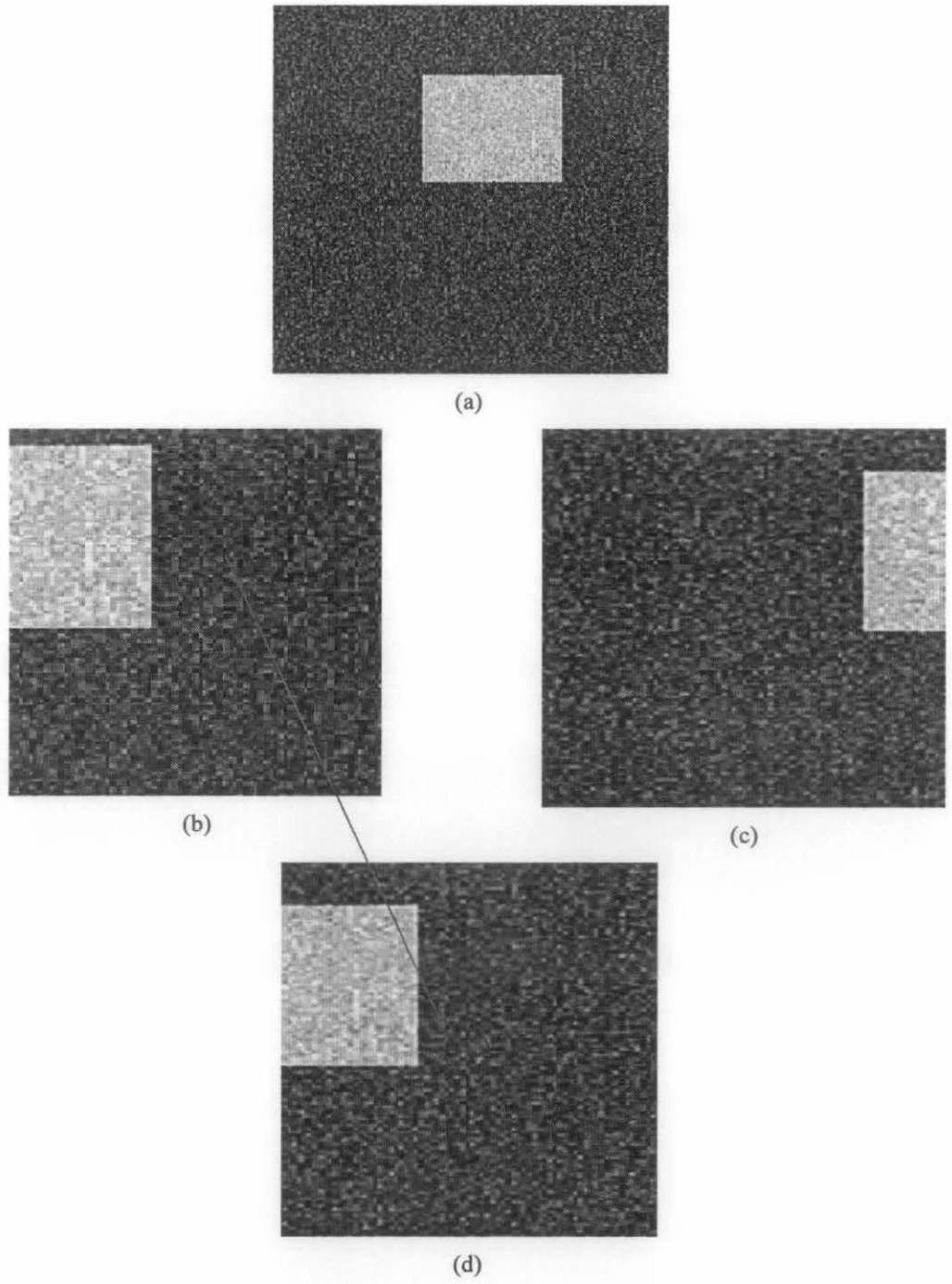

Figure 4.27 The result of (a) reference image D with noise (9 dB); (b) Skin areas due to melanin- (c) Skin areas due to haemoglobin; (d) Closed up of skin repigmentation areas, the repigmentation area in the center of the lesion is not visible again.

4.3.9 Analysis

To measure the accuracy of the vitiligo monitoring system, tests are performed involving reference models A, B, C, and D. As depicted in Figures 4.14-4.17, the method is able to discern vitiligo lesion, the healthy skin and the skin repigmentation areas. Moreover, it can determine skin repigmentation area down to 1-by-1 pixel (Figure 4.17).

Then, the reference images are added with noise before being analyzed by the system. The range of signal-to-noise ratios used for the test is varying from 20 dB to 1 dB. It is found that the method is able to discern the repigmentation areas of reference images A, B, and C even though the signal-to-noise ratio is 1 dB (Figures 4.18, 4.19, and 4.20).

For reference image D, it is shown that if the signal-to-noise ratio is less than 15 dB, the method can not determine the repigmentation areas that are located on the border of vitiligo lesions and skin, as shown in Figures 4.21, 4.22 and 4.23. The method is however still able to identify repigmentation area that are located in the center of the vitiligo lesion area. The repigmentation area located in the center of the vitiligo lesion area can not be captured when the signal-to-noise ratio is less than 10 dB (Figures 4.24, 4.25, and 4.26).

The method is able to capture vitiligo in different areas. It is also shown that it is able to capture small repigmentation areas regardless of the position of the repigmentation areas. However, the method will deteriorate if signal-to-noise ratio decreases. When signal-to-noise ratio is low, the method can not capture small repigmentation areas. The performance of the method also depends on the position of the repigmentation areas. The repigmentation areas that are located on the border of vitiligo and normal skin (Figure 4.23) are harder to be captured than the repigmentations that are located on the center of vitiligo lesion (Figure 4.26).

4.4 Summary

Chapter 4 discussed the development of vitiligo monitoring system algorithm. It also covered the development of skin model and noise generator in order to measure the performance of the developed algorithm in the controlled environment.

Skin color is due to the combination of skin chromophores, namely pigment melanin and haemoglobin. However in digital color image, color is created by combining three different spectral bands: red, green, and blue (RGB). In [Tsumura, 1999], it is found that the spatial distribution of melanin and haemoglobin in skin can be separated by employing linear independent component analysis of a skin color image. The analysis is based on the skin color model with three assumptions. Firstly, it is assumed linearity in the optical density domain of RGB channels. The second and third assumptions state that the spatial variations of skin image color are caused by two skin choromophores, namely melanin and haemoglobin and their quantities are mutually independent, as shown in Figure 4.2. Using this skin color model (Figure 4.3), the developed vitiligo monitoring system converts RGB skin images into images that represent skin areas due to melanin and hemoglobin.

The vitiligo monitoring system is employed in the controlled environment in order to measure its performance and limitation. There are four types of reference images, namely Reference Model Image A, Reference Model Image B, Reference Model Image C, and Reference Model Image D (Figure 4.13). Reference image A is a skin image with vitiligo lesion. Reference image B is similar to reference image A. However, in its vitiligo lesion areas, there are three areas of skin repigmentation. The size of each repigmentation areas is 5-by-5 pixels. Reference image C and reference image D are similar to reference image B. The differences are on the size of the skin repigmentation areas. The size of the repigmentation areas is 3-by-3 pixels, in the reference image C and 1-by-1 pixel, in the reference image D.

References Images are modeled based on the distribution of color combinations in the three spectral bands, namely Red, Green and Blue. Samples of skin color are taken randomly from 6 patients. Next, the distribution of each spectral value is modeled using normal distribution (Gaussian distribution). Noise generator is constructed based on white Gaussian noise.

From experiments, it is found that the developed vitiligo monitoring system can discern the vitiligo lesion, healthy skin and skin repigmentation areas of reference image A, B and C even though the SNR is 1 dB (Figure 4.18, Figure 4.19 and Figure 4.20). For reference image D, it is shown that if the signal-to-noise ratio is less than 15 dB, the system can not determine the repigmentation areas that are located on the border of vitiligo lesions and skin, as shown in Figures 4.21, 4.22 and 4.23. The system is however still able to identify repigmentation area that are located in the center of the vitiligo lesion area. The repigmentation area located in the center of the vitiligo lesion area can not be captured when the signal-to-noise ratio is less than 10 dB (Figures 4.24, 4.25, and 4.26).

The overall trend is the system will deteriorate if signal-to-noise ratio decreases. When signal-to-noise ratio is low, the system can not capture small repigmentation areas. The performance of the system also depends on the position of the repigmentation areas. The system tends to deteriorate more if the repigmentation areas are located on the border of the vitiligo lesion and normal skin.

Chapter 5

RESULTS AND ANALYSIS

5.1 Introduction

As described in Chapter 2, the developed vitiligo monitoring system is employed on the real images provided by Hospital Kuala Lumpur, Malaysia. The collaborative research is focused on developing an objective and accurate skin repigmentation assessment tool for vitiligo monitoring.

Patients for this collaborative research are chosen by a dermatologist. The images of the vitiligo lesions are the taken using Nikon digital camera SLR D100. The research was divided into two phases, namely preliminary study and pre-clinical trial. For the first phase of the development of the vitiligo monitoring system, historical data was used. To further validate and improve the system, a second data set was taken during pre-clinical trial.

5.2 Preliminary Study

The preliminary study involved images of vitiligo lesion taken from historical data of 4 different patients taken before treatment and during treatment. The vitiligo monitoring system was used to determine the repigmentation by comparing the images. Figure 5.1 shows images of vitiligo skin samples from patient 1, patient 2, patient 3 and patient 4. The images refer to the same skin area and were taken during the course of treatment. As seen from the figures, the progression of the repigmentation is clearly visible for patient 1, patient 2 and patient 3 after more than 10 months of treatment. However, for patient 4, in which case the treatment has been going on for only 4 months, repigmentation is not visible from the figure.

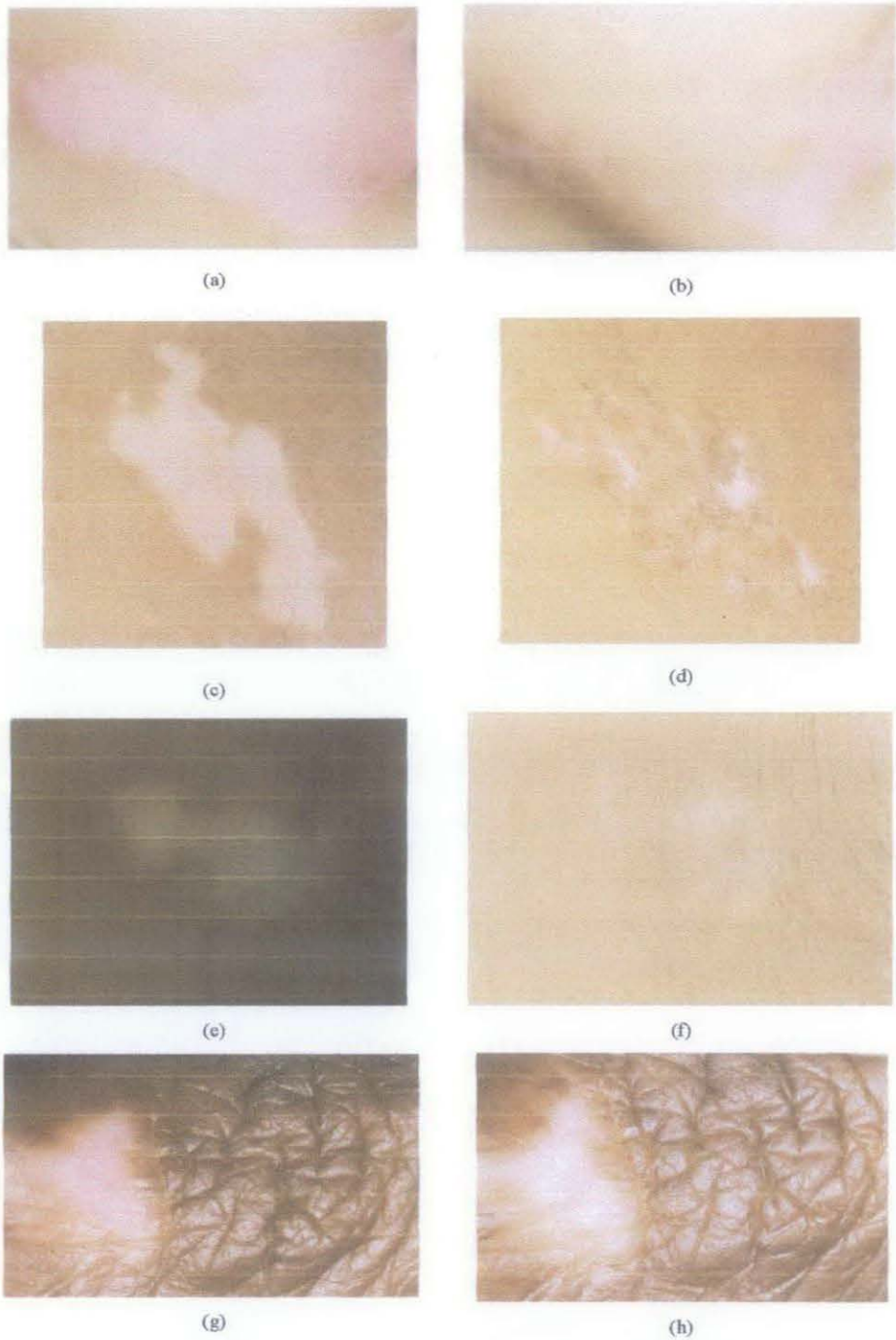

Figure 5.1 Patient 1 (a) RGB image taken on November 2003 (b) RGB image taken on November 2004; Patient 2 (c) RGB image taken on July 2004 (d) RGB image taken on July 2005;Patient 3 (e) RGB image taken on March 2003 (f) RGB image taken on October 2004; Patient 4 (g) RGB image taken on October 2005, (h) RGB image taken on February 2006

The vitiligo monitoring system applied on the RGB skin images of patients 1, 2, 3 and 4 produced images that now represent the skin due to melanin and haemoglobin only as shown in Figure 5.2.

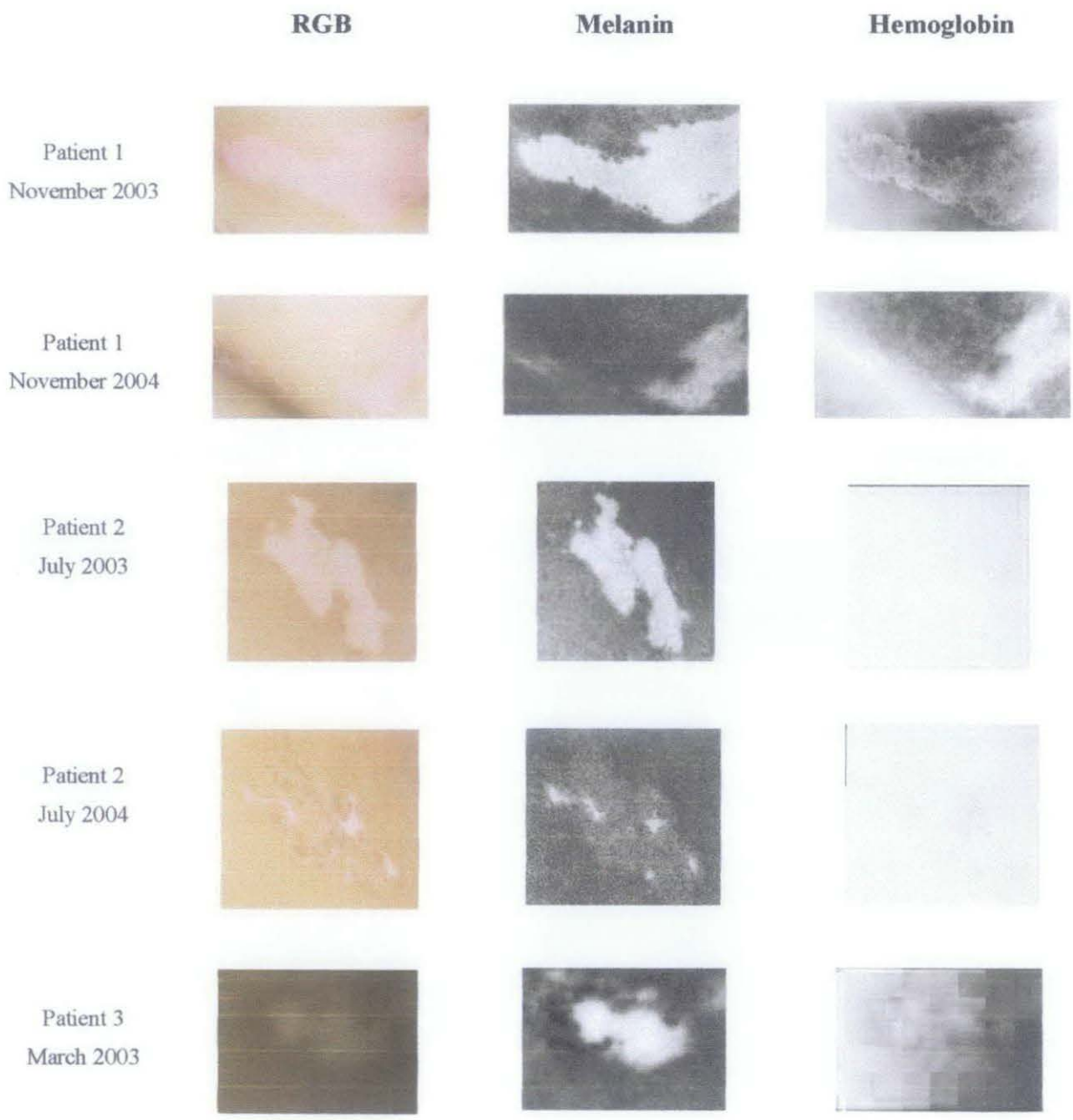

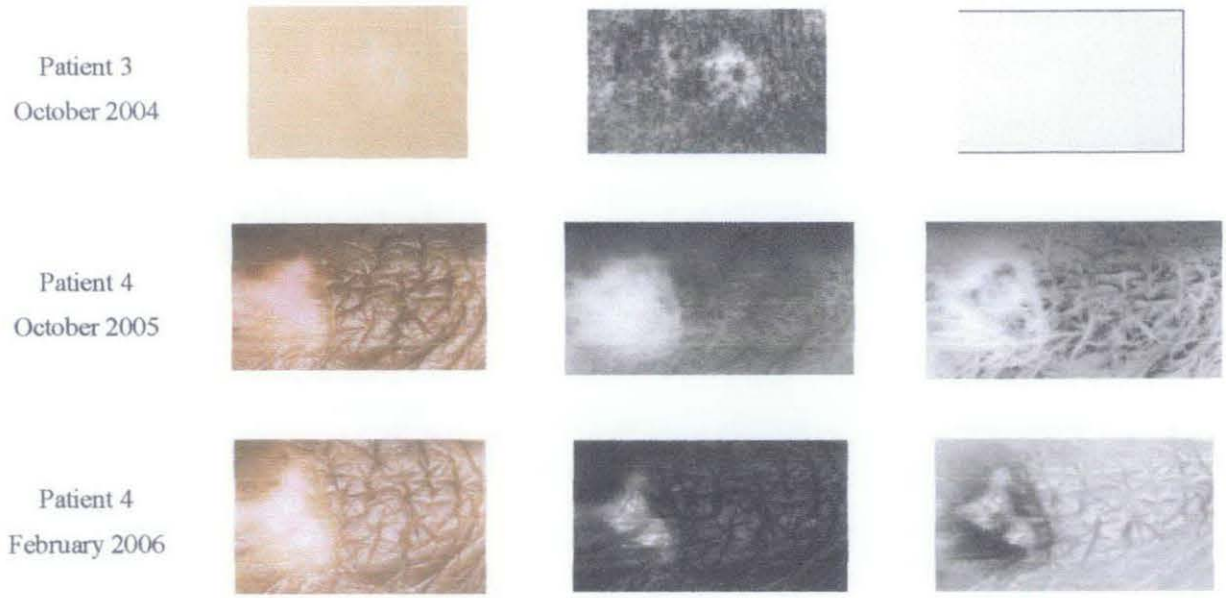

Figure 5.2 Processed images of Patients 1, 2, 3 and 4

Segmentation performed on the melanin images as shown in Figure 5.3. The segmented images of melanin represent vitiligo lesion areas. The non-melanin/vitiligo lesion areas after treatment can be seen smaller due to repigmentation, even for patient 4. In the historical data, the images that refer to the same lesion areas are assumed to have similar size. If the size is not the same, the images are adjusted accordingly. This is to ensure the accuracy and the objectivity of the system.

The system computed that for patient 1, the determined non-melanin area for November 2003 image is 26,263 pixels and for November 2004 image, the area is 8,907 pixels indicating repigmentation progression of 66 %. For patient 2, the non-melanin area for July 2003 image is 20,848 pixels and for July 2004 image, the areas is 1,543 pixels indicating repigmentation progression of 94%. For patient 3, the non-melanin area for March 2003 image is 1,656 pixels and for October 2004 image, the area is 133 pixels indicating repigmentation progression of 92%. For patient 4, the non-melanin area for October 2005 image is 585 pixels and for February 2006 image, the areas is 432 pixels indicating repigmentation progression of 26%. In comparison, the dermatologist

repigmentation score and scale based on Physician's Global Assessment is found to be in moderate scale (51%-75% range) for patient 1, and mild (0-25% range) for patient 4.

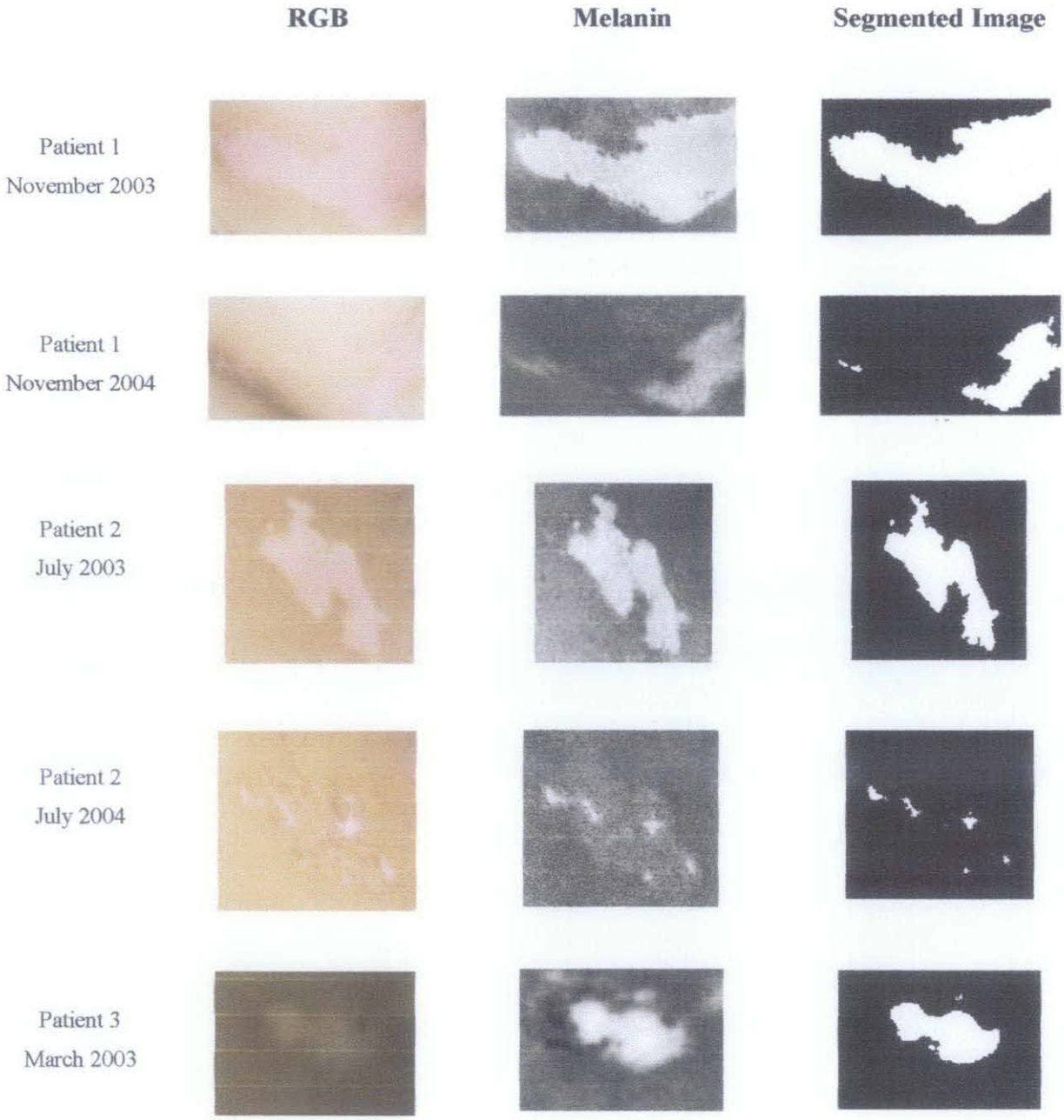

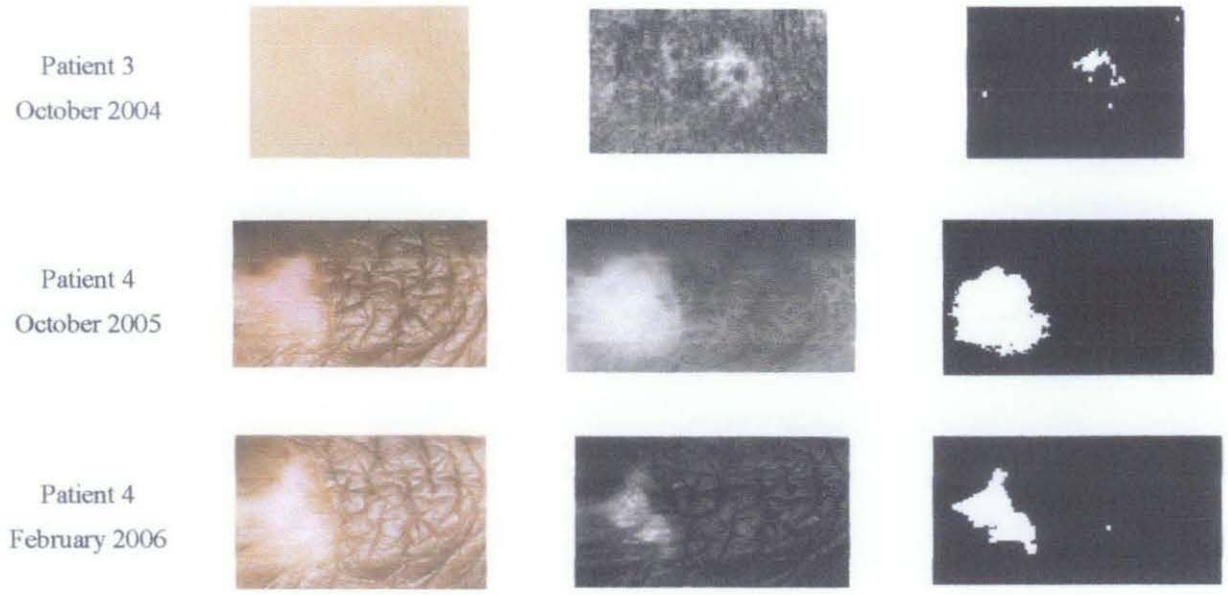

Figure 5.3 Segmented images of Patients 1, 2, 3 and 4

Using the measurements provided in Table 5.1, the repigmentation progression due to the vitiligo treatment can be determined objectively in percentages as shown in Table 5.2. Table 5.2 also compares repigmentation assessment by Physician's Global Assessment and our proposed method.

Table 5.1 Determination of vitiligo skin areas using developed method

	Time Interval	Vitiligo Skin Areas (pixels)
Patient 1	November 2003	26,263
	November 2004	8,907
Patient 2	July 2004	20,848
	July 2005	1,535
Patient 3	March 2003	1,656
	October 2004	133
Patient 4	October 2005	585
	February 2006	432

Table 5.2 Comparison between physician's global assessment (PGA) and developed method

	PGA	Developed Method
Patient 1	51%-75%	66%
Patient 2	76%-100%	94%
Patient 3	76%-100%	92%
Patient 4	0-25%	26%

It is clearly seen that the percentages obtained using the vitiligo monitoring system are within the Physician's Global Assessment ranges except for the case of Patient 4. In the case of Patient 4, the images were taken within 4 months of treatment therefore repigmentation has occurred on a smaller area. It is difficult for dermatologist to discern visually small repigmentation progression due to the treatment. The vitiligo monitoring system however, is able to capture small repigmentation progression objectively and proves to be potentially superior as it allows monitoring on a smaller time frame.

5.3 Pre-Clinical Trial Study

During clinical trial study, 5 patients are chosen by dermatologists as our data set. The data set involves images of vitiligo lesion taken from 4 patients. The images are taken before and after treatment with smaller interval of 6 weeks. The patients come from different ethnic origins.

5.3.1 Reference Images

From the preliminary study, it is imperative to determine the true image size and area to make accurate comparisons. Since the position or distance of the photographer from the patient is not necessity the same every time during data collection, a reference image of

known size and area is needed during data collection. A reference object of a known size and area is placed on the skin.

Gonzales suggested having green color as color background in order to focus solely on the region of interest [Gonzales, 2003]. We use a rectangular green tape as a reference image of known size on the skin under investigated. Figure 5.2 shows an example of a reference image in the data. The actual of this reference image is 1.13×10^2 mm^2.

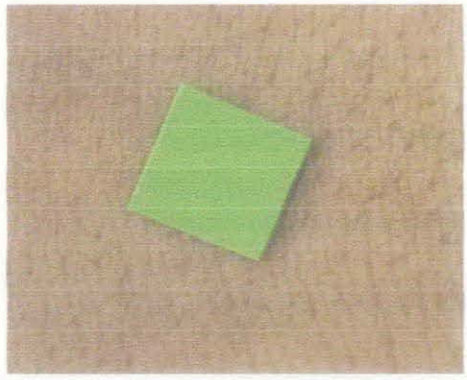

Figure 5.4 1.13×10^2 mm^{2}green tape as a reference

In order to determine the area represented by 1 square pixel, we segment the reference from the image. This is achieved by performing an image segmentation process. From the green spectral band of image, the green reference is segmented by employing Otsu's method. This technique has been described earlier in Section 3.

Figure 5.5 shows the green spectral band of Figure 5.4. The threshold selection is then selected by maximizing the between class variance within the histogram data (Section 3), as shown in figure 5.6. The result is a logical image, as shown in Figure 5.7. The reference image is found to have an area of 24625 pixels. It can be concluded that in that particular image (Figure 5.4), 1-by-1 pixel represents 4.5888×10^{-3} mm^2.

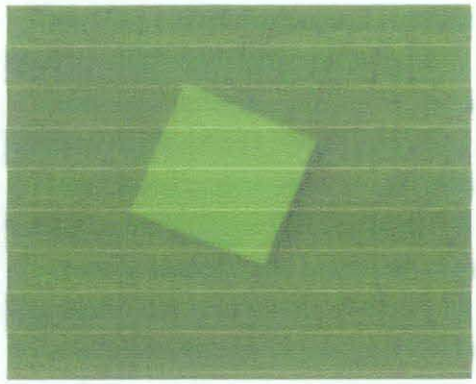

Figure 5.5 Green band of reference image

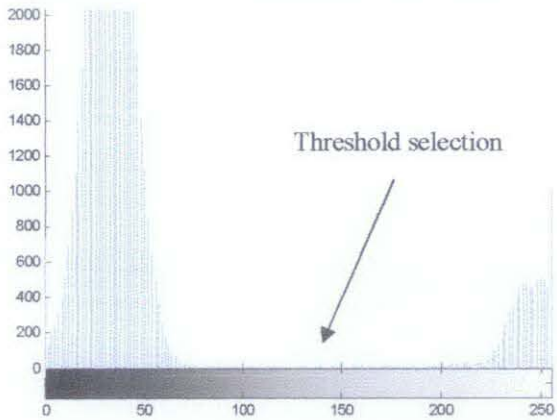

Figure 5.6 Histogram of reference image

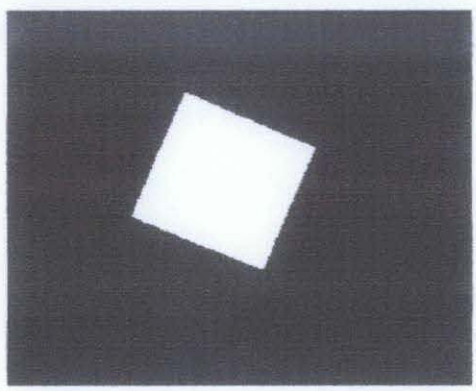

Figure 5.7 Logical image of reference image

5.3.2 Patient Data

Skin images of patient are taken with digital camera SLR Nikon D-100. The first RGB images are used as a base liner and are all taken on 17th July 2007. For treatment, all of the patients are given tacrolimus ointment. The second RGB images are then taken after 6 weeks of treatment. Figures 5.8-5.16 show the skin images of patient A, B, C, D, and E before and after 6 weeks of treatment. Figure 5.8 shows vitiligo lesion areas on the face of patient A. Patient B has two vitiligo lesion areas. Figure 5.9 and 5.10 show the lesion areas of patient B, one on the lower limb and the other on the feet, respectively. Figure 5.11 shows vitiligo lesion areas on face of patient C. Similar to patient B, patient D has more than one location of vitiligo areas. There are four locations, one on the neck, one on the trunk, one on the upper limb and the last one is on the lower limb area. Figure 5.12, Figure 5.13, Figure 5.14 and Figure 5.15 show the lesion areas of Patient D. Figure 5.16 shows the vitiligo lesion areas on the face of patient E.

Patient A

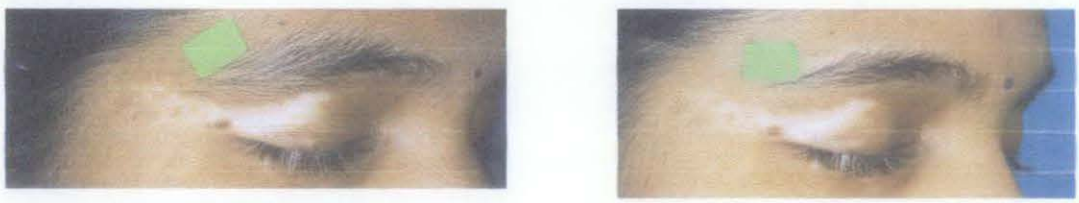

(a) (b)

Figure 5.8 (a) RGB image taken on 17th July 2007, (b) RGB image taken on 28th August 2007

Patient B – Lower Limb

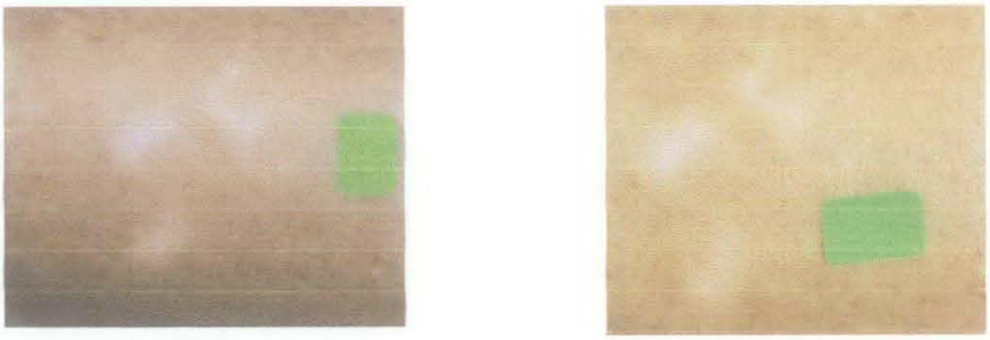

(a) (b)

Figure 5.9 (a) RGB image taken on 17th July 2007, (b) RGB image taken on 28th August 2007

Patient B – Feet

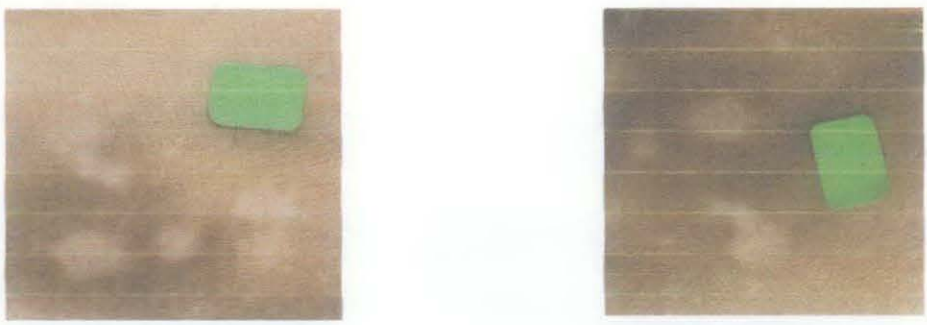

(a) (b)

Figure 5.10 (a) RGB taken on 17th July 2007, (b) RGB taken on 28th August 2007

Patient C – Face

(a) (b)

Figure 5.11 (a) RGB image taken on 17th July 2007, (b) RGB image taken on 28th August 2007

Patient D – Neck

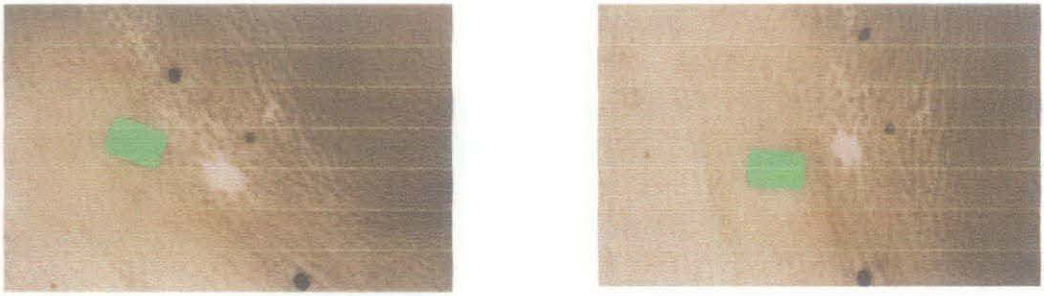

(a) (b)

Figure 5.12 (a) RGB image taken on 17th July 2007, (b) RGB image taken on 28th August 2007

Patient D – Trunk

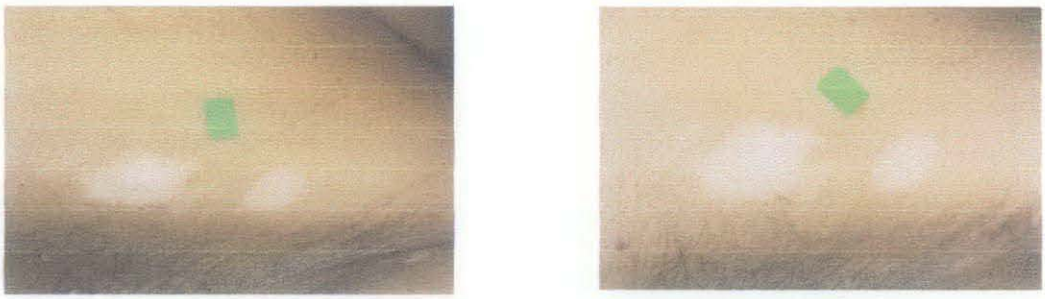

(a) (b)

Figure 5.13 (a) RGB image taken on 17th July 2007, (b) RGB image taken on 28th August 2007

Patient D – Upper Limb

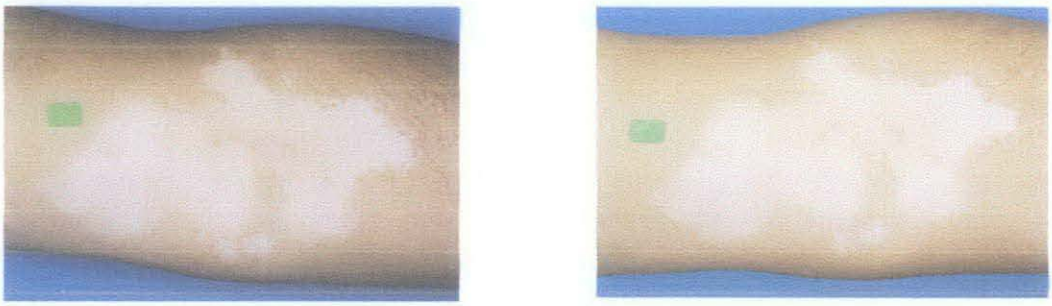

(a) (b)

Figure 5.14 (a) RGB image taken on 17th July 2007, (b) RGB image taken on 28th August 2007

Patient D – Lower Limb

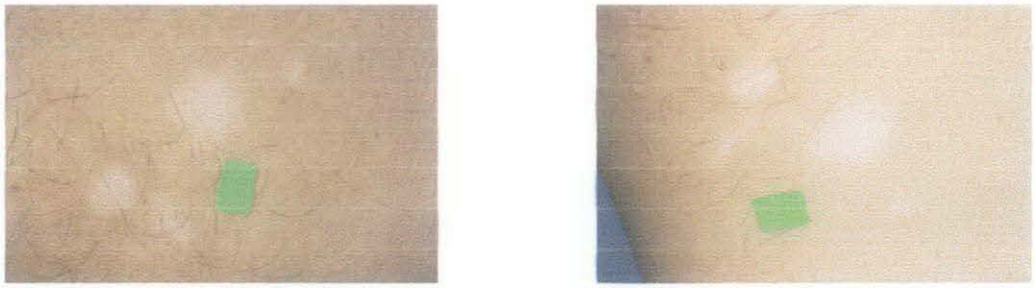

(a) (b)

Figure 5.15 (a) RGB image taken on 17th July 2007, (b) RGB image taken on 28th August 2007

Patient E – Face

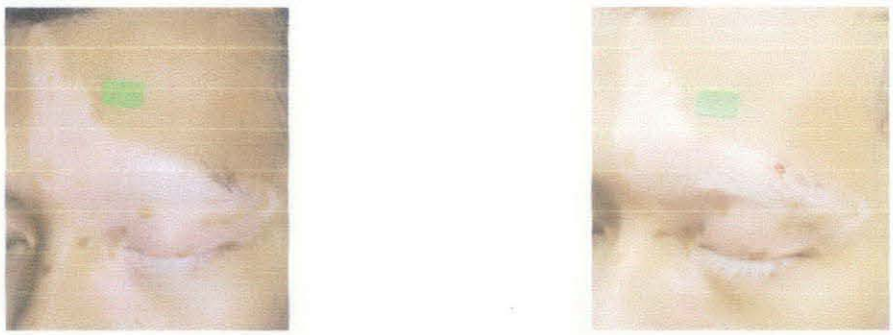

(a) (b)

Figure 5.16 (a) RGB image taken on 17 July 2007, (b) RGB image taken on 28th August 2007

The vitiligo monitoring system applied on the RGB skin images of patients A, B, C, D and E produced images that now represent the skin due to melanin and haemoglobin only as shown from Figure 5.17 to Figure 5.25.

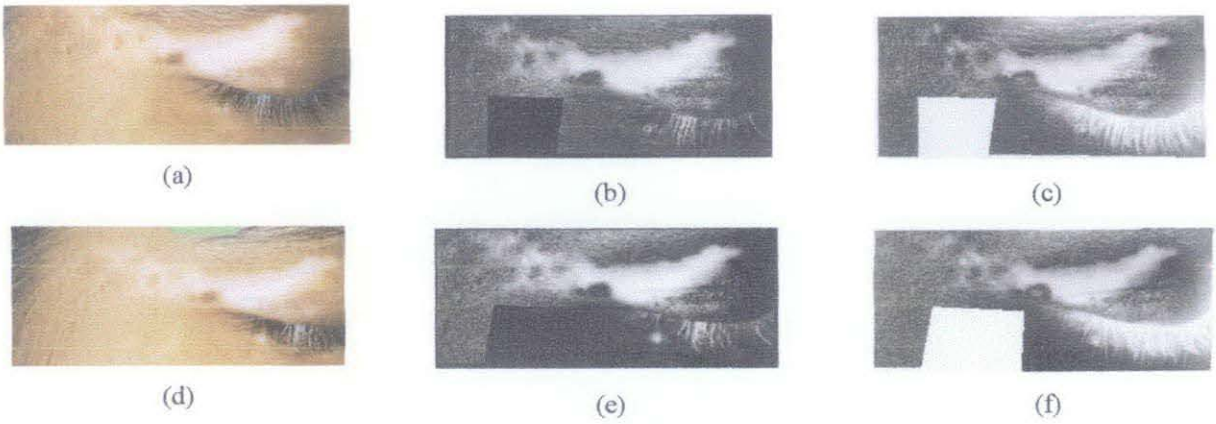

Figure 5.17 Processed images of lesions on the face of patient A: (a) RGB image – 17th July 2007 (b) Melanin-17th July 2007, (c) Haemoglobin -17th July 2007, (d) RGB image – 28th August 2007, (e) Melanin – 28th August 2007, (f) Haemoglobin – 28th August 2007

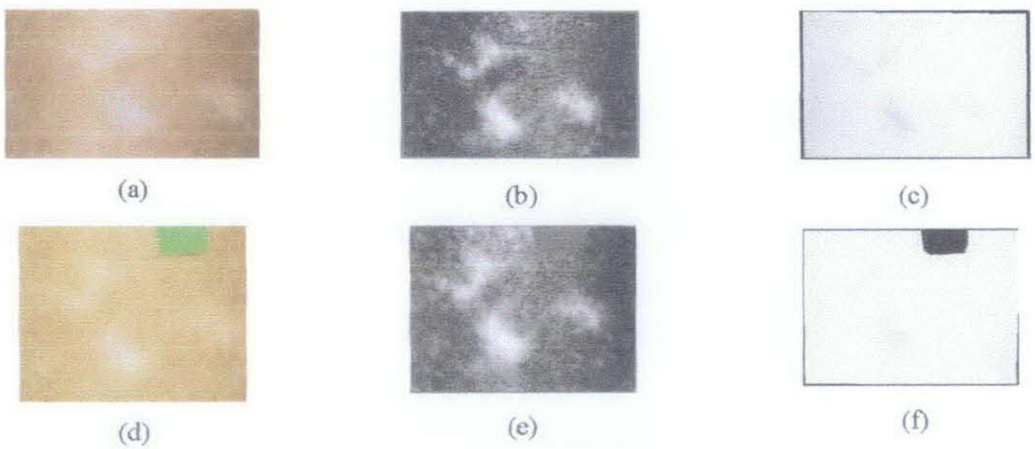

Figure 5.18 Processed images of lesions on the lower limb of Patient B: (a) RGB image – 17th July 2007, (b) Melanin-17th July 2007, (c) Haemoglobin -17th July 2007, (d) RGB image – 28th August 2007, (e) Melanin – 28th August 2007, (f) Haemoglobin – 28th August 2007

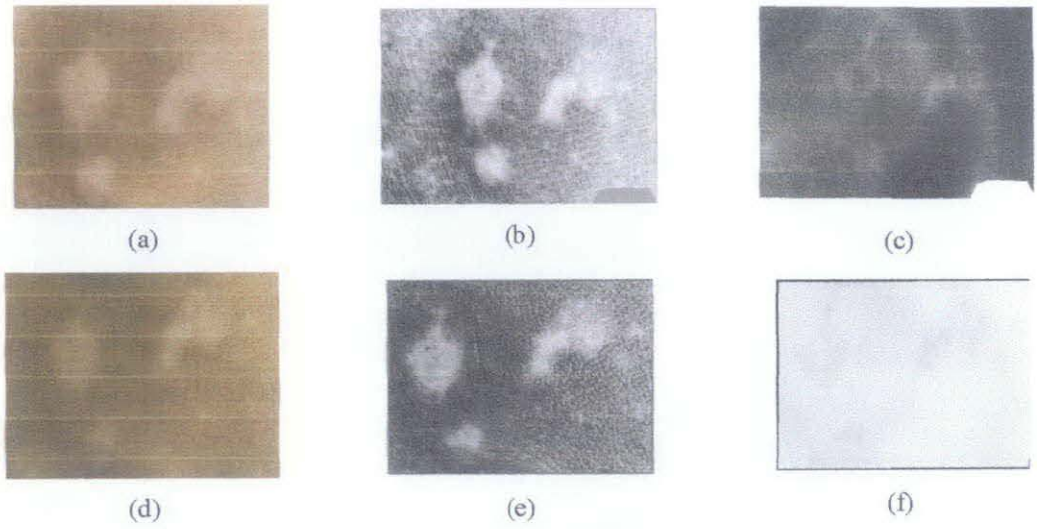

Figure 5.19 Processed images of lesions on feet of Patient B: (a) RGB image – 17th July 2007, (b) Melanin-17th July 2007, (c) Haemoglobin -17th July 2007, (d) RGB image – 28th August 2007 (e) Melanin – 28th August 2007, (f) Haemoglobin – 28th August 2007

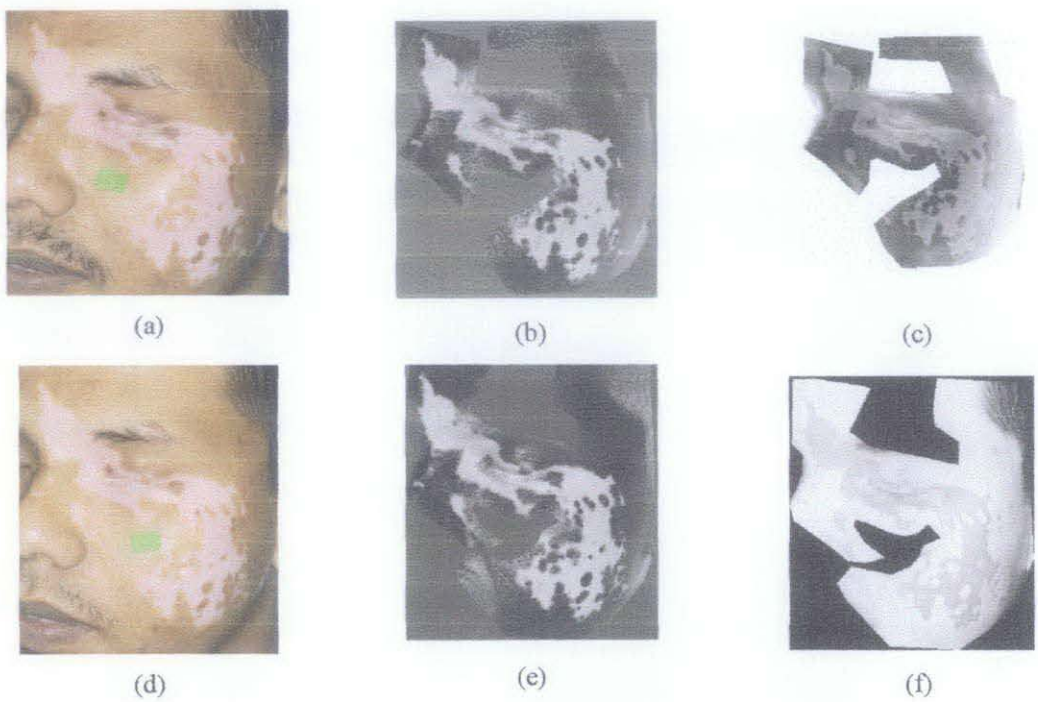

Figure 5.20 Processed images of lesions on the face of Patient C: (a) RGB image – 17th July 2007, (b) Melanin-17th July 2007, (c) Haemoglobin -17th July 2007, (d) RGB image – 28th August 2007, (e) Melanin – 28th August 2007, (f) Haemoglobin – 28th August 2007

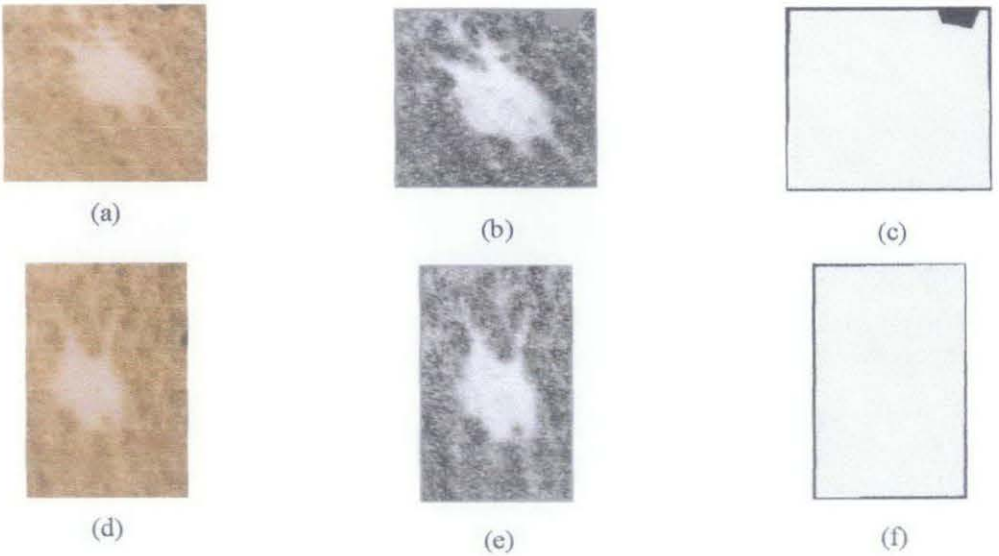

Figure 5.21 Processed images of lesions on the neck of Patient D: (a) RGB image – 17th July 2007, (b) Melanin-17th July 2007, (c) Haemoglobin -17th July 2007, (d) RGB image – 28th August 2007, (e) Melanin – 28th August 2007, (f) Haemoglobin – 28th August 2007

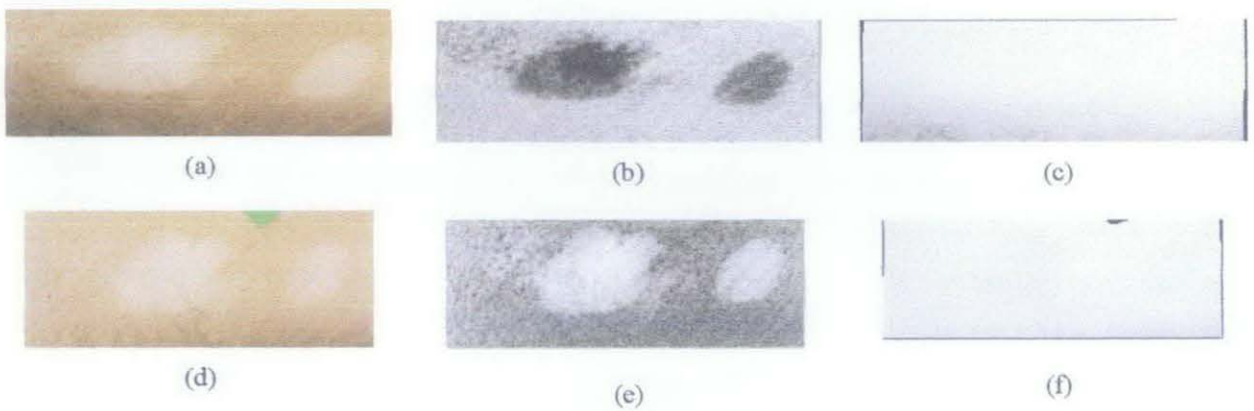

Figure 5.22 Processed images of lesions on the trunk of Patient D: (a) RGB image – 17th July 2007, (b) Melanin-17th July 2007, (c) Haemoglobin -17th July 2007, (d) RGB image – 28th August 2007, (e) Melanin – 28th August 2007, (f) Haemoglobin – 28th August 2007

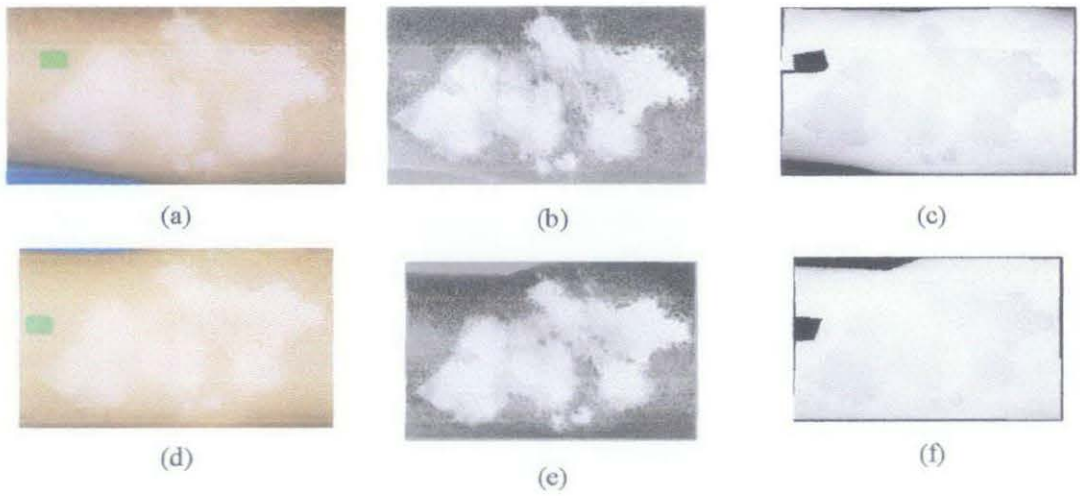

Figure 5.23 Processed images of lesions on the upper limb of Patient D: (a) RGB image – 17th July 2007, (b) Melanin-17th July 2007, (c) Haemoglobin -17th July 2007, (d) RGB image – 28th August 2007, (e) Melanin – 28th August 2007, (f) Haemoglobin – 28th August 2007

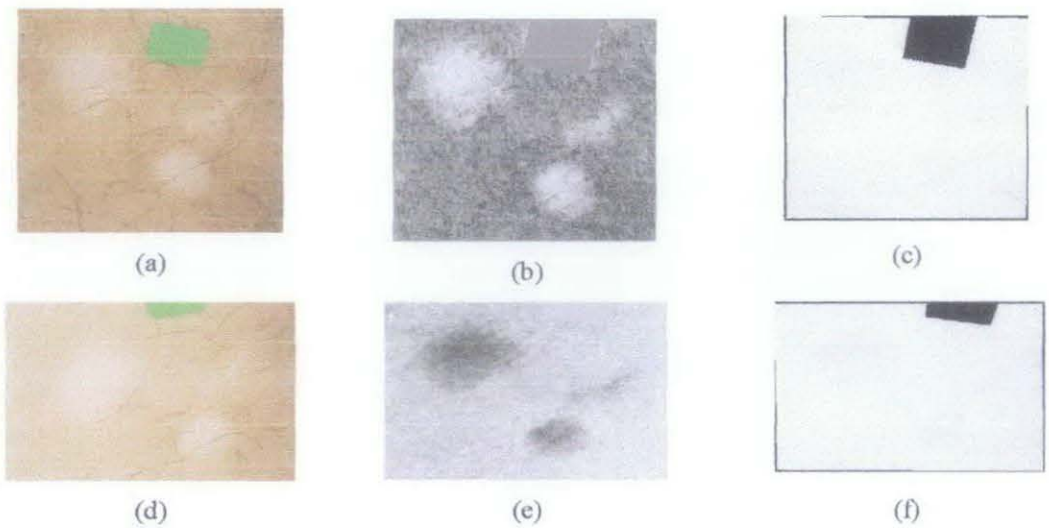

Figure 5.24 Processed images of lesions on the lower limb of Patient D: (a) RGB image – 17th July 2007, (b) Melanin-17th July 2007, (c) Haemoglobin -17th July 2007, (d) RGB image -28th August 2007, (e) Melanin – 28th August 2007, (f) Haemoglobin – 28th August 2007

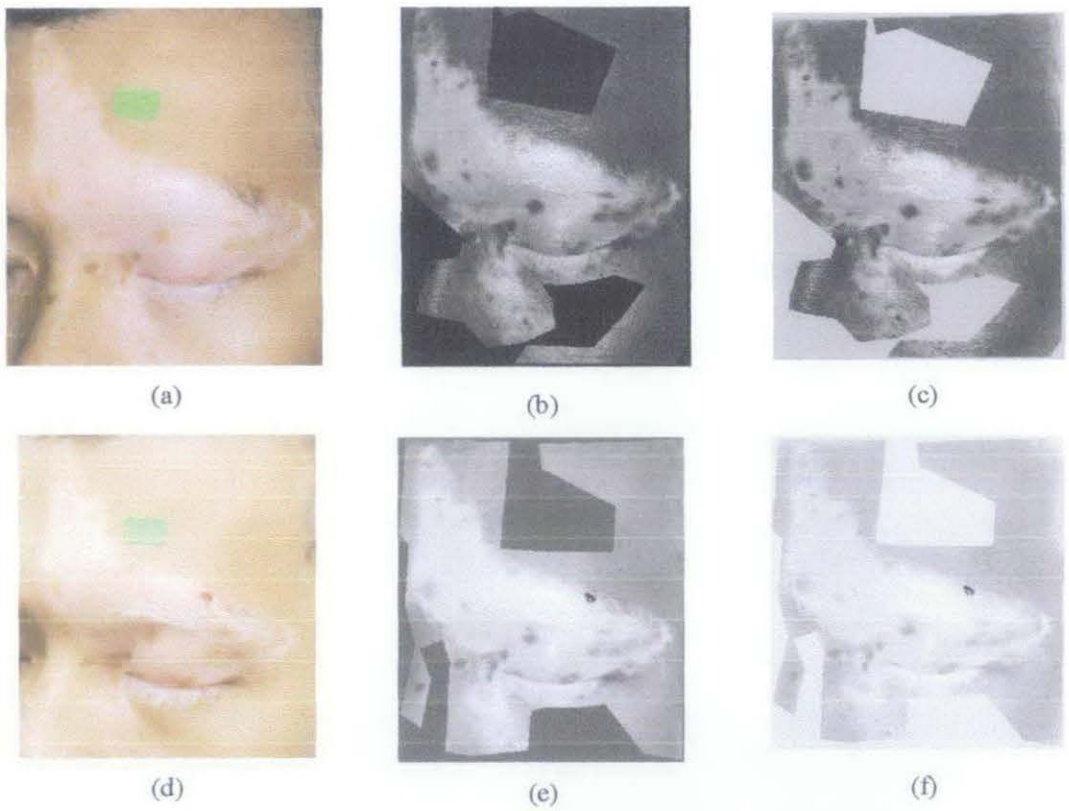

Figure 5.25 Processed images of lesions on the face of Patient E: (a) RGB image – 17th July 2007, (b) Melanin-17th July 2007, (c) Haemoglobin -17th July 2007, (d) RGB image – 28th August 2007, (e) Melanin – 28th August 2007, (f) Haemoglobin – 28th August 2007

Segmented melanin images are shown in Figures 5.26 - 5.34. To ensure the accuracy of the system, the actual size of the pixel in each image is estimated using the reference image. For example, 1 pixel in Figure 5.17(a) represents $113/45972\,mm^2$ or 2.458×10^{-2} mm^2, 1 pixel in Figure 5.17(d) represents $113/50249\,mm^2$ or 2.2488×10^{-2} mm^2 and so on. This process is performed in every pre-clinical image before we measure the vitiligo lesion area in the image.

It is found that for patient A, the determined non-melanin area (vitiligo lesion area) on 17th July 2007 image is 170.3 mm^2 and 161.1 mm^2, on 28th August 2007 image. For patient B, the non-melanin area (vitiligo lesion area) on the lower limb on 17th July 2007 image is 217 mm^2 and 161.1 cm^2, on 28th August 2007 image. The non-melanin area (vitiligo lesion area) on the feet on 17th July 2007 image is 177.9 mm^2 and 121.2 mm^2, on 28th August 2007 image. From Figure 5.29, the non-melanin area (vitiligo lesion area) of

patient C is found to be 2447.6 mm^2 on 17th July 2007 image and 2227.4 mm^2, on 28th August 2007 image. Patient D has four locations of vitiligo areas. For vitiligo lesion areas on the neck, the non-melanin area (vitiligo lesion areas) is 66.9 mm^2 and 54.3 mm^2, on 17th July 2007 and 28th August 2007 respectively. For vitiligo lesion areas on the trunk, the non-melanin area (vitiligo lesion area) on 17th July images is 578 mm^2 and 511.6 mm^2, on 28th August 2007 image. For vitiligo lesion areas on the upper limb, the lesion area on 17th July images is 3632.5 mm^2 and 3595 mm^2, on 28th August 2007 image. For vitiligo lesion areas on the lower limb, the lesion area on 17th July images is 282.3 mm^2 and 249.9 mm^2, on 28th August 2007 image. From Figure 5.34, it is found that for patient E, the determined non-melanin area is 3102.6 mm^2 on 17th July 2007 image and 3049.7 mm^2, on 28th August 2007 image.

(a) (b)

Figure 5.26 Patient A-face (a) segmented melanin image- 17th July 2007, (b) Segmented melanin image –28th August 2007

(a) (b)

Figure 5.27 Patient B-lower limb, (a) segmented melanin image- 17th July 2007, (b) Segmented melanin image –28th August 2007

(a) (b)

Figure 5.28 Patient B-feet (a) segmented melanin image- 17th July 2007, (b) Segmented melanin image –28th August 2007

(a) (b)

Figure 5.29 Patient C-face (a) segmented melanin image- 17th July 2007, (b) Segmented melanin image –28th August 2007

(a) (b)

Figure 5.30 Patient C-neck (a) segmented melanin image- 17th July 2007, (b) Segmented melanin image –28th August 2007

(a) (b)

Figure 5.31 Patient C-trunk (a) segmented melanin image- 17th July 2007, (b) Segmented melanin image –28th August 2007

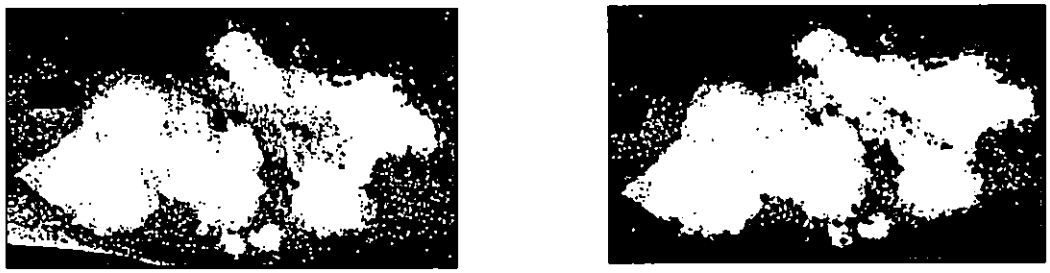

(a) (b)

Figure 5.32 Patient D-upper limb (a) segmented melanin image- 17th July 2007, (b) Segmented melanin image –28th August 2007

(a) (b)

Figure 5.33 Patient D-lower limb (a) segmented melanin image- 17th July 2007, (b) Segmented melanin image –28th August 2007

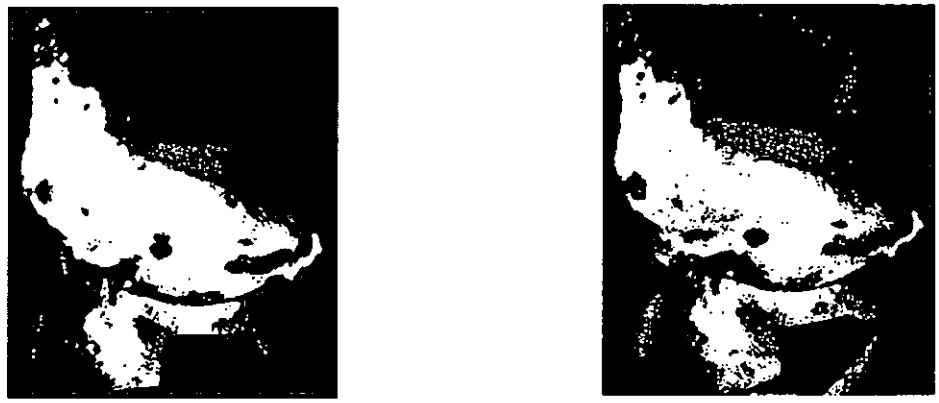

(a) (b)

Figure 5.34 Patient E-face (a) segmented melanin image- 17th July 2007, (b) Segmented melanin image –28th August 2007

The vitiligo skin areas from 17th July 2007 and 28th August 2007 images are tabulated in table 5.3.

Table 5.3 Determination of vitiligo skin areas using developed method

	Body Parts	Vitiligo Skin Areas (mm^2)		Deviation
		17th July 2007	28th August 2007	
Patient A	Face	170.3	161.1	0.092
Patient B	Lower Limb	217	187.4	0.296
	Feet	177.9	121.2	0.567
Patient C	Face	2447.6	2227.4	2.202
Patient D	Neck	66.9	54.3	0.126
	Trunk	578	511.6	0.664
	Upper Limb	3632.5	3595	0.375
	Lower Limb	282.3	249.9	0.324
Patient E	Face	3102.6	3049.7	0.529

5.3.3 Physician's Global Assessment (PGA)

Physician's Global Assessment (PGA) is the current scoring system used to evaluate the progression of vitiligo treatment. The score of PGA can be seen in Table 1.1. For our pre-clinical trial analysis, the results of the vitiligo monitoring system are being compared with Physician's Global scorings of two dermatologists in Hospital Kuala Lumpur, Malaysia. Using the measurements provided in Table 5.3, the repigmentation progression due to the vitiligo treatment can be determined objectively in percentages as shown in Table 5.4. Table 5.4 also compares repigmentation assessment by Physician's Global Assessment and our proposed method.

Table 5.4 Comparison between Physicians's Global Assessment and the developed method

	Body Parts	PGA	Vitiligo Monitoring System
Patient A	Face	0-25%	5.4%
Patient B	Lower Limb	0-25%	13.6%
	Feet	0-25%	31.87%
Patient C	Face	0-25%	8.99%
Patient D	Neck	0-25%	18.8%
	Trunk	0-25%	11.49%
	Lower Limb	0-25%	1%
	Upper Limb	0-25%	11.5%
Patient E	Face	0-25%	1.7%

For patient A, the PGA score is mild (0-25%). For patient B, the score of lesion areas on lower limb and on feet are both mild. Patient C also has mild score. For patient D, all of the lesion areas (neck, trunk, lower limb and upper limb) have mild scores. For patient E, the vitiligo lesion areas have mild score.

5.3.4 Analysis

As recorded in Table 5.3, after 6 weeks of treatment, there are repigmentation progressions on every case of our clinical trial study. In other words, we can find repigmentation areas on the vitiligo lesion areas after 6 weeks of treatment. However these repigmentation areas are so small (Figure 5.8 to Figure 5.16), as a result, our dermatologists find it difficult to discern these areas visually from the images.

The vitiligo monitoring system however has been able to quantify the repigmentation progression on the lesion areas objectively as shown in Table 5.4. It is found that after 6 weeks of treatment, the vitiligo lesion areas are reduced. In comparison to Physician's Global Assessment scores (Table 5.4), the percentages obtained using the developed method are within the Physician's Global Assessment range except for the case of vitiligo lesion on feet of Patient B.

In the case of Patient B, there are areas of vitiligo lesion that can be seen clearly in Figure 5.28 but in Figure 5.10 these areas are not so clear to be discerned visually. The developed system however is able to capture these areas (Figure 5.28). It is shown that the vitiligo monitoring system is superior as it is able to capture small repigmentation areas.

In the processed images (Figure 5.17 – Figure 5.25) from RGB images, one may find dark and black areas on the images due to melanin and haemoglobin only. These are areas of reference and reflective surfaces. From our experiments, we find that the presence of reference (green tape) and reflective surfaces can affect the analysis of the vitiligo monitoring system. Together with dermatologists, we try to minimize the effects of these areas by setting it aside from the process of the vitiligo monitoring system. The region of interest on every image was chosen carefully with dermatologist.

Reflective surfaces are due to the direct reflectance of the light when the light comes into contact with the skin surfaces. The reflectance light is only 5% of the total light coming in contact with skin surfaces (Section 2.7.1). However in our experiments, this reflectance can be irritating on certain skin areas, most likely face and feet. It is found that most of patients have oily skin surfaces on their face. The oily surfaces can affect the determination of melanin on skin. For the feet, the reflective surfaces are due to the tibia bones. It is observed that in tibia bones area, the skin will look glossy and shinny on images. Figure 5.8, Figure 5.11 and Figure 5.16 show the vitiligo lesion areas on the face of our patients. It is found that the reflectance on these figures can affect the selection of regions of interest. Even dermatologists find it hard to determine regions of interest in these images. To overcome this problem, the selection of regions of interest are performed together with dermatologists when the patients coming for the evaluation to hospital.

The dark and black areas resulted by the selection process may affect the process transformation of RGB images to images due to melanin and haemoglobin only. However due to the Principal Component Analysis, we ensure that these dark and black areas are not affecting the whole process.

Principal Component Analysis (PCA) transforms the data sets into new data sets such that the greatest variance by any projection of the data comes to lie on the first principal component of the new data sets, the second greatest variance on the second principal component of the new data sets, and so on (Section 3.4). The dark and black areas have small variance in comparison to color areas on the image. As a result, they will lie on the last principal component of RGB image data sets. Since the PCA only use the first and the second principal components, we can conclude that dark and black areas do not affecting the system.

5.4 Summary

Chapter 5 describes the results of vitiligo monitoring system. The vitiligo monitoring system is employed on the real data provided by Hospital Kuala Lumpur. The research was divided into two phases, namely preliminary study and pre-clinical trial. For the first phase of the development of the vitiligo monitoring system, historical data was used. To further validate and improve the system, a second data set was taken during pre-clinical trial.

The vitiligo monitoring system transforms the RGB images into images due to melanin and haemoglobin only. The repigmentation progression is quantified from the segmented melanin images and results are shown in Table 5.1. Results obtained are compared with the Physician's Global Assessment scores (Table 5.2). It is seen that the percentages obtained using the vitiligo monitoring system are within the Physician's Global Assessment ranges except for the case of Patient 4. In the case of Patient 4, the images were taken within 4 months of treatment therefore repigmentation has occurred on a smaller area. The dermatologist find it hard to discern these repigmentation areas visually. The developed system however, is able to capture small repigmentation progression objectively and proves to have the potential as it allows monitoring on a smaller time.

The second data set comes from pre-clinical trial study. The images were taken from 5 patients (patient A, patient B, patient C, patient D and patient E). The patients are coming from three different ethnic origins, namely Malay, Chinese and Indian. Each patient has two images that are taken at different time and refer to the same skin areas. The first set of images was taken on 17th July 2007. The second set of images was taken after 6 weeks of treatment (28th August 2007). The developed method is then applied on these images.

The developed system quantifies the repigmentation progression of the vitiligo lesion areas from each case of patients as shown in Table 5.3. It can be seen that there are

repigmentation areas on every case of the clinical trial data. However these repigmentation areas are so small (Figure 5.8 to Figure 5.16), as a result, dermatologists find it difficult to discern these areas visually. The developed method however has been able to determine the repigmentation progression on the lesion areas objectively as shown in Table 5.4. It is concluded that after 6 weeks of treatment, the vitiligo lesion areas are reduced.

The comparison between Physician's Global Assessment and developed method can be seen in Table 5.4. It is seen that the percentages obtained using the developed method are within the Physician's Global Assessment ranges except for the case of Patient B. In the case of Patient B, there are areas of vitiligo lesion that can be seen clearly in Figure 5.27 but in Figure 5.10 these areas are not so clear to be discerned visually. The developed system however is able to capture these areas (Figure 5.27). It is shown that the developed method is superior as it is able to capture small repigmentation areas

Chapter 6

CONCLUSIONS

6.1 Introduction

Vitiligo is an acquired pigmentary skin disorder characterized by depigmented macules that result from damage to and destruction of epidermal melanocytes. Visually, the vitiligo areas are paler in contrast to normal skin or completely white due to the lack of pigment melanin [Roberts, 2003]. In this thesis, statistical signal and image processing techniques are applied to develop a vitiligo monitoring system that determines repigmentation progression during the course of treatment of vitiligo disease.

6.2 Discussion

Vitiligo is a skin disorder that visually makes the skin areas paler in contrast to normal skin or completely white due to the lack of pigment melanin. Pigment melanin is color pigment found in skin, eyes and hair. It is produced by melanocytes through processes called melanogenesis [Romero-Graillet 1996, Ito 2003]. Melanocytes reside on the bottom lines of dermis.

Vitiligo treatment aims to re-pigment skin in order to obtain normal skin tone. To evaluate the therapeutic response of vitiligo, dermatologists currently employ Physician's Global Assessment (PGA). This scale is based on the degree of repigmentation within lesions over time. However, it is found that PGA is subjective as it has intra and inter variations. The objective of the thesis is to develop image processing algorithm and analysis that able to determine and quantify the repigmentation progression objectively. This vitiligo monitoring system will be used as a tool for assisting dermatologist monitor vitiligo lesion during the course of treatment.

In this research, it is important to determine the reflectance captured by the monitoring system. Light reflections of skin could be defined by several components. 5% of the incident light coming in contact to skin is directly reflected at the surface. Most of the incident light (nearly 95%) penetrates into skin and follows a complex path until it exits back out of the skin or gets attenuated by skin choromophores [Preece, 2004]. It can be concluded that the light coming from skin carries information of the structure within skin layers.

This incoming light is capture by digital camera to get the skin image. Digital color camera usually uses a Bayer mask over the CCD to generate a digital color image. Bayer mask is a color filter array used for arranging red, green and blue (RGB) color filters on a square grid of CCD sensor [Bayer 1976]. The mask pattern is 50% green, 25% red and 25% blue. As a result, in digital imaging, color is produced by combining three different bands, namely: red band, green band and blue band.

Essentially, skin color is due to the combination of skin histological parameters, namely pigment melanin and haemoglobin. However in digital imaging, color is represented by three spectral bands: red, green, and blue (RGB). It is therefore necessary to find a robust algorithm to extract skin histological parameters from the RGB image. In this thesis, statistical signal and image processing techniques are applied to determine melanin and hemoglobin from skin images.

It is stated by N.Tsumura that the spatial distribution of melanin and haemoglobin in skin could be separated by employing linear independent component analysis of a skin color image [Tsumura, 1999]. The analysis is based on the three assumptions. Firstly, it is assumed linearity in the optical density domain of RGB channels. The second and third assumptions state that the spatial variations of skin image color are caused by two skin choromophores, namely melanin and haemoglobin and their quantities are mutually independent, as shown in Figure 4.2.

Figure 4.3 shows the skin model used of the analysis. It is shown that skin color distribution lies on a two-dimensional melanin-haemoglobin color subspace. Using Principal Component Analysis as a dimensional reduction tool, the two-dimensional subspace can be represented by its first and second principal components. Principal Component Analysis is orthogonal linear transformation that computes the most meaningful basis to re-express a data set and used widely as a dimension reduction tool. It is reported that the values of the RGB skin image can be adequately represented by using two principal components with an accuracy of 99.3 %. In addition, it is also necessary to make the two-dimensional subspace zero mean and unit variance in order to get stronger independence condition.

Independent Component Analysis (ICA) is employed on the two-dimensional color space in order to determine images due to melanin and hemoglobin only. Independent Component Analysis (ICA) is a multivariate data analysis for source separation. The source separation (blind source separation) is a problem in signals processing where the source of the observed signals were mixed are unknown [Roberts 2001]. As depicted in Figure 3.14, the goal of ICA is to find a linear transformation of input that makes the output independent as possible. In ICA, independence means that the multivariate probability density function of the sources, in our case, melanin and hemoglobin, can be written as the product of marginal independent distributions. Figure 4.2 shows that melanin and hemoglobin are independent therefore we can employ ICA for the analysis of melanin and hemoglobin.

In the thesis, we apply the Fast ICA algorithm developed by Aapo Hyvarinen [Hyvarinen, 1997; Hyvarinen, 1999; Hyvarinen, 2000] to our vitiligo technique. As depicted in Figure 4.4, the ICA method finds a liner transformation, w, of the two-dimensional melanin-haemoglobin color subspace, v, that makes the output, u, independent as possible. The matrix w is computed so that the mutual information of s is minimized. This is roughly equivalent to finding directions in which the negentropy is maximized. Negentropy is a measure of nongaussianity (Equation 3.41). However, instead of measuring negentropy, the method employs the approximation of negentropy

(Equation 4.5). To find the maxima of the approximation of negetropy, Newton iterative method (Equation 4.7) is used.

The PCA/ICA process produces skin images due to melanin and hemoglobin only. Segmentation of vitiligo lesion areas is then performed on image due to melanin. As mentioned earlier, vitiligo lesion areas are skin areas that are lacking pigment melanin. A threshold selection based on median cut algorithm is employed to segment non-melanin areas and melanin areas on the image due to melanin only. The determined non-melanin areas represent the vitiligo lesion areas.

The changes in the vitiligo surface areas of skin images before and after treatment are quantified by comparing the size of non-melanin areas before and after treatment. The changes are expressed as a percentage of repigmentation to reflect the repigmentation progression of vitiligo lesion areas.

The performance of the vitiligo monitoring system is investigated in controlled environments. Here, we construct images of skin model and vitiligo lesion model. The skin and vitiligo model are developed using patients data. It is assumed that the spatial distribution of skin and vitiligo lesion can be expressed by Gaussian distribution. These images are then distorted by controlled noise. The result shows the developed is able to determine a vitligo lesion down to 1-by-1 pixel in an image that has no noise as depicted in Figure 4.17. However if we add noise to the image, the developed system is able to determine a 1-by-1 pixel vitiligo lesion area for signal to noise ratios 15 dB, as shown in Figure 4.21.

The vitiligo monitoring system is tested against real images provided by Department of Dermatology, Hospital Kuala Lumpur. Tests are performed on historical data and pre-clinical trial data sets. The historical data set consists of images taken from 4 patients (patient 1, patient 2, patient 3 and patient 4). From the study of historical data, it is found that the percentages obtained using the developed method are within the Physician's Global Assessment ranges except for the case of Patient 4 as shown in Table 5.2. In

patient 4, the repigmentation areas are small due the briefness of the treatment (4 months) compared to the other patients. It is difficult for dermatologists to discern visually small repigmentation progression due to the treatment. The vitiligo monitoring system is however able to capture small repigmentation progression objectively and thus can be potentially used as it allows monitoring on a shorter time frame.

In the pre-clinical trial, the images are taken from 5 patients (patient A, patient B, patient C, patient D and patient E). Each lesion areas on a patient have two images. The images are taken at different time (6 weeks different). The first images were taken on 17th July 2007 and the second images on 28th August 2007. As shown in Table 5.3, there are repigmentation progressions on every case of our pre-clinical trial study. However these repigmentation areas are so small (Figure 5.8 to Figure 5.16), as a result, dermatologists find it difficult to discern these areas visually in the images. The system however has been able to quantify the repigmentation progression on the lesion areas objectively as shown in Table 5.4. In comparison to Physician's Global Assessment scores (Table 5.4), the percentages obtained using the developed method are within the Physician's Global Assessment range except for the case of vitiligo lesion on feet of Patient B. In the case of Patient B, there are areas of vitiligo lesion that can be seen clearly in Figure 5.27 but in Figure 5.10 these areas are not so clear to be discerned visually. The developed system however is able to capture small repigmentation areas (Figure 5.27).

6.3 Contribution and Future Work

The main contribution of this thesis is in the development of a system that enable dermatologist to monitor the repigmentation progression of vitiligo lesion on a shorter time frame. The developed system is able to determine and quantify repigmentation areas objectively, enabling treatment efficacy to be determined earlier.

A new approach for measuring the vitiligo lesion areas has been developed. The analysis is based on the combination of statistical signal and image processing algorithms. Principal Component Analysis and Independent Component Analysis are used to

transform skin RGB images into images due to melanin and hemoglobin only. This is followed by segmentation process.

It is shown that the processed images are being influenced by the direct reflectance of light. This can be overcome by utilizing polarized filter in the digital camera lens. Polarizing filter should be able to filter the direct reflectance of the light coming in contact to skin.

An intensive clinical trial is currently undertaken in Hospital Kuala Lumpur using our system.

REFERENCE

A. Hameed, Z. Rani and A. Kazmi (2005). *Vitiligo:new-etiology based treatment.* Journal of Pakistan Association of Dermatologists 15: 252-260.

A. Hyvärinen and E. Oja (1997). *A Fast Fixed-Point Algorithm for Independent Component Analysis.* Neutral Computation 9: 1483-1492.

A. Hyvärinen and E. Oja (2000). *Independent Component Analysis: Algorithms and Applications.* Neural Networks 13: 411-430.

A. Taneja, M. Trehan and C. R. Taylor (2003). *308-nm Excimer Laser for The Treatment of Localized Vitiligo.* International Journal of Dermatology 42(8): 658-662.

A.Manios, A.Tosca, E. Volakakis, M. Laivadara and D.Tsiftsis (2003). *Computer Assisted Evaluation of Wound Healingn in Chronic Ulcers.* Computers in Biology and Medicine 33(4): 311-317.

B.Jung, B. Choi, A.J. Durkin, K. M. Kelly and J. S. Nelson (2004). *Characterization of Port Wine Stain Skin Erythema and Melanin Content using Cross-Polarized Diffused Reflectance Imaging.* Lasers Medical Science 34: 174-181.

B.R. Boersma, W. Westerhof and J. D. Bos (1995). *Repigmentation in Vitiligo Vulgaris by Autologous Minigrafting: Results in Nineteen Patients.* Journal of American Academy of Dermatology 33: 990-995.

Bayer, B. E. (1976). *Color Imaging Array.* U. S. Patent No. 3,971,065.

C.M. Issa, J Rehder and M. B. Taube (2003). *Melanocyte Transplantation for the Treatment of Vitiligo: Effects of Different Surgical Techniques.* European Journal of Dermatology 13(1): 34-39.

D. Nakao, N. Tsumura and Y. Miyake (2001). *Real-time multi-spectral image processing for mapping pigmentation in human skin.* Proceedings of IS&T/SID's 9th Color Imaging Conference, Color Science, Systems and Applications, 80-84.

D.R. Revis and M. B. Seagle. (2006). *Skin, Anatomy* Retrieved January 2006, from http://www.emedicine.com.

DA Smith, SJ Tofte and J. Hanifin (2002). *Repigmentation of Vitiligo with Topical Tacrolimus.* Dermatology 205(3): 301-303.

E. Baltas, Z. Csoma and F. Ignacz (2002). *Treatment of Vitiligo with 308 nm Xenon Excimer Laser.* Archives of Dermatology 138(12): 1619-1620.

F. Chang, Z. Ma and W. Tian (2007). *A Region-Based Skin Color Detection Algorithm.* Proceedings of the 11th Pacific-Asia Conference on Knowledge Discovery and Data Mining, Nanjing, China, 417-424.

F.Tomaz, T. Candeias and H. Shahbazkia (2004). *Fast and Accurate Skin Segmentation in Color Images.* Proceedings of the First Canadian Conference on Computer and Robot Vision, 180-187.

Fukunaga, K. (1972). *Introduction to Statistical Pattern Recognition,* Academic Press.

G. Menchini, E.Tsoureli–Nikittta and J. G. Hercogova (2003). *Narrow-band UVB Micro-phototherapy: A New Treatment for Vitiligo.* Journal of the European Academy of Dermatology and Venereology 17(2): 171-177.

G.N. Stamatas, B.Z. Zmudzka, N. Kollias and J. Beer (2004). *Review: Innovative Technology, Non-Invasive Measurements of Skin Pigmentation In Situ.* Pigment Cell Res. 17: 618-626.

Gomez, G. (2002). *On Selecting Colour Components for Skin Detection.* Proceedings of the16th International Conference on Pattern Recognition 961-964.

Grimes, P. E. (2005). *New Insight and New Therapies in Vitiligo.* Journal of America Medical Association 293: 730-735.

H. Nugroho and M. H. Ahmad Fadzil (2007). *Skin Segmentation using Principal Component Analysis.* Proceedings of the 3rd nternational Colloquium on Signal Processing and its Application, 764-769.

H. Takiwaki, S. Shirai, Y. Kanno, Y. Watanabe and S. Arase (1994). *Quantification of Erythema and Pigmentation using a Video Microscope and a Computer.* British Journal of Dermatology 131: 85-92.

Hamadani, N. (1981). *Automatic Target Cueing in IR Images.* Master's Thesis, Air Force Institute of Technology, 1981.

Hamzavi, I., H. Jain, D. MecLean, J. Shapiro, H. Zeng and H. Lu (2004). *Parametric Modeling of Narrowband UV-B Phototherapy for Vitiligo using a Novel Quantitative Tool- the Vitiligo Area Scoring Index.* Archives of Dermatology 140: 677-683.

Heckbert, P. S. (1980). *Color Image Quantization for Frame Buffer Display.* Bachelor of Science, Massachusetts Institute of Technology, 1980.

Hong Li and Y. Sun (2005). *The Study and Test of ICA Algorithms.* Proceedings of International Conference on Wireless Communications, Networking and Mobile Computing, 602-605.

Hvyarinen, A. (1998). *New approximations of differential entropy for independent component analysis and projection pursuit.* Advances in Neural Information .Processing System 10(273-279).

Hyvarinen, A. (1999). *Fast and Robust Fixed-Point Algorithms for Independent Component Analysis*. IEEE Transaction on Neural Networks 10(3): 626-634.

I. Maglogiannis (2003). *Automated Segmentation and Registration of Dermatological Images*. Journal of Mathematical Modelling and Algorithms 2: 277-294.

I. Maglogiannis, E. Zafiropoulos and C. Kyranoudis (2006). *Intelligent Segmentation and Classification of Pigmented Skin Lesions in Dermatological Images*. Proceedings of Hellenic Conference on Artificial Intelligent, 214-223.

I. Maglogiannis, S. Pavlopoulos and D. Koutsouris (2005). *An Integrated Computer Supported Acquisition, Handling, and Characterization System for Pigmented Skin Lesions in Dermatological Images*. IEEE Transactions on Information Technology in Biomedicine 9(1): 86-98.

Ito, S. (2003). *The IFPCS presidential lecture: a chemist's view of melanogenesis*. Pigment Cell Res. 16(3): 230-236.

J. Karhunen, E. Oja, L. Wang, R. Vigario and J. Joutsensalo (1997). *A Class of Neural Networks for Independent Component Analysis*. IEEE Transactions on Neural Networks 8(3): 486-504.

J. Liu and Y. H. Yang (1994). *Multiresolution Color Image Segmentation*. IEEE Transaction on Pattern Analysis and Machine Intelligence 16(7): 674-693.

J. Porter, A. Beuf and J. Nordlund (1979). *Psychological Reaction to Chronic Skin Disorders*. General Hospital Psychiatry 1: 73-77.

J. Yi, J. Park, J. Kim and J. Choi (2003). *Robust Skin Color Segmentation Using a 2D Plane of RGB Color Space*. Proceedings of International Symposium on Intelligent Control 413-420.

J.B. Kim, S.W. Jung and H. J. Kim (2002). *Face Detection by Integrating Multiresolution-Based Watersheds and a Skin-Color Model.* Proceedings of the 15th International Conference on Industrial and Engineering Applications of Artificial Intelligence and Expert Systems: Developments in Applied Artificial Intelligence, 715-724.

J.J. Dios and N. García (2005). *Feature Extraction Used for Face Localization Based on Skin Color.* Proceedings of International Conference on Image Analysis and Recognition, 1032-1039.

Kampen, N. G. v. (1981). *Stochastic Processes in Physics and Chemistry.* New York, North-Holland.

Keener, R. W. (2006). *Statistical Theory: Notes for a Course in Theoritical Statistics,* Springer.

Kenny, J. (1971). *Vitiligo treated by psoralens: a long term follow-up study of the permanency of repigmentation.* Archives of Dermatology 103: 475-480.

Kovacs, S. (1998). *Continuing Medical Education: Vitiligo.* Journal of the American Academy of Dermatology 38: 647-666.

L. Mostafa and S. Abdelazeem (2005). *Face Detection Based on Skin Color Using Neural Networks,* Proceedings of International Conference on Graphics, Vision and Image Processing Cairo, Egypt.

Lay, D. (2000). *Linear Algebra and It's Applications.* New York, Addison-Wesley.

Lerner, A. (1959). *Vitiligo.* Journal of Invest Dermatology 32: 285-310.

M. Harville, H. Baker, N. Bhatti and S. Süsstrunk (2005). *Consistent Image-Based Measurement and Classification of Skin Color.* Proceedings of IEEE International Conference on Image Processing, Genoa, Italy, II-374-377.

M.J. Jones and J. M. Rehg (2002). *Statistical Color Models with Application to Skin Detection.* International Journal of Computer Vision 46(1): 81-96.

M.J. Seow and V.K.Asari (2004). *Recurrent Network as a Nonlinear Line Attractor for Skin Color Association.* Proceedings of International Symposium on Neural Networks 870-875.

M.Storring (2004). *Computer Vision and Human Skin Colour.* Ph.D. Dissertation, Aalborg University, 2004.

MA Middelkamp-Hup, JD Bos, F Rius-Diaz, S Gonzalez and W. Westerhof (2007). *Treatment of vitiligo vulgaris with narrow-band UVB and oral Polypodium leucotomos extract: a randomized double-blind placebo-controlled study.* Journal of the European Academy of Dermatology and Venereology 21(7): 942-950.

MJ. Zhang, WQ Wang, QF Zheng and W. Gao (2004). *Skin-Color Detection Based on Adaptive Thresholding.* Proceedings of the 3rd International Conference on Image and Graphics, 250-253.

MMU. (2006). *Centre of Image Processing and Telemedicine* Retrieved June 2007, from http://fet.mmu.edu.my/fet/research/ciptem/.

N. Tsumura, H. Haneishi and Y. Miyake (1999). *Independent Component Analysis of Skin Color Image.* Journal of the Optical Society of America A 16: 2169-2176.

N. Tsumura, H. Haneishi and Y. Miyake (2000). *Independent Component Analysis of Spectral Absorbance Image in Human Skin.* Optical Review 7: 479-482.

N. Tsumura, M. Kawabuchi, H. Haneishi and Y. Miyake (2000). *Mapping pigmentation in human skin by multivisible-spectral imaging by inverse optical scattering technique.* Proceedings of IS&T/ SID's 8th Color Imaging Conference, Color Science, Systems and Applications, 81-84.

N. Tsumura, N. Ojima, K. Sato, M. Shiraishi, H. Shimizu, H. Nabeshima, S. Akazaki, K. Hori and Y. Miyake (2003). *Image-based skin color and texture analysis/synthesis by extracting hemoglobin and melanin information in the skin.* ACM Transactions on Graphics 22(3): 770-779.

N. van Geel, K Ongenae and J. Naeyaert (2001). *Surgical techniques for Vitiligo: A Review.* Dermatology 202(2): 162-166.

N. van Geel, Yves Vander Haeghen, K. Ongenae and J. M. Naeyert (2004). *A New Digital Image Analysis System Useful for Surface Assessment of Vitiligo Lesions in Transplantation Studies.* European Journal of Dermatology 14: 150-155.

N.Roberts and M. Lesage (2003). *Vitiligo: Causes and Treatment.* The Pharmaceutical Journal 270: 440-442.

Norashikin, S. (2007). *Physician's Global Assessment (PGA).* Private communication. Kuala Lumpur.

Ohno, Y. (2000). *CIE Fundamentals for Color Measurements.* Proceedings of the IS&T NIP16 Conference, 540-545.

Otsu, N. (1979). *A Threshold Selection Method from Gray-Level Histograms.* IEEE Transactions on Systems, Man, and Cybernetics 9(1): 62-66.

P. Tichavský, Zbyn˘ek Koldovský and E. Oja (2006). *Performance Analysis of the FastICA Algorithm and Cramér–Rao Bounds for Linear Independent Component Analysis*. IEEE Transactions on Signal Processing 54(4): 1189-1203.

P.Schmid and S. Fischer (1997). *Colour Segmentation for The Analysis of Pigmented Skin Lesions*. Proceedings of the Sixth International Conference on Image Processing and Its Applications, Dublin, Ireland, 688-692.

Peterson, C. (2001). *How It Works, The Charged-Coupled Device or CCD.* Journal of Young Investigators 3.

Preece, S. J. and E.Claridge (2004). *Spectral Filter Optimization for the Recovery of Parameters which Describe Human Skin.* IEEE Transaction on Pattern Analysis and Machine Intelligence 28(7): 913-922.

Q. Zhu, KT. Cheng, CT. Wu and Y. Wu (2004). *Adaptive Learning of an Accurate Skin-Color Model.* Proceedings of the Sixth IEEE International Conference on Automatic Face and Gesture Recognition, 37-42.

R. C. Gonzalez and R. E. Woods (1992). *Digital Image Processing.* Boston, Addison-Wesley Longman Publishing .

R.M. Gray and L. D. Davisson (2004). *An Introduction to Statistical Signal Processing*, Cambridge University Press.

R.R. Anderson and J. A. Parrish (1981). *The Optics of Human Skin.* Journal of Investigative Dermatology 77: 13-19.

Ritter, G. X. and J. N. Wilson (2000). *Handbook of Computer Vision Algorithms in Image Algebra*, CRC Press.

Rosebury, T. (1969). *Life on Man*, Secker & Warburg.

Rosenfeld, A. and A. Kak (1982). *Digital Picture Processing* New York, Academic Press.

S. Cooray and N. O'Connor (2004). *Facial Feature Extraction and Principal Component Analysis for face Detection in Colour Images.* Proceedings of the International Conference on Image Analysis and Recognition 741-749.

S. Fischer, P.Schmid and J. Guillod (1996). *Analysis of Skin Lesions with Pigmented Networks*. Proceedings of International Conference on Image Processing, Lausanne, France, 323-326.

S. Roberts and R. Everson (2001). *Independent Component Analysis: Principles and Practice*, Cambridge University Press.

S.Barnett (2005). *SLR vs All-in-One: Which Way to Go?* Imaging Resources.

S.D. Cotton and E. Claridge (1996). *Developing A Predictive Model of Human Skin Colouring*. Proceedings of the SPIE Medical Imaging 814-825.

S.D. Cotton, E. Claridge and P. Hall (1997). *Noninvasive Skin Imaging*. Lecture Notes In Computer Science 1230: 501-506.

S.E. Umbaugh, G.A. Hance, R.H. Moss and W. V. Stoecker (1996). *Unsupervised Color Image Segmentation with Application to Skin Tumor Borders*. IEEE Engineering in Medicine and Biology 15(1): 104-111.

S.E. Umbaugh, R.H. Moss, W.V. Stoecker and G. A. Hance (1993). *Automatic Color Segmentation Algorithms With Application to Skin Tumor Feature Identification.* IEEE Engineering in Medicine and Biology 12(3): 75-82.

S.L. Phung, A. Bouzerdoum and D. Chai (2005). *Skin Segmentation Using Color Pixel Classification: Analysis and Comparison.* IEEE Transaction on Pattern Analysis and Machine Intelligence 27(1): 148-154.

S.L. Phung, D. Chai and A. Bouzerdoum (2003). *Adaptive Skin Segmentation in Color Images.* Proceedings of IEEE Intemational Conference on Acoustics, Speech, & Signal Processing, Hong Kong, 173-176.

Sahbi, H. and N. Boujemaa (2002). *Coarse to Fine Face Detection Based on Skin Color Adaption.* Proceedings of the International ECCV 2002 Workshop Copenhagen on Biometric Authentication, 112-120.

T.S. Caetano and D. A. C. Barone (2001). *A Probabilistic Model for the Human Skin Color.* Proceedings of 11th International Conference on Image Analysis and Processing, 279-283.

Takiwaki, H. (1998). *Measurement of Skin Color: Pratical Application and Theoretical Considerations.* Journal of Medical Investigation 44: 121-125.

Tonsi, A. (2004). *Vitiligo and Its Management Update: A Review.* Pakistan Journal of Medical Science 20(3): 242-247.

Umbaugh, S. E. (2005). *Computer Imaging: Digital Image Processing and Analysis,* CRC Press.

V Lepe, B Moncada and J. Castanedo-Cazares (2003). *A double- blind randomized trial of 0.1% tacrolimus vs 0.05% clobetasol for the treatment of childhood.* Archives of Dermatology 139(5): 581-585.

Y.J. Kim, B.S. Chung and K. C. Choi (2001). *Depigmentation Therapy with Q-switched Ruby Laser after Tanning in Vitiligo Universalis*. Dermatologic Surgery 27(11): 969-970.

Y.W. Lim and S. U. Lee. (1990). *On the color image segmentation algorithm based on the thresholding and the fuzzy c-means techniques*. Pattern Recognition 23(9): 935-952.

Yves Vander Haeghen, N. van Geel, K. Ongenae, M. De Mil, C. Vervaet and J. M. Naeyaert (2004). *Double-blind Placebo-Controlled Study of Autologous Transplanted Epidermal Cell Suspensions for Repigmenting Vitiligo*. Archives of Dermatology 140: 1203-1208.

Z. Fan and B. Lu (2004). *An Adjusted Gaussian Skin-Color Model Based on Principal Component Analysis*. Proceedings of International Symposium on Neural Networks, Dalian, China, Springer, 804-809.